Final Technical Report
WP-1184

Electrostatic Fuel Atomization for Gas Turbines

Naval Surface Warfare Center

David Guimond
Code 9823
5001 S. Broad St.
Philadelphia, PA 19112

CFD Research Corporation
Matthew Thomas
Adam Elliott
215 Wynn Drive
Huntsville, Al 35805

CFDRC Report: 8445/6

REPORT DOCUMENTATION PAGE

Form Approved
OMB No. 0704-0188

Public reporting burden for this collection of information is estimated to average 1 hour per response, including the time for reviewing instructions, searching existing data sources, gathering and maintaining the data needed, and completing and reviewing this collection of information. Send comments regarding this burden estimate or any other aspect of this collection of information, including suggestions for reducing this burden to Department of Defense, Washington Headquarters Services, Directorate for Information Operations and Reports (0704-0188), 1215 Jefferson Davis Highway, Suite 1204, Arlington, VA 22202-4302. Respondents should be aware that notwithstanding any other provision of law, no person shall be subject to any penalty for failing to comply with a collection of information if it does not display a currently valid OMB control number. **PLEASE DO NOT RETURN YOUR FORM TO THE ABOVE ADDRESS.**

1. REPORT DATE *(DD-MM-YYYY)*
30-Jun-2006

2. REPORT TYPE
Final

3. DATES COVERED *(From - To)*
1-Mar-2001 - 1-Sep-2005

4. TITLE AND SUBTITLE
Electrostatic Fuel Atomization for Gas Turbines

5a. CONTRACT NUMBER

5b. GRANT NUMBER

5c. PROGRAM ELEMENT NUMBER
0603716D

5d. PROJECT NUMBER
WP-1184

5e. TASK NUMBER

5f. WORK UNIT NUMBER

6. AUTHOR(S)
Matthew Thomas
Adam Elliott
David P. Guimond

7. PERFORMING ORGANIZATION NAME(S) AND ADDRESS(ES) AND ADDRESS(ES)

CFD Research Corporation
215 Wynn Drive
Huntsville, AL 35805

Naval Surface Warfare Center
Carderock Division
5001 S. Broad St
Philadelphia, PA 19112-5083

8. PERFORMING ORGANIZATION REPORT NUMBER
NSWCCD-98-TR-2006/06+CR

9. SPONSORING / MONITORING AGENCY NAME(S) AND ADDRESS(ES)
Strategic Environmental R&D Program
Weapons Systems and Platforms
901 N. Stuart St., Suite 303
Arlington, VA 22203-1853

10. SPONSOR/MONITOR'S ACRONYM(S)
SERDP

11. SPONSOR/MONITOR'S REPORT NUMBER(S)

12. DISTRIBUTION / AVAILABILITY STATEMENT
Approved for public release; distribution is unlimited

13. SUPPLEMENTARY NOTES

14. ABSTRACT
Recent breakthroughs in the field of hydrocarbon fuel electrostatic charging techniques permitted the opportunity to evaluate this technology within shipboard gas turbines. This technology demonstration effort focused on electrostatic atomization insertion within a U.S. Navy Shipboard Rolls Royce Corporation 501K research engine at the Naval Surface Warfare Center, Carderock Division (NSWCCD). Specific milestones achieved during this effort included:1.)Electrostatic charging effect measurements on the droplet size and patternation of 501-K primary simplex atomizer configurations. 2.)Spray demonstration of an electrostatic boosted 501-K gas turbine airblast fuel injector prototype at fuel flows from 40 PPH to 250 PPH. 3.)Numerical modeling of electrostatic charging on secondary atomization breakup and prediction of particulate emissions.4.)Fabrication, installation and test prototype engine injectors in the RR501K engine. This report documents results associated with injector conceptual design, electrode integration, atomization measurements, and numerical modeling and fuel injection system integration and engine test.

15. SUBJECT TERMS
Gas Turbines, Fuel Injection, Electrostatics, Emissions

16. SECURITY CLASSIFICATION OF:			17. LIMITATION OF ABSTRACT	18. NUMBER OF PAGES	19a. NAME OF RESPONSIBLE PERSON
					David Guimond
a. REPORT	b. ABSTRACT	c. THIS PAGE			19b. TELEPHONE NUMBER *(include area code)*
UNCLASSIFIED	UNCLASSIFIED	UNCLASSIFIED	UL	93	215-897-8641

Standard Form 298 (Rev. 8-98)
Prescribed by ANSI Std. Z39.18

This report was prepared under contract to the Department of Defense Strategic Environmental Research and Development Program (SERDP). The publication of this report does not indicate endorsement by the Department of Defense, nor should the contents be construed as reflecting the official policy or position of the Department of Defense. Reference herein to any specific commercial product, process, or service by trade name, trademark, manufacturer, or otherwise, does not necessarily constitute or imply its endorsement, recommendation, or favoring by the Department of Defense.

TABLE OF CONTENTS

	Page
EXECUTIVE SUMMARY	IX
1. BACKGROUND	**1**
2. OBJECTIVE	**5**
3. TECHNICAL APPROACH	**6**
4. PROTOTYPE ATOMIZER DEVELOPMENT	**7**
4.1 SIMPLEX INJECTOR DEVELOPMENT	7
4.2 AIRBLAST INJECTOR DEVELOPMENT	16
4.3 ATOMIZATION TESTING	20
4.4 COMBUSTION TESTING	23
4.5 CFD MODELING OF THE ENGINE COMBUSTION PROCESS	25
5. RR501K ENGINE COMBUSTION SYSTEM IMPLEMENTATION	29
5.1 ENGINE ELECTROSTATIC FUEL INJECTION SYSTEM	29
5.2 ENGINE IMPLEMENTATION	34
5.3 RR501K ENGINE TEST AND EVALUATION	35
6. SUMMARY	40
7. REFERENCES	41
APPENDIX A- ASME Paper	42
APPENDIX B - ERC Report	49

LIST OF FIGURES

	Page
FIGURE 1. ROLLS ROYCE CORPORATION 501-K ENGINE	1
FIGURE 2. DEMONSTRATED SECONDARY ATOMIZATION PROCESS THAT COULD BE LEVERAGED IN THE RR501K FUEL INJECTION SYSTEM	3
FIGURE 3. SECONDARY ATOMIZATION BREAKUP DUE TO ELECTROSTATIC CHARGING	3
FIGURE 4. ELECTROSTATIC CHARGING APPROACHES CONSIDERED FOR IMPLEMENTATION INTO AN RR501K ENGINE	4
FIGURE 5. ELECTROSTATIC FUEL ATOMIZATION DEVELOPMENT APPROACH	6
FIGURE 6. AIR ASSISTED SIMPLEX ELECTROSTATIC NOZZLE DESIGN	7
FIGURE 7. 501-K SIMPLEX NOZZLE AND RADIAL ELECTRODE	8
FIGURE 8. 501-K SIMPLEX NOZZLE AND DOWNWARD ELECTRODE	8
(A) RADIAL ELECTRODE CONFIGURATION RESULTS	9
(B) DOWNWARD ELECTRODE CONFIGURATION RESULTS	9
FIGURE 9. ELECTRODE CONFIGURATION EFFECT ON FLUID CHARGE DENSITY	9
FIGURE 10. TEST SETUP USED FOR SMD AND OPTICAL PATTERNATION TESTS	10
FIGURE 11. ELECTROSTATIC SIMPLEX TEST FIXTURE TESTED WITH DIESEL FUEL	11
FIGURE 12. TYPICAL SMD DATA FOR ELECTROSTATIC ATOMIZER	11
FIGURE 13. OPTICAL PATTERNATION TEST IN PROGRESS	12
FIGURE 14. PATTERNATION DATA FN=0.5 AT 25 PSI, 3 INCH AXIAL POSITION	13
FIGURE 15. PATTERNATION DATA FN=0.5 AT 50 PSI, 3 INCH AXIAL POSITION	14
FIGURE 16. PATTERNATION DATA FN=10 AT 100 PSI, 3 INCH AXIAL POSITION	14
FIGURE 17. AIR ASSISTED SIMPLEX ELECTROSTATIC NOZZLE	15
FIGURE 18. CFD ANALYSIS RESULTS OF THE ENGINE PROTOTYPE INJECTOR CONFIGURATION	16
FIGURE 18. PURE AIRBLAST ELECTROSTATIC NOZZLE DESIGN	17
FIGURE 19. SOLID MODEL OF THE SINGLE SWIRLER ELECTROSTATIC FUEL NOZZLE CONCEPT.	18
FIGURE 20. AXIAL VELOCITY NEAR THE COMBUSTOR DOME; SINGLE SWIRLER ELECTROSTATIC FUEL NOZZLE WITH DOME SWIRLER.	18
FIGURE 21. AXIAL VELOCITY NEAR THE COMBUSTOR DOME; TWO-SWIRLER ELECTROSTATIC FUEL NOZZLE, COWL REMOVED FROM DOME SWIRLER..	19
FIGURE 22. DETAIL DESIGN OF TWO INJECTOR PROTOTYPES EVALUATED BY CFDRC	19
FIGURE 23. INJECTOR PROTOTYPES FABRICATED FOR DEVELOPMENT TEST AND EVALUATION	20
FIGURE 24. VISUAL SPRAY TESTING AT RR 501K IGNITION CONDITION	21
FIGURE 25. CHARGED INJECTION DATA FOR BOTH PROTOTYPE INJECTOR CONFIGURATIONS	22
FIGURE 26. RR501K FUEL INJECTOR AMBIENT COMBUSTION TEST RIG	23
FIGURE 27. RR501K ELECTROSTATIC CHARGED NOZZLE OPERATING IN COMBUSTION RIG	24
FIGURE 28. CFDRC'S MEXA-554JU EMISSIONS ANALYZER	24
FIGURE 29. SIMULATION OF EXISTING ALLISON 501-K COMBUSTOR	26
FIGURE 30. RRA 501-K COMBUSTION SOOT PREDICTIONS	27
FIGURE 31. SMOKE NUMBER MEASUREMENTS AND SOOT PREDICTION IN THE 501-K	28
FIGURE 32. RR 501K ENGINE ELECTROSTATIC INJECTOR DESIGN	30
FIGURE 32. RR501K PROTOTYPE ENGINE INJECTOR	31
FIGURE 33. RR501K ENGINE CONFIGURED ELECTROSTATIC CHARGED FUEL INJECTOR SET	31
FIGURE 34. CUSTOMIZED POWER SUPPLY FOR ELECTROSTATIC CHARGE CONTROL	32
FIGURE 35. SCHEMATIC OF CORONA-DISCHARGE IN A LABORATORY COMBUSTOR AND THE NECESSARY CONTROL CIRCUITRY	33
FIGURE 36. ELECTROSTATIC FUEL NOZZLE CONTROLLER	33

FIGURE 37. RR 501K GAS TURBINE AT NSWCCD PHILADELPHIA 34
FIGURE 38. PHOTOGRAPH OF ELECTROSTATIC INJECTOR INSTALLATION WITHIN A RR501K ENGINE 35
FIGURE 39. OPTIMIZED RR501K ENGINE START SCHEDULE 38

Abbreviations

A/D	Analog/Digital
BTU	British Thermal Units
ºC	degrees Centigrade
CCD	Charged-Coupled Device
CFD	Computational Fluid Dynamics
CFDRC	CFD Research Corporation
CO	Carbon Monoxide
CO_2	Carbon Dioxide
D/A	Digital/Analog
EP	End Point
ERC	Energy Research Consultants
ºF	degrees Fahrenheit
FN	Flow Number
g	grams
GPM	Gallons Per Minute
H_2	Hydrogen
H_2O	Water
hr	hour
kg	kilogram
kV	Kilo-Volt
L	Liter
lb	pound
mW	milliWatts

NO_X	Nitrogen Oxides
NSWCCD	Naval Surface Warfare Center Carderock Division
O_2	Oxygen
PC	Personal Computer
PM2.5	Particulate Matter < 2.5 Microns in Diameter
PPH	Pounds per Hour
ppm	parts per million
PSIG	Pounds per Square Inch Gage
SAE	Society of Automotive Engineers
SMD	Sauter Mean Diameter
SO_2	Sulfur Dioxide
SSGTG	Ship Service Gas Turbine Generator
THC	Total Hydrocarbons
V	Volts
wt	weight

Administrative Information

This effort was accomplished under Program Element 0603716D by CFD Research Corporation, Huntsville, AL and the Energy Conversion R & D Branch (Code 985); Machinery Research and Silencing Division (Code 98); Naval Surface Warfare Center, Carderock Division (NSWCCD) Philadelphia. The work was sponsored by the Strategic Environmental Research and Development Program (SERDP). Program Manager at SERDP is Mr. Charles Pellerin, Weapons Systems and Platforms (WP).

EXECUTIVE SUMMARY

Recent breakthroughs in the field of hydrocarbon fuel electrostatic charging techniques permitted the opportunity to evaluate this technology within shipboard gas turbines. This technology demonstration effort focused on electrostatic atomization insertion within a U.S. Navy Shipboard Rolls Royce Corporation 501K research engine at the Naval Surface Warfare Center, Carderock Division (NSWCCD). Specific milestones achieved during this effort included:

1. Electrostatic charging effect measurements on the droplet size and patternation of 501-K primary simplex atomizer configurations.
2. Spray demonstration of an electrostatic boosted 501-K gas turbine airblast fuel injector prototype at fuel flows from 40 PPH to 250 PPH.
3. Numerical modeling of electrostatic charging on secondary atomization breakup and prediction of particulate emissions.
4. Fabrication, installation and test prototype engine injectors in the RR501K engine.

This report documents results associated with injector conceptual design, electrode integration, atomization measurements, and numerical modeling and fuel injection system integration and engine test.

1. BACKGROUND

The Rolls Royce RR501-K engine in Figure 1 serves as the prime mover for ship service gas turbine generator sets (SSGTGs) of the U.S. Navy's DDG 51 Class ships [1]. The 501-K engine features a single shaft with a 14-stage axial compressor, a combustor with six equally spaced combustion liners, and a four-stage turbine. At the present time the RRC 501-K34 serves as the prime mover for SSGTGs on DDG 51 Class ships with the RRC 501-K17 being used on DD 963 and CG 47 Class ships.

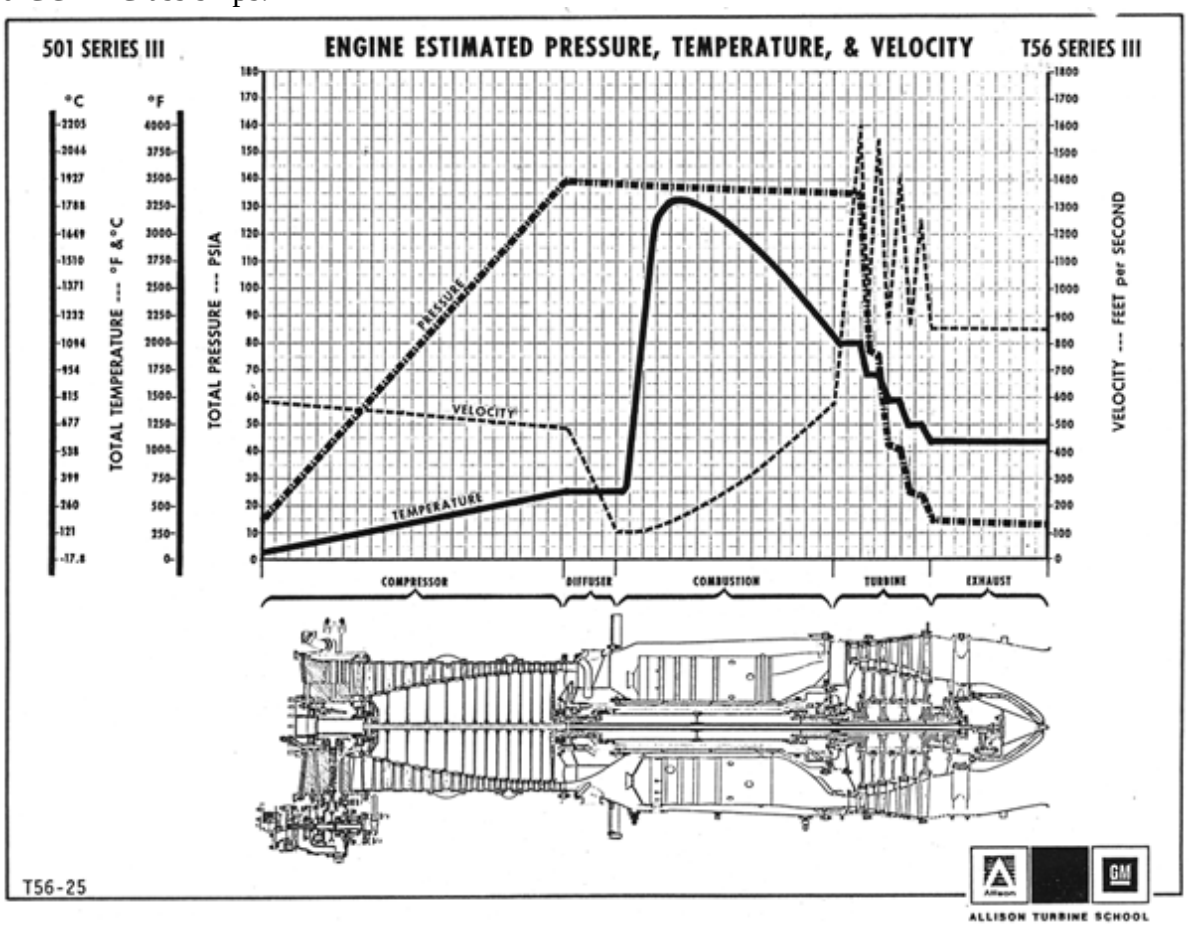

Figure 1. Rolls Royce Corporation 501-K Engine

The combustion section of the Navy's 501K engine shown in Figure 1 has traditionally proven to be where the bulk of the routine in-service maintenance takes place.

- The combustion liners historically last about 2,200 hours before replacement is required. The Navy is currently shifting to a new liner design in an effort to improve service life. The new effusion cooled liner is similar to other low emissions designs. Prototype effusion liners have operated in the Fleet for 15,000+ hours with only minor cracking noted.
- Fuel nozzle reliability is difficult to quantify. They are typically the first components to be replaced when t troubleshooting engine starting problems. They are also replaced when the temperature spread between combustion liners exceeds preset limits. The normal nozzle failure mode is that the pilot tip becomes clogged and prevents turbine starting.

Fouling of the secondary flow passages is significantly less common. The current nozzle design is a piloted dual entry type that lends itself to electrostatic charging.

The presence of electric charge on the fuel droplets within the well-defined geometry of the combustor allows for spray distance, angle, and charge levels to be adjusted for optimum evaporation and combustion. There are several methods available to impart charge to droplets. Among the most common we have induction charging, corona charging, and charge injection. Electrostatic spraying is an efficient and cost effective process to use in preparing fuel for combustion in gas turbine engines commonly found in Navy shipboard operations. Using electronically controlled electrostatic atomization, droplet size and particularly dispersion can be manipulated, independent of flow velocity, aerodynamics or other mechanisms. As a result, the electrostatic boosted gas turbine engine fuel injection preparation approach described here offers significant potential in an engine insertion role. Figure 4 summarizes two fundamental electrostatic fuel-charging approaches CFDRC has examined through the ambient gas turbine fuel injection demonstration phase. The approach selected for test and evaluation in the RR501K industrial gas turbine engine is the induction charging approach.

Numerous researchers [1] have demonstrated that when a charged drop loses mass by evaporation, charge is not lost during the evaporation process. This loss of mass but retention of charge leads to an increase in drop charge-to-mass ratio until the Rayleigh limit is reached. Droplet disruption then occurs with ejection of highly charged smaller drops from the larger ‘mother drop’. The largest ‘daughter drop’, perhaps 75% of the mass of the original ‘mother drop’ remains, and maintains electrostatic stability until evaporation once again diminishes its surface area to its Rayleigh charge density limit. Figure 2 shows the experimental data of Abbas [2]. The middle curve shows how drop radius decreases with time due to evaporation until there is an abrupt decrease in mother drop radius at the Rayleigh limit. The upper curve is remarkable in that it shows that there is **NO LOSS OF CHARGE DURING EVAPORATION**. There is, of course, an abrupt loss of charge the instant the Rayleigh limit is reached when about 25% of the charge of the mother drop is ejected onto its daughter drop(s). The lower curve illustrates clearly that when the Rayleigh limit is attained abrupt changes in charge and radius are observed. This process of secondary atomization breakup due to electrostatic charge has yet to be investigated as a process capable of enhancing the combustion process in gas turbine combustor configurations.

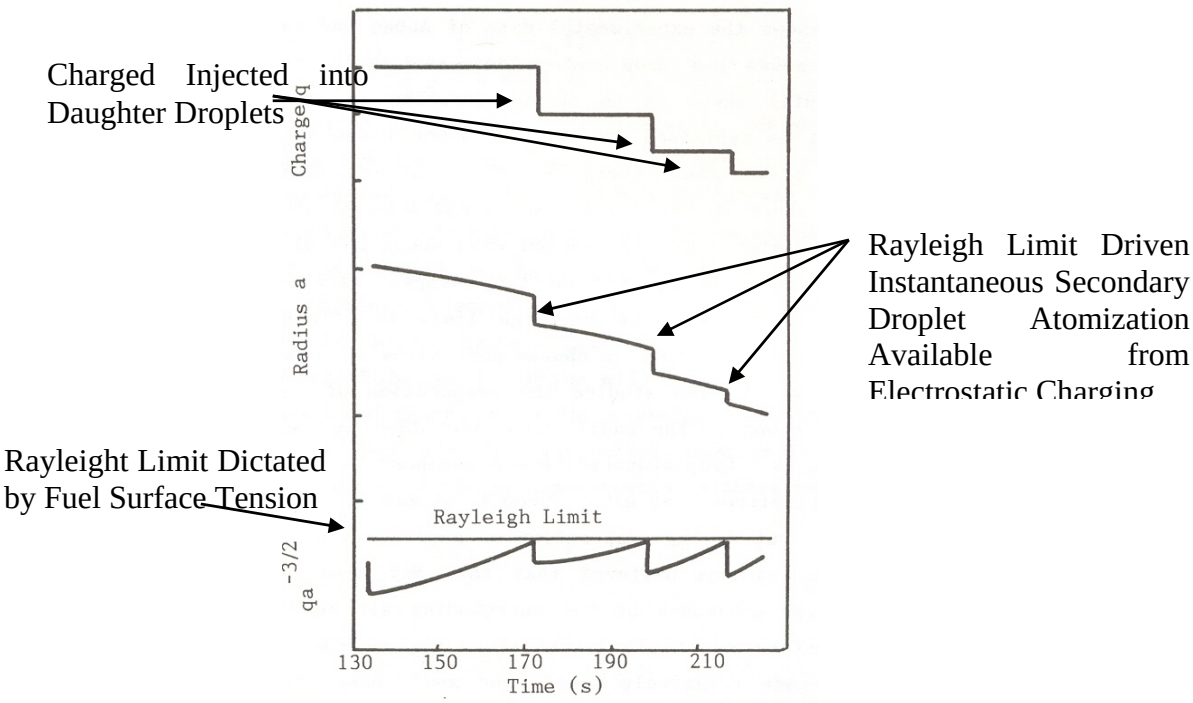

Figure 2. Demonstrated Secondary Atomization Process That Could be Leveraged in the RR501K Fuel Injection System

CFDRC has developed a lumped parameter model for this process as shown in Figure 3. As stated earlier, when droplet mass and corresponding diameter decay due to evaporation the charge concentration on the droplet surface reaches a level that the repulsive forces due to charge exceed that of the retention force due to surface tension. Instantaneous droplet shattering occurs as a result. This lumped parameter model [3] has been incorporated into our in-house CFD software to support modeling electrostatic charging within combustion chambers.

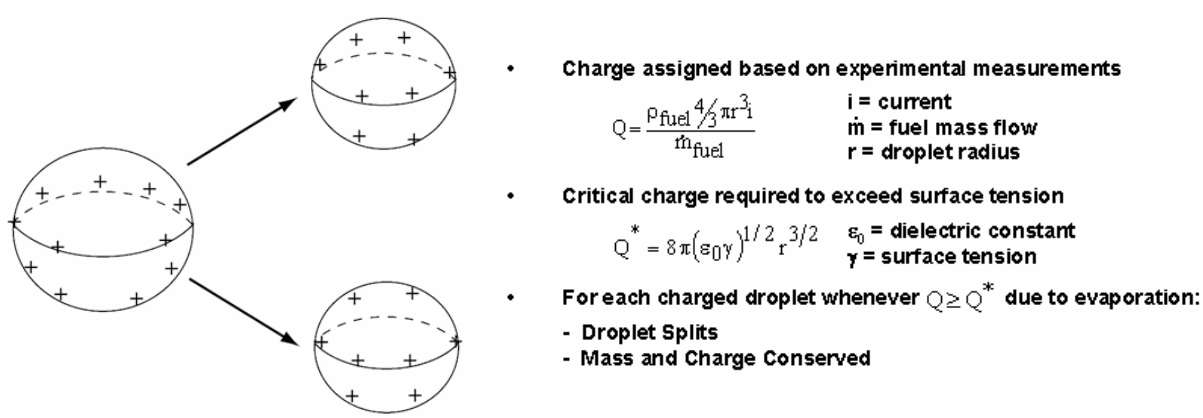

Figure 3. Secondary Atomization Breakup Due to Electrostatic Charging

The formation of particulate matter during the gas turbine combustion process is directly related to the fuel droplet size entering the combustion zone and secondary droplet atomization/coalescence. The influence of mean droplet size on particulate emissions derives from the manner in which each individual droplet evaporates. The presence of an electrostatic

charge can significantly accelerate this evaporation process as well as impede any tendency for the droplets to coalesce. Published data shows that droplet size reduction will have a first order effect on PM2.5 reduction. Prior CFDRC simulations have indicated that particulate formation can be enhanced up to 75% as a result of accelerated secondary atomization and impeded droplet coalescence. CFDRC's unique electrostatic fuel atomization charging approach has the ability to inject maximum charge into airblast generated droplet distributions with maximum self-dispersal qualities and enhanced secondary droplet breakup. This atomization charging process is simple, rugged, compact and low cost, thereby enabling this technology to be retrofitted to existing gas turbine engines. The insensitivity to flow rates and fuel properties offers maximum technology flexibility within the gas turbine community. As a result, the electrostatic gas turbine engine fuel injection charging offers unparalleled potential in an engine insertion role.

Contact Charging [4]

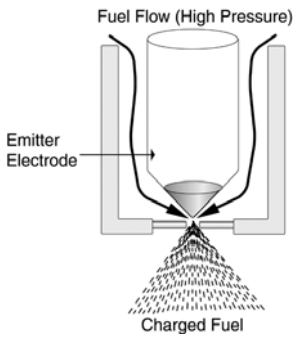

- Requires low fluid conductivity
- Demonstrated at low fuel flows (less than 10 PPH)
- Not commercially available
- Requires hydraulic power for atomization unavailable in 501K installations
- Susceptible to fuel coking

Induction Charging [5]

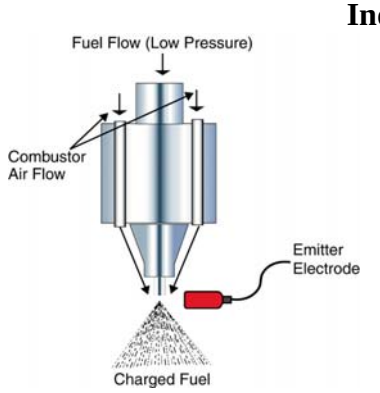

- Functional at any conductivity
- Demonstrated up to 250 PPH in a single injector
- Commercially demonstrated
- Requires pneumatic power for atomization available through combustor
- Failsafe operation (i.e. nozzle atomization operational without electrostatic charging)

Figure 4. Electrostatic Charging Approaches Considered for Implementation into an RR501K Engine

Induction charging allows higher fuel flow rates than other charging approaches. Air from the engine compressor in addition to high fuel pressure is used to assist in the atomization process. This approach allowed for failsafe operation of the atomizer. If the electronic charging circuit should fail, there would still be sufficient atomization of the fuel for the engine to operate without damaging the combustor or turbine section.

2. OBJECTIVE

The research objective of this project is to develop and evaluate the capability of electrostatic charged fuel injection technology to achieve an 80% reduction in PM2.5 emissions in a RR 501-K gas turbine engine. Specific objectives of this project goal include:

1. Design and fabrication of a one prototype Allison 501-K electrostatic fuel injector based on the integration of CFDRC's successful electrostatic automotive prototypes and patented fuel nozzle technology.
2. PDPA atomization measurement comparison between current Allison 501-K production fuel injector technology and the prototype electrostatic fuel injector.
3. Atomization test and evaluation of a single injector within a University combustion research test environment at typical operating conditions.
4. Assembly of an Allison 501-K engine fuel injection system retrofit kit.
5. Coordinate with NSWCCD to insert and test of one electrostatic fuel injection retrofit kit within a U.S. Navy shipboard 501-K gas turbine engine.
6. Inititation of working relationships with Parker Hannifin and/or Delavan to procedure the final retrofit kit.

3. TECHNICAL APPROACH

To achieve the objectives of this project, The Naval Surface Warfare Center Carderock Division (NSWCCD) has teamed with CFD Research Corporation (CFDRC) to develop electrostatic charged fuel injection technology for gas turbine engines culminating with a proof of concept test using an RR 501-K engine. NSWCCD's approach for development of electrostatic charged atomization technology centers on the design and development of the atomizer and controller. The approach is shown in Figure 5. All of the aspects involved in the integration of an electrostatic atomizer into a fuel injector suitable for operation in the RR 501-K engine are currently being addressed in this program.

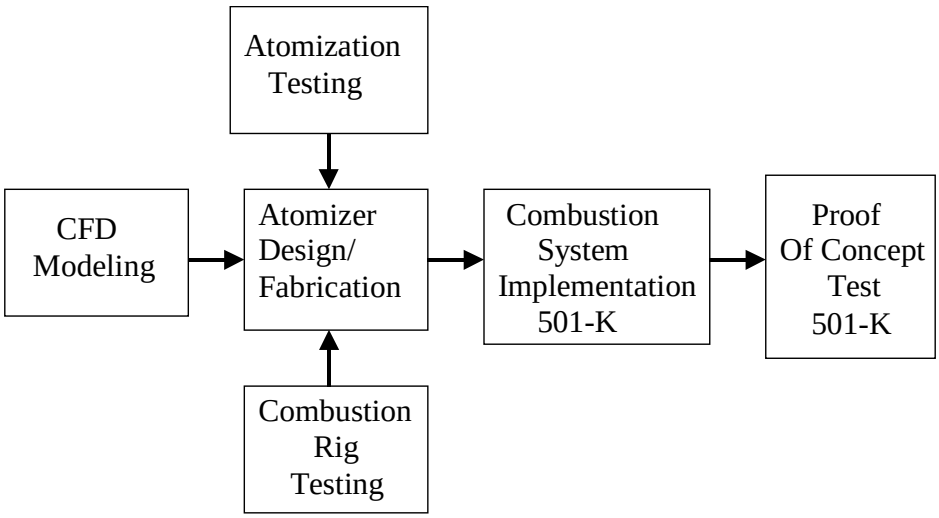

Figure 5. Electrostatic Fuel Atomization Development Approach

4. PROTOTYPE ATOMIZER DEVELOPMENT

Prior to implementation into the RR501K engine a significant amount of preliminary research and development was required to maximize the potential of success during engine test and evaluation. These efforts included preliminary design, numerical modeling, prototype fabrication, and spray test and evaluation of both induction charged simplex and airblast based injector technologies. Upon conclusion of these efforts ambient combustion testing of the airblast nozzle was conducted.

4.1 Simplex Injector Development

CFDRC developed several conceptual designs for an electrostatic fuel nozzle in the 501-K combustor. The first design was an air assisted simplex nozzle illustrated in Figures 6. The airblast injector configuration selected for engine test and evaluation is discussed later.

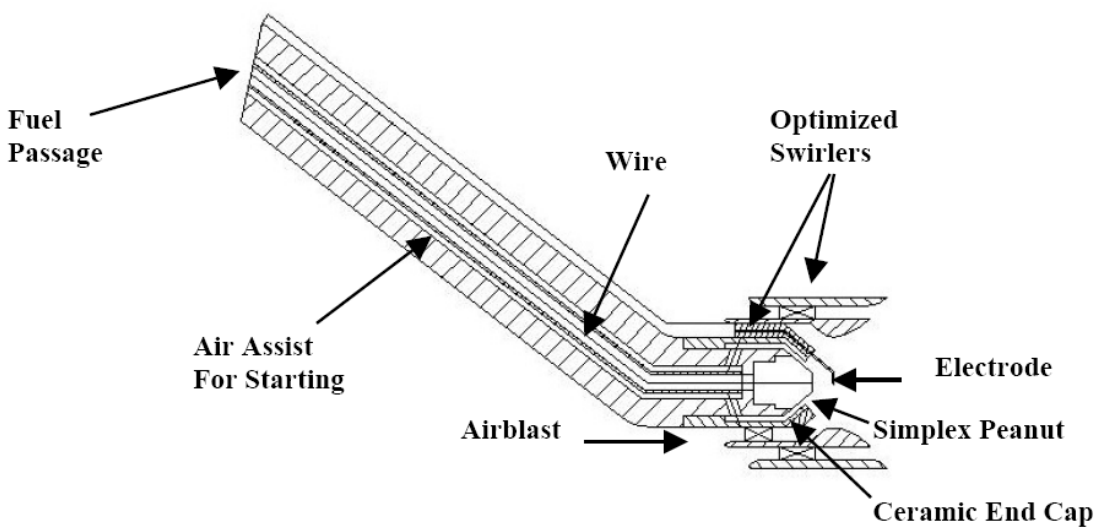

Figure 6. Air Assisted Simplex Electrostatic Nozzle Design

During the first year the simplex atomizer selected for installation into the 501-K engine was tested with diesel fuel. The atomizer flow number selected was 20. Atomizers of this type constructed of stainless steel are available off-the-shelf. Three flow rates, two electrode configurations, and voltages ranging from 40kV to 80 kV were tested. The test matrices for the two electrode configurations with the flow are shown in Tables 1 and 2. Pictures of the actual electrode configurations are shown in Figures 7 and 8 as well as the actual test matrix.

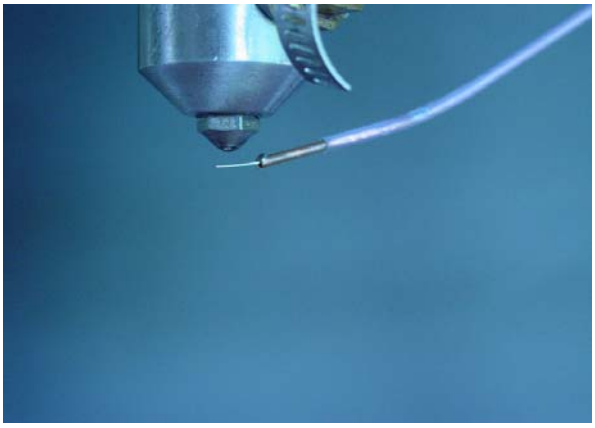

(a) Radial Electrode Configuration

Test Number	Electrode Configuration	Nozzle (Flow Number)	Flowrate (lb/hr)	Nominal Voltage (kV)
1	Radial	20	173	40
2	Radial	20	173	48
3	Radial	20	173	56
7	Radial	20	173	56
4	Radial	20	173	64
5	Radial	20	173	72
8	Radial	20	173	72
9	Radial	20	122	40
10	Radial	20	122	48
11	Radial	20	122	56
12	Radial	20	122	64
13	Radial	20	122	72
15	Radial	20	147	40
16	Radial	20	147	48
17	Radial	20	147	56
18	Radial	20	147	64
19	Radial	20	147	72
20	Radial	20	147	80

(b) Test Matrix

Figure 7. 501-K Simplex Nozzle and Radial Electrode

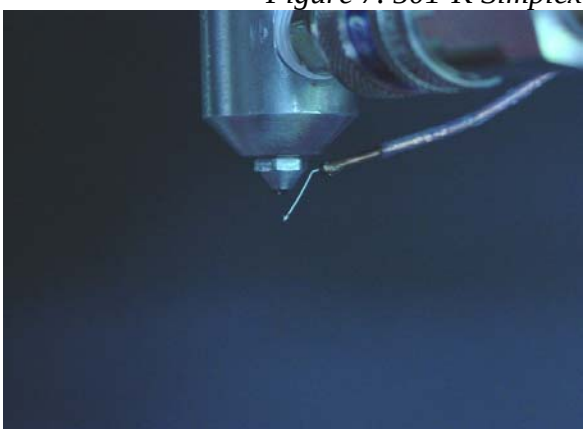

(a) Downward Electrode Configuration

Test Number	Electrode Configuration	Nozzle (Flow Number)	Flowrate (lb/hr)	Nominal Voltage (kV)
21	Downward	20	173	40
22	Downward	20	173	48
23	Downward	20	173	56
24	Downward	20	173	64
25	Downward	20	173	72
26	Downward	20	173	80
27	Downward	20	147	40
28	Downward	20	147	48
29	Downward	20	147	56
30	Downward	20	147	64
31	Downward	20	147	72
32	Downward	20	147	80
33	Downward	20	122	40
34	Downward	20	122	48
35	Downward	20	122	56
36	Downward	20	122	64
37	Downward	20	122	72
38	Downward	20	122	80

(b) Test Matrix

Figure 8. 501-K Simplex Nozzle and Downward Electrode

Figure 9 summarizes the results of the radial electrode configuration tests. In these tests, an erratic behavior of the test data was realized and resulted in a visual inspection of the electrode during operation. Droplets of diesel were forming on the electrode and then breaking away suddenly. This caused the charge collection data to have an erratic behavior and a variable spray cone distribution. As a result, the downward facing electrode configuration was used. This configuration change eliminated the tendency for droplet formations on the electrode. As shown in Figure 9, the charge per liter increases with higher electric fields. The amount of charge present in each of the flow rates varies only slightly due to several factors. First, the electric field for these tests was low as a result of the test facility being configured for the lowest electric field possible. Further tests have been completed with higher electric fields that yielded even higher amounts of charge per liter.

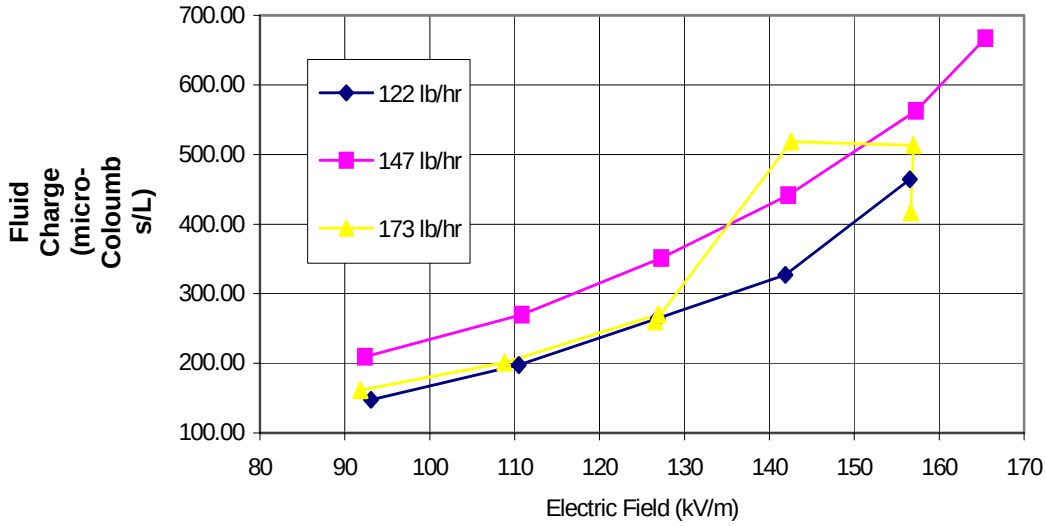

(a) Radial Electrode Configuration Results

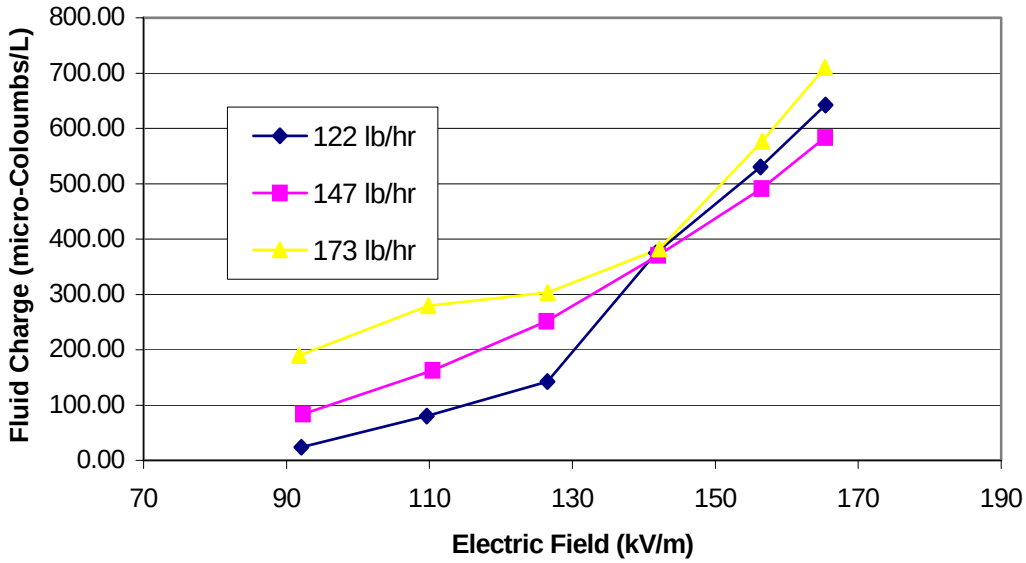

(b) Downward Electrode Configuration Results

Figure 9. Electrode Configuration Effect on Fluid Charge Density

Effective atomization and droplet dispersion occurs when the electrostatic atomizer operating voltage is properly matched to the flow rate. Vigorous, penetrating sprays have been demonstrated at RR 501-K flow rates when the applied voltage is maintained just below the flow rate dependent, maximum charging level. Also, the physical placement of the electrode in the atomizer design has a first order effect on the maximum charging capability. Following baseline electrode testing CFDRC tasked Energy Research Consultants (ERC) to perform a qualitative optical patternation and Sauter Mean Diameter (SMD) measurements of four simplex atomizers. Appendix A contains the summary report ERC submitted to CFDRC at the conclusion of this test

series. The test setup is shown in Figure 10. These atomizers had a wide range of flow numbers (FN = 0.5, 3, 7.4, and 10). Each atomizer was tested at four different pressures with and without the electrostatic atomization. This resulted in 16 optical patternation tests and 32 (4 different positions) SMD measurements for each atomizer.

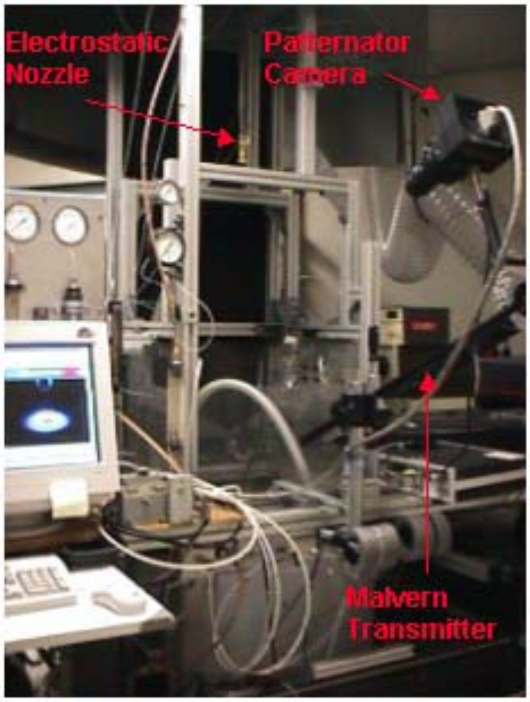

Equipment:
- Malvern 2600
- Data Acquisition
- Ventilation System
- Prototype Optical Patternator
- Nozzle Spray Apparatus

Figure 10. Test Setup used for SMD and Optical Patternation Tests

Figure 11 shows one of the simplex atomizers operating in uncharged (a) and charged (b) mode. These spray photographs illustrate the failsafe operation of the induction charging approach chosen for this project. There is sufficient atomization of the fuel without the electrostatic charging circuit being active. With electrostatic charging it is anticipated that the engine would still operate without damage but at a higher level of emissions.

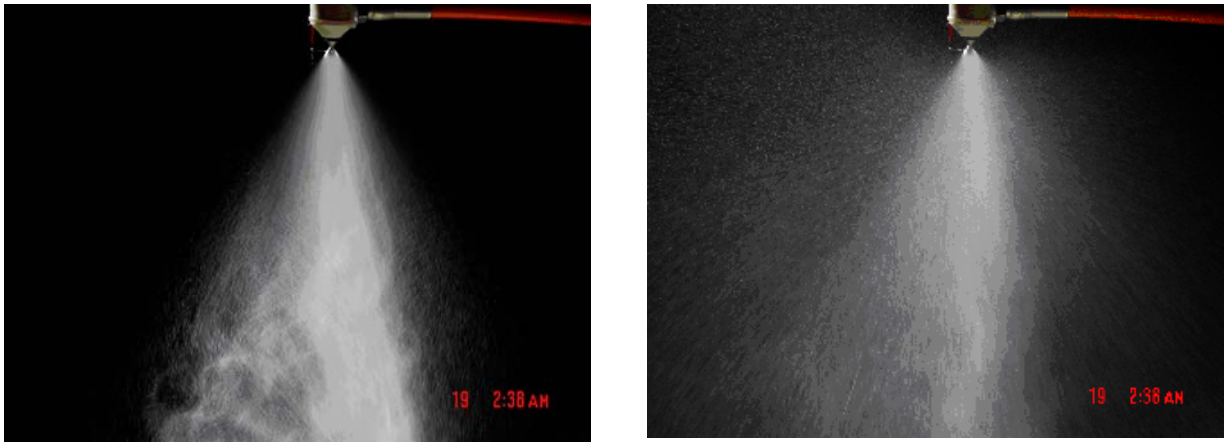

a) Uncharged operation b) Charged operation

Figure 11. Electrostatic Simplex Test Fixture Tested with Diesel Fuel

A typical set of data from the SMD measurements is shown in Figure 12. This data is for a high flow condition (FN=10). The data shows a reduction in droplet size and an improvement in the uniformity of the spray.

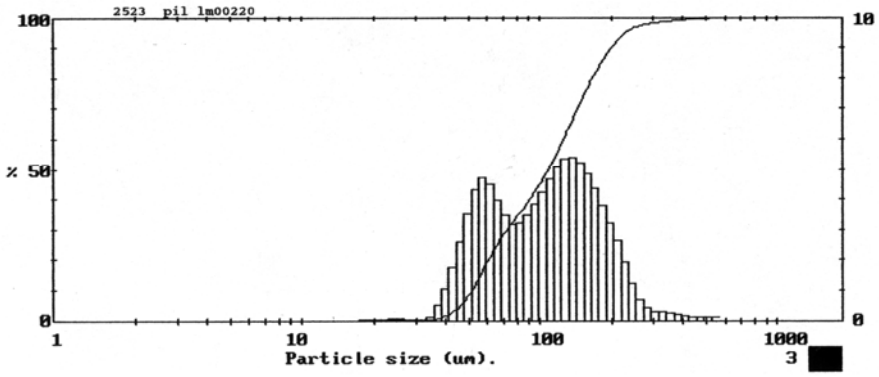

a) with electrostatic charging

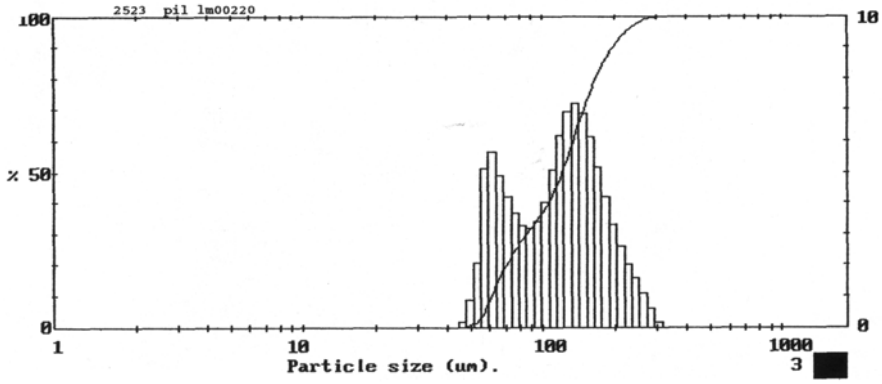

b) without electrostatic charging

Figure 12. Typical SMD Data for Electrostatic Atomizer

For the optical patternation tests, the setup remained the same as in the SMD measurements. The camera for capturing the patternation data was a CCD camera located above the spray cone. In each case, 9 images were obtained. The exposure varied from about 0.5 sec to about 4.0 sec in an effort to obtain relatively consistent pixel intensities from case to case. In all cases, at least 4.5 seconds (0.5 sec * 9 images) of data were obtained (the total exposure time associated with all 9 images). The laser power before the collimating lens was maintained at 200 mW. Data processing involved an average of the 9 images for each case. Since the camera obtained images at an angle, the image was affine transformed. A circular mask was placed at the nozzle geometric centerline of the affined image so that the corners of the images were not included in patternation analysis. A mask radius of 240 pixels (about 5.68 inches) was chosen. A picture of an optical patternation test is shown in Figure 13.

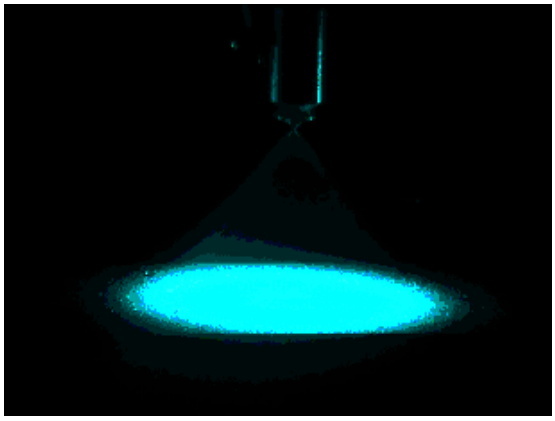

Figure 13. Optical Patternation Test in Progress

The patternation numbers were calculated by dividing the image into eight areas. The image was divided into one circle near the center and seven annular areas, all with equal radii. The eight areas were the same for all the images and were chosen from the largest spray image obtained. For each area, the pixel intensities were summed. The total sum was obtained. Examples of two patternation images along with the accompanying patternation numbers are shown in Figure 14.

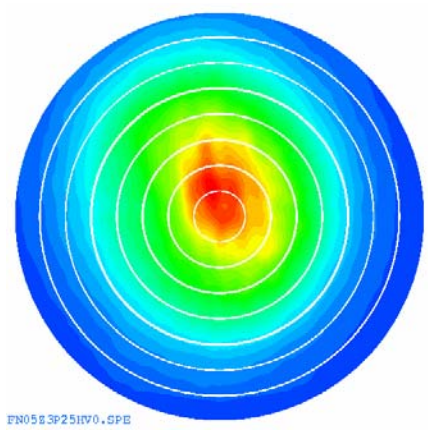

Without Electrostatics

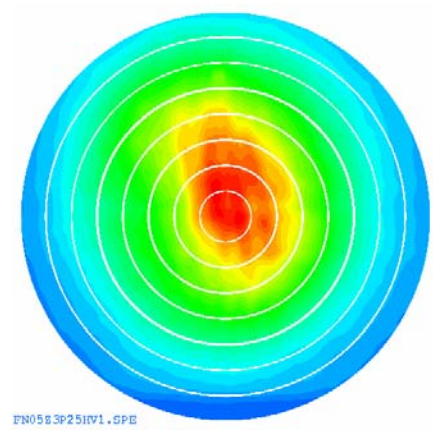

With Electrostatics

FN05Z3P25HV0.SPE

RING#	I,s I,s/I,tot (%)	
1	1.97969E+07	4.61
2	5.17662E+07	12.05
3	7.09702E+07	16.52
4	7.64231E+07	17.79
5	7.06724E+07	16.45
6	5.78486E+07	13.47
7	4.53542E+07	10.56
8	3.66680E+07	8.54

I,tot = 4.29500E+08

FN05Z3P25HV1.SPE

RING#	I,s I,s/I,tot (%)	
1	2.21136E+07	3.59
2	5.90367E+07	9.59
3	8.57843E+07	13.94
4	9.98985E+07	16.23
5	1.01750E+08	16.53
6	9.38039E+07	15.24
7	8.26377E+07	13.43
8	7.04666E+07	11.45

I,tot = 6.15492E+08

Figure 14. Patternation Data FN=0.5 at 25 psi, 3 inch axial position

Figures 15 & 16 show patternation images for a relatively low flow rate and number versus a high flow rate and number respectively. The images reveal that the lower flow rate and number sprays are more spread out with the electrostatic forces present. The effect of electrostatic forces is less pronounced with the higher flow rate and number sprays. However, the effect of electrostatic charging on droplet coalescence is still significant in both cases.

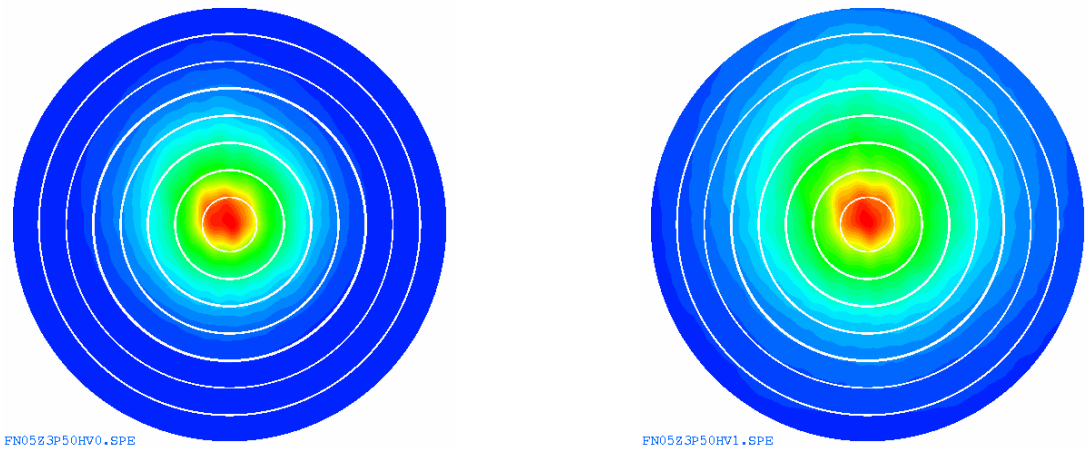

Without Electrostatics With Electrostatics

Figure 15. Patternation Data FN=0.5 at 50 psi, 3 inch axial position

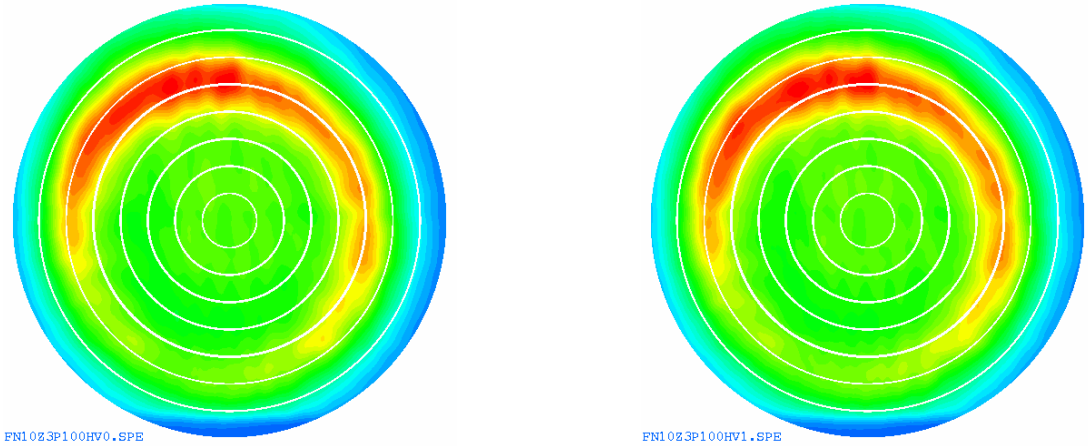

Without Electrostatics With Electrostatics

Figure 16. Patternation Data FN=10 at 100 psi, 3 inch axial position

Rigorous detail design and analysis of an air assisted simplex-based electrostatic atomizer was completed. Figure 17 summarizes this nozzle. The injector features a high flow number simplex atomizer surrounded by both an air assist passage and a primary injector air swirler. This air assist was used to achieve good atomization during startup when fuel pressures are very low. The injector air swirler features curved vanes to minimize the air pressure drop and maximize the amount of airflow. The air from the swirler protects the nozzle face, provides air to assist in atomization, and prevents fuel from reaching the electrode casing. The electrodes are housed in a ceramic layer around the outside of the injector. CFDRC developed multiple research prototypes for this electrostatic simplex-based fuel nozzle prior to fabrication and assembly of the final prototype shown in figure 17.

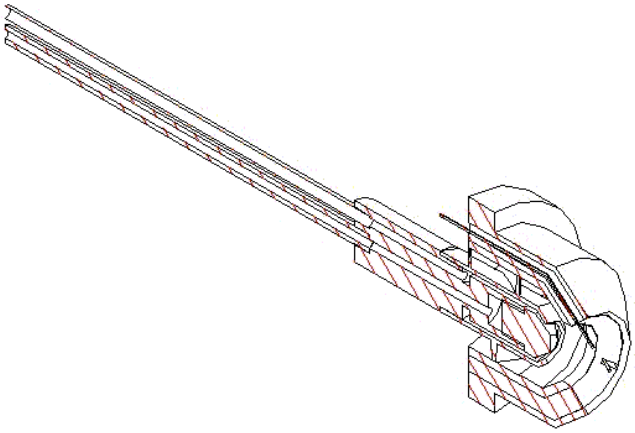

(a) Conceptual Design

(b) Operational Prototype

Figure 17. Air Assisted Simplex Electrostatic Nozzle

Numerous 2D CFD simulations of the injector in operation within the combustion chamber were completed to assess its analytically predicted performance. Axial velocity and temperature contours of a typical simulation are shown in Figure 18.

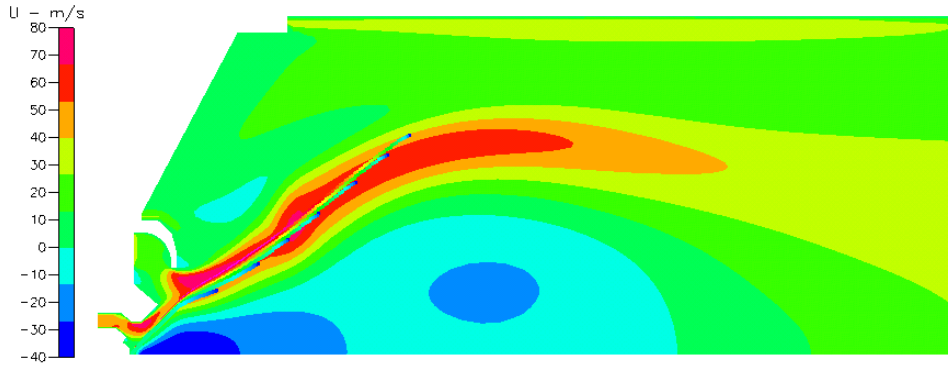

(a) Axial velocity contours in the 501-K combustor

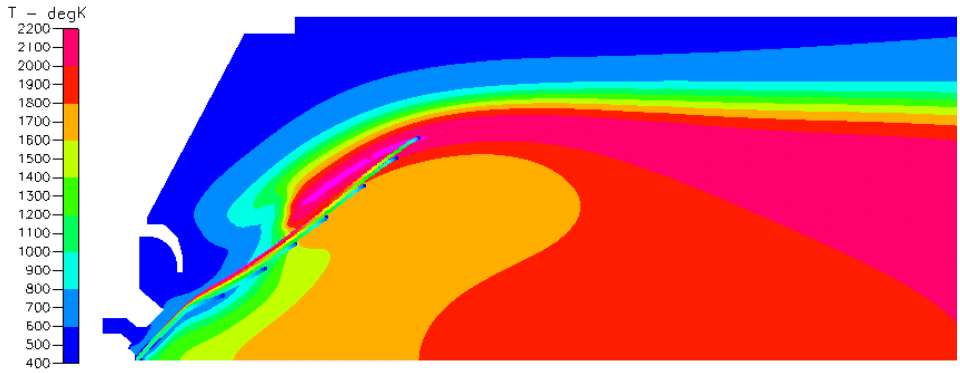

(b) Temperature contours in the 501-K combustor

Figure 18. CFD Analysis Results of the Engine Prototype Injector Configuration

Approximately halfway through this program effort the RR501K program office elected to convert the RR501K engine injectors from a dual orifice injection system into an airblast injector configuration. The primary reason for this was a chronic fuel coking problem within the primary simplex injector flow passage. Even though the flow number of the injector configuration summarized in figure 17 is quite high the need to convert to an electrostatic charged airblast configuration was deemed necessary.

4.2 Airblast Injector Development

One of CFDRC's early airblast injector configurations is shown in Figure 18. This injector configuration was conceived to install directly into the combustion chamber and utilize the combustor dome swirler as an independent source of combustion air similar to the approach being utilized by the RR501K project office. The configuration below features an electrode configuration devised to charge up the spray inductively and by direct contact to the spray as it exits the airblast prefilmer. A more detailed assessment of this injector revealed the electrode configuration as conceived could fail very early in its operational cycle as a result the high cycle vibrational fatigue during nominal engine operation. As a result a more robust electrode configuration was required.

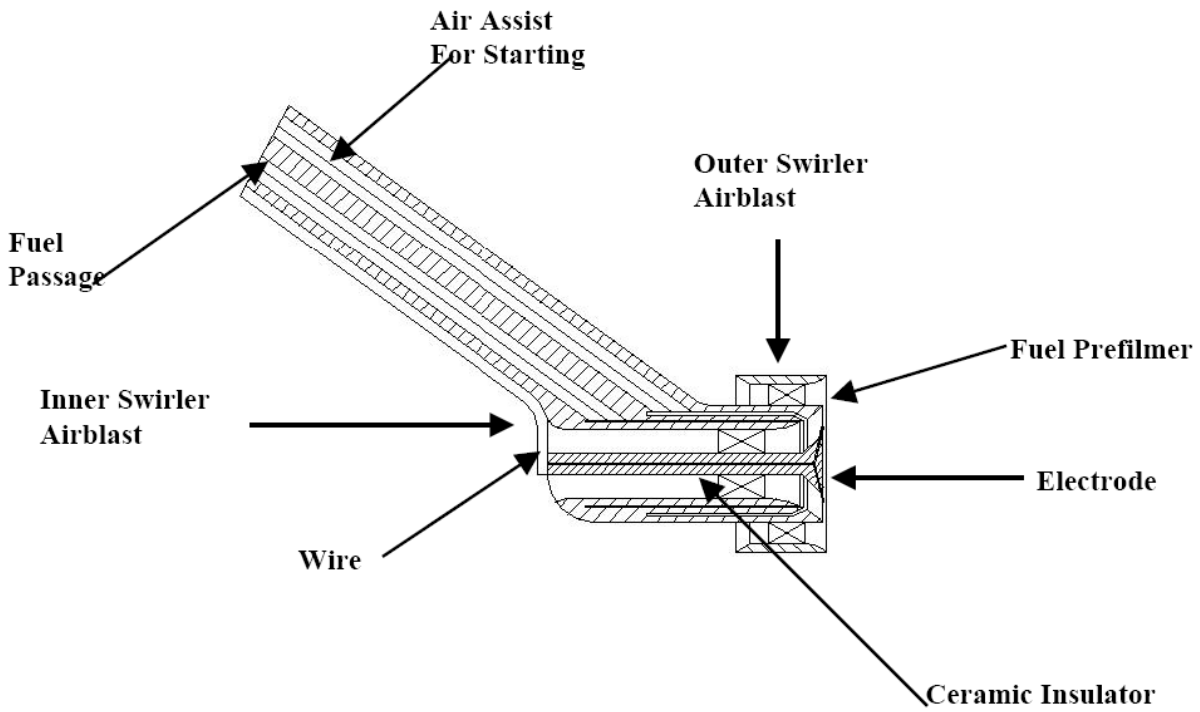

Figure 18. Pure Airblast Electrostatic Nozzle Design

Rolls Royce provided CFDRC detailed drawings of the latest combustor being retrofitted to Navy 501K engines. This is now the only combustor used in all Navy 501K engines. This combustor features a dome swirler with an inner cowl that directs the swirled air down toward the centerline. Any nozzle installed in the combustor should utilize this air for airflow distribution and fuel atomization. The airblast design considered optimal for the electrostatic nozzle could use a single inner airflow swirler on one side of the filmer, with the airflow from the dome swirler on the other side to assist in atomization. This basic design concept is shown in Figure 19.

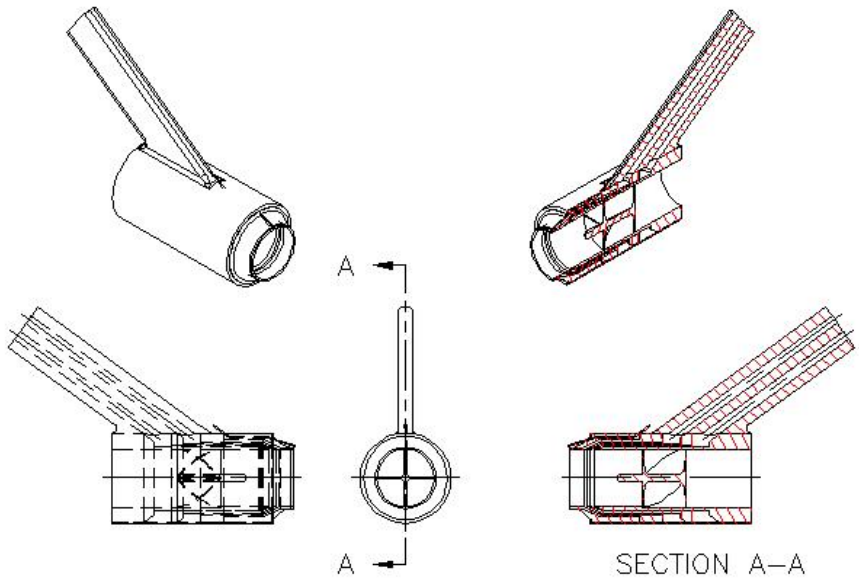

Figure 19. Solid model of the single swirler electrostatic fuel nozzle concept.

Figure 20 shows a contour plot of axial velocity that shows how the dome swirler airflow interacts with the fuel nozzle flow. A single heavy-duty electrode was installed along the centerline of the fuel injector.

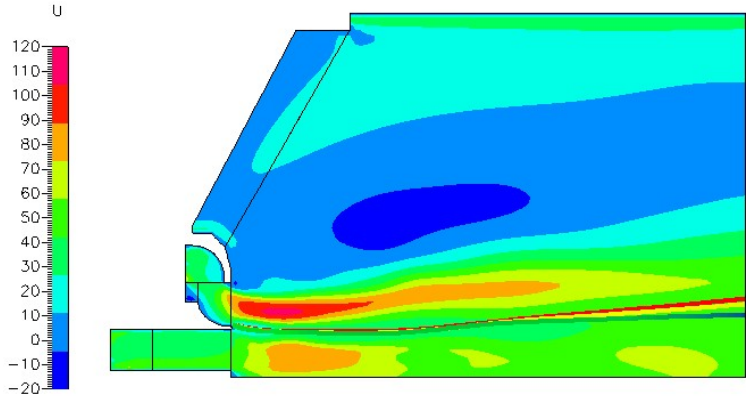

Figure 20. Axial velocity near the combustor dome; single swirler electrostatic fuel nozzle with dome swirler.

This single swirler electrostatic fuel nozzle produces a flow and flame structure very similar to what is produced in the combustor by the original conventional nozzle design. To significantly improve the aerodynamics in the combustor, the cowl over the dome swirler could be removed to allow the swirling air to move away from the centerline and form a central recirculation zone. This flow structure would increase fuel air mixing and produce a much more compact flame. Axial velocity contours for this nozzle configuration are shown in Figure 21. In this concept, the nozzle would feature two swirling airflow passages on either side of the fuel filmer. The electrode would be installed on the nozzle centerline. Although advantageous in terms of combustor performance, this option would require permanent modifications to the combustor

liners and would make the modified combustors incompatible with any of the conventional fuel nozzles currently in use.

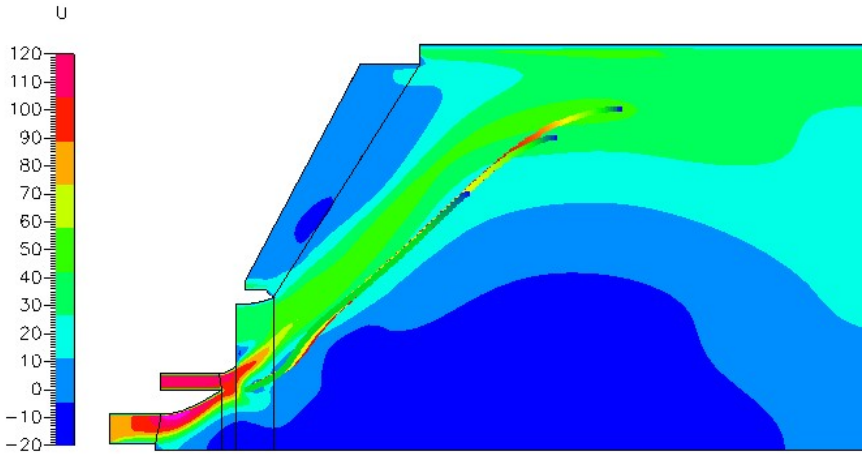

Figure 21. Axial velocity near the combustor dome; two-swirler electrostatic fuel nozzle, cowl removed from dome swirler..

In summary the original program focused on charging the simplex atomization approach found in the baseline RR501K gas turbine. However, when the Navy transitioned to a Delavan air-blast injector configuration CFDRC elected to electrostatic charge an air-blast nozzle capable of potential retrofit within the Delavan injector. Detail designs of the original simplex injector and the final prototype air-blast configuration are shown in Figure 22.

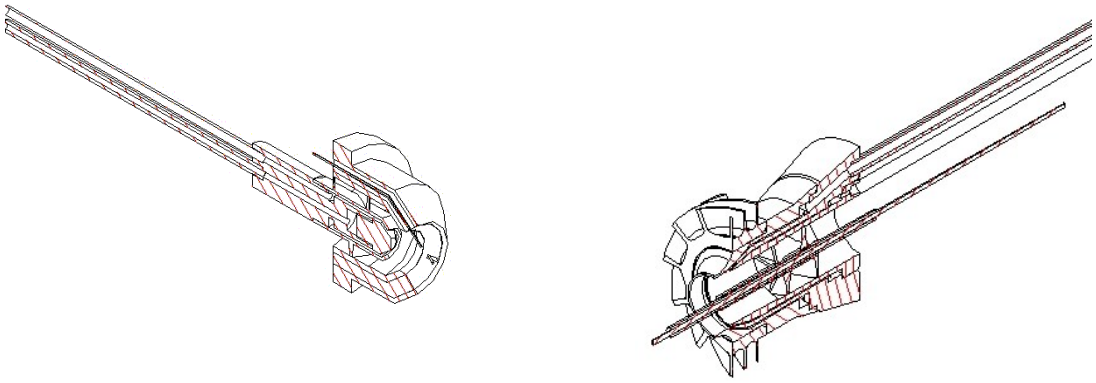

a) Charged Simplex b) Charged Airblast (Dome Swirler Shown)

Figure 22. Detail Design of Two Injector Prototypes Evaluated by CFDRC

In the air-blast design air from the engine compressor is utilized rather than high fuel pressure to assist in the atomization process. During engine starting the compressor discharge air is too low in pressure to effectively atomize the fuel, consequently air assist (external to the engine) is utilized to assist in the atomization process. This passage is shown in the figure 22b. Also shown in Figure 22b is the approximate location of the electrostatic charging electrode. Both fuel injector designs were conceived to insure that if the electronic charging circuit should fail, there is sufficient atomization of the fuel for the engine to operate without damaging the combustor or turbine section. However, it is anticipated there will be significant increase in emissions, particularly PM2.5.

During the second year of the program prototype fabrication and assembly of the electrostatic charged air-blast nozzle shown in Figure 22b was completed. Figure 23 compares prototype test versions of both the air-assisted simplex and air-assisted airblast injectors. Included in both photographs is the combustor dome swirler. The combustor dome swirler, although not a part of the fuel injector, has a first order effect on the spray pattern exiting both nozzles, but in particular the airblast nozzle. Consequently its presence was included in all development testing associated with each fuel injector spray pattern.

(a) Simplex Based Injector

(b) Air-Blast Based Injector

Figure 23. Injector Prototypes Fabricated for Development Test and Evaluation

4.3 Atomization Testing

In the second year of the program CFDRC focused on effective electrostatic charging of an air-blast type nozzle. Preliminary efforts to efficiently charge fuel as it uniformly exited an annular prefilmer were problematic at best. As a result it was decided to position the electrode along the nozzle centerline and downstream of the prefilmer exit. This configuration, summarized in Figures 23b proved highly effective. Following successful electrode integration into the air-blast version of the nozzle a significant amount of spray testing at ambient ignition conditions, as well as corrected full power conditions, was completed. Figure 24 compares the ignition condition of each nozzle. The air-blast nozzle, with air assist, possesses a significantly improved ignition spray pattern. Financial resources prohibited additional droplet size measurements at ERC, consequently this injector test and evaluation phase transitioned to ambient combustion testing.

(a) Simplex Based Injector

(b) Air-Blast Based Injector

Figure 24. Visual Spray Testing at RR 501K Ignition Condition

Figure 25 summarizes the results of electrostatic charging capacity for both injector types. As shown in Figure 25, the charge per liter increases with increased electrode voltage and associated higher electric fields. The amount of charge injected into each flow rate increases proportionally with the flow rate. This trend is similar to other mature electrostatic spray technology fields (painting, agriculture, etc.). Fuel flow testing above 200 lb/hr exceeded CFDRC's in house capability, however the trends shown in Figure 25 are not anticipated to vary.

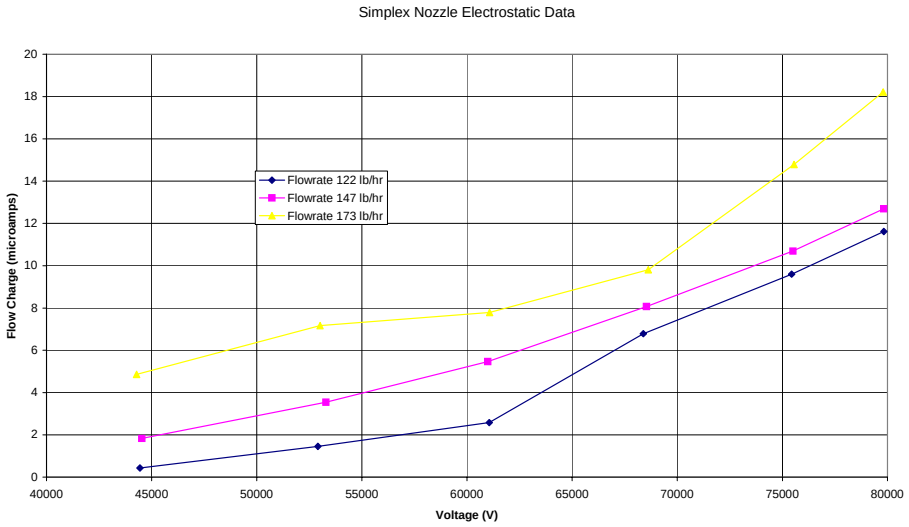

a) Simplex Injection Technology Charging

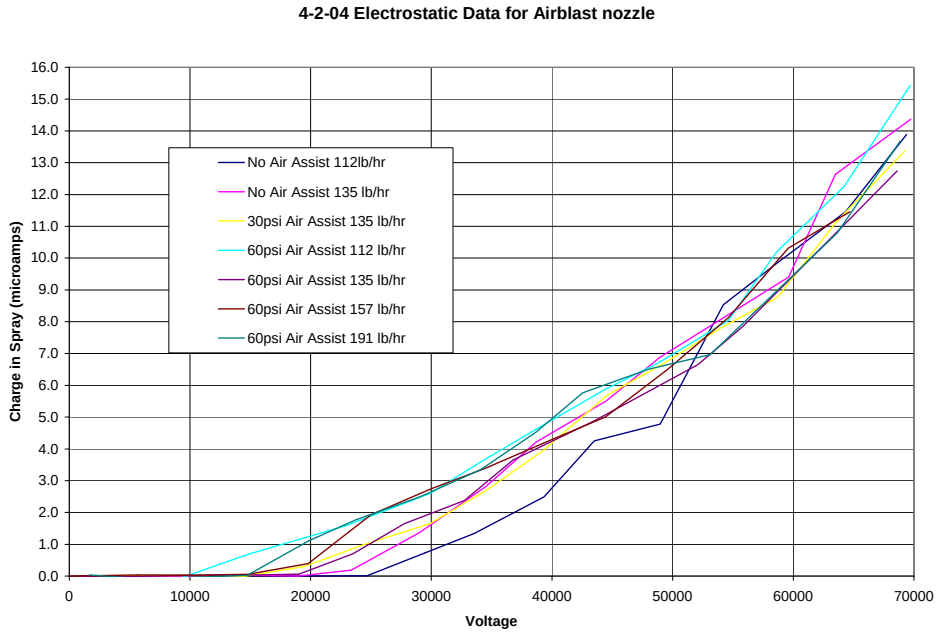

b) Air-blast Injector Charging

Figure 25. Charged Injection Data for Both Prototype Injector Configurations

4.4 Combustion Testing

Following ambient spray testing, both injectors were installed in the combustion rig shown in Figure 26. Upon installation significant problems associated with electrostatic field line containment using the simplex injector geometry within an enclosed metallic combustor environment were observed. These problems were manifest in the form of random voltage discharge (corona discharge) toward the injector housing and chamber walls. The reason for this process is hypothesized to be associated with large metallic objects near the electrode that inductively build up charge as a result of close proximity to the electrode. This charge buildup, upon reaching critical charge density, results in random discharges. This problem became acute once the electrode voltage input exceeded 7000-8000 volts in the charged simplex injector. This voltage is approximately half of what is desired to electrostatic charge fuel at conventional gas turbine injector flows. Resources and measurement technology limited CFDRC's ability to quantify this problem beyond these observations. This phenomenon also presented a potential operational hazard associated with electronic instrumentation.

However, the centrally located electrode in the air-blast nozzle provided for the electrostatic field lines to uniformly propagate from the electrode. This created a highly uniform ionization field much more conducive to uniform electrostatic charging of the spray and the ensuing combustion process. Additional research measurements outside the scope and resource allocations of this project precluded a more in depth assessment of these phenomena. As a result of these observations, electrostatic charging of the simplex injector design was abandoned while combustion testing of the air-blast injector configuration ensued.

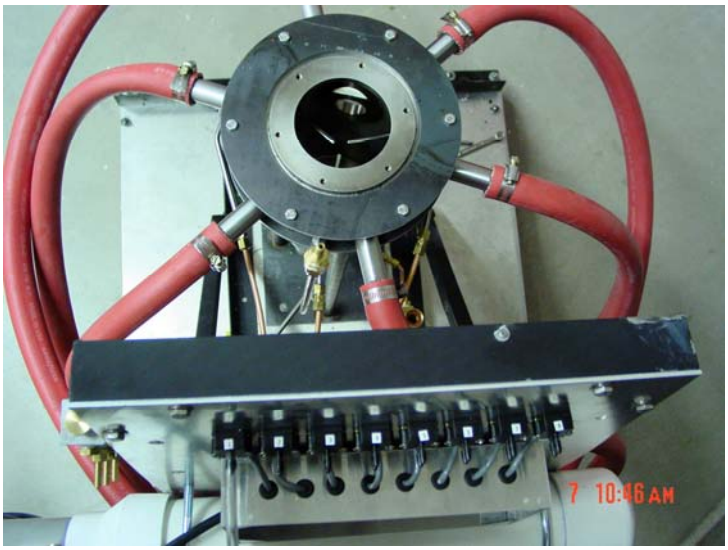

Figure 26. RR501K Fuel Injector Ambient Combustion Test Rig

This air-blast injector was subsequently placed in the rig shown in Figure 26 and significant ambient combustion testing was completed. Random inductive charging of the combustor and/or nozzle housing was not observed using the centrally located electrode throughout the combustion test operations shown in Figure 27 unless the charge potential exceeded 70,000 volts. This level of voltage is well in excess of the 40,000 to 50,000 volts, as shown in figure 25, necessary to

effectively charge the injector configuration. This can be explained as a result of the electrode's position effectively and uniformly increases the ionization level of the inner airblast passage that is critical to the atomization process. More precise instrumentation and associated testing outside the scope of this effort will ultimately be required to fully quantify these effects.

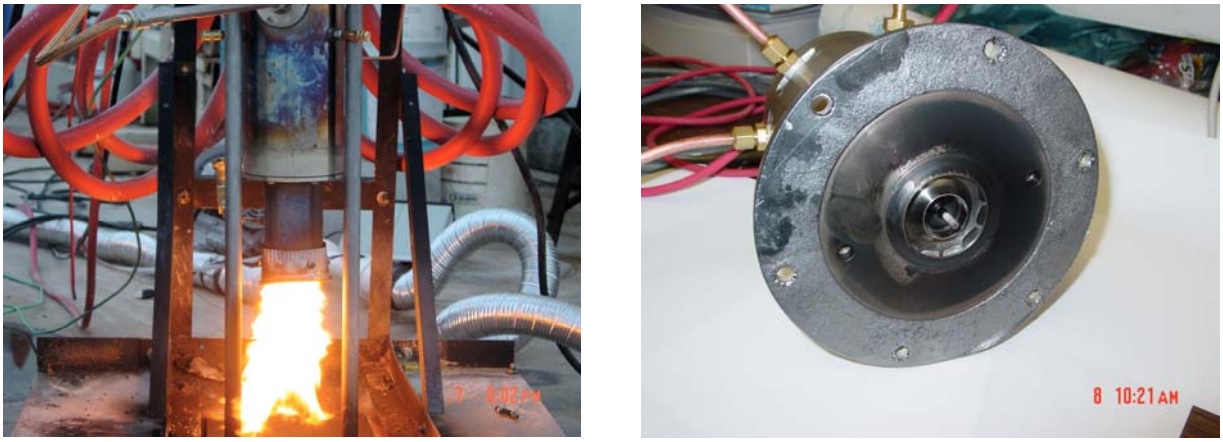

(a) Combustion Operation (b) Electrode Inspection

Figure 27. RR501K Electrostatic Charged Nozzle Operating in Combustion Rig

Emissions measurements of this combustion process were completed using a Horiba MEXA-554JU emission analyzer summarized in Figure 28. These preliminary emissions results were utilized to assist in refining the airblast injector design prior to configuring the injector for installation into the engine.

Figure 28. CFDRC's Mexa-554JU Emissions Analyzer

Table 1 summarizes the emissions measurements completed during the combustion testing described earlier. More sophisticated instrumentation will be required to ultimately assess the emissions of the RR 501K engine.

	Without Electrostatics	With Electrostatics	Without Electrostatics	With Electrostatics
CO (%vol)	0.06	0.08	0.25 - 0.30	0.20 - 0.22
HC (ppm)	16	11	60-120	32-50
CO2 (%vol)	10.4	10.2	7.35	7.1 - 7.7
Fuel to Air Ratio	0.033	0.033	0.047	0.047
O2 (%vol)	10.36	10.4	10.4	10.7
Fuel Mass Flow Rate (lb/hr)	50	50	33.66	33.66
Air Mass Flow Rate (lb/hr)	1510	1510	709.1	709.1
Voltage (V)	0	3150	0	13000
Current (mA)	0	6.23	0	<< 1

Table 1. Combustion Emissions Using Electrostatic Charging Approach Shown in Figure 11b

1.1 4.5 CFD Modeling of the Engine Combustion Process

Prior to installation of this injector design into the engine CFD Research Corporation completed several numerical simulations of electrostatic fuel injection within the RR 501-K combustor. These simulations provided confidence that the nozzle design selected for testing is theoretically capable of meeting one of the original programs goals of 80% reduction in PM 2.5 emissions.

CFD-ACE$^+$, the code used during all calculations presented in this report, includes the following basic capabilities in addition to a long list of specialized physical models:

1. co-located, fully implicit and strongly conservative finite volume formulation;
2. solution of two- and three-dimensional Navier-Stokes equations for incompressible and compressible flows;
3. pressure-based solution algorithms including SIMPLE and a variant of SIMPLEC;
4. non-orthogonal curvilinear coordinates;
5. multi-block and many-to-one grid topology, allowing for local grid refinement;
6. unstructured grids with any cell type and with arbitrary interfaces at domain interfaces;
7. parallel processing;
8. fourth order compact, second order central (with damping), second order upwind, and Osher-Chakravarthy spatial differencing schemes;
9. standard, low-Reynolds number, and RNG turbulence models for steady-state models;
10. instantaneous and finite-rate, one-step, and four-step heat release and emission kinetics models;
11. 2-scalar prescribed PDF, eddy breakup, and eddy dissipation turbulence-chemistry interaction models;
12. NO_x and CO emissions models;
13. conjugate heat transfer with radiation; and
14. spray models for trajectory tracking, vaporization, etc.

Combustion was modeled using a one-step finite rate reaction with equilibrium products of CO_2, H_2O, CO, H_2, OH, and O. The fuel is injected as the specie $C_{12}H_{23}$ with properties designed to imitate DF-2. The reaction rate is adapted from Westbrook and Dryer [6] with modifications that adjust for the equilibrium product flame temperature.

The 501-K combustor flow field inside and outside the liner was modeled in order to provide the most accurate simulation possible. A baseline simulation performed on the 501-K combustor is shown in Figure 29.

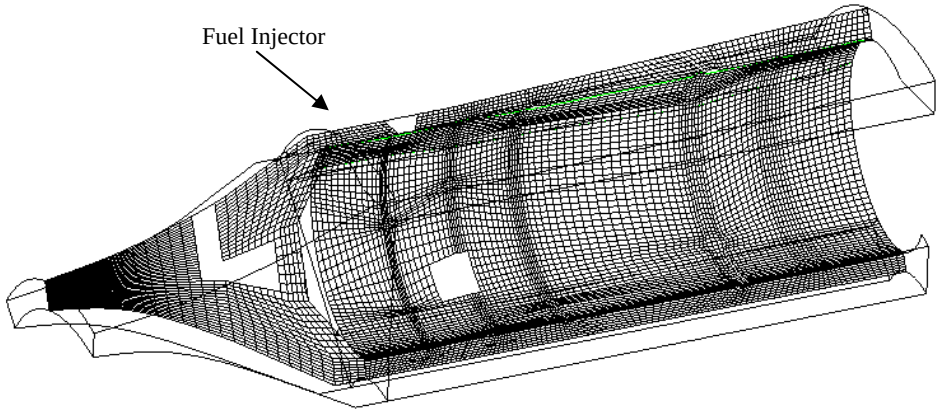

Combustor Grid Model

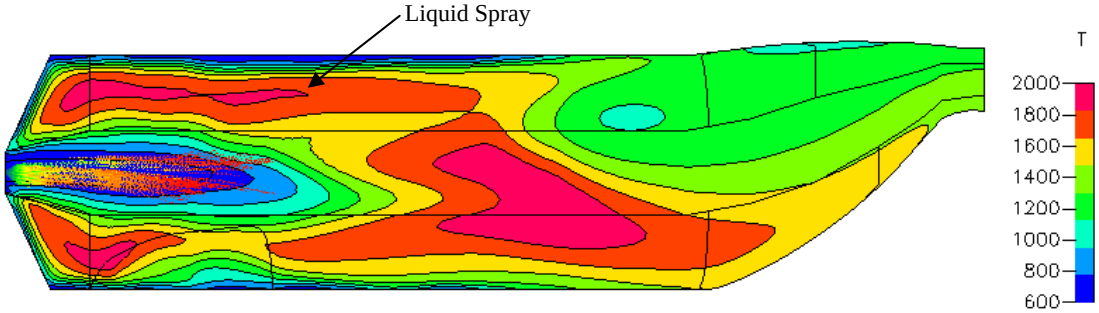

Inner Combustor Temperature
(Plane Through Nozzle Centerline)

Figure 29. Simulation of Existing Allison 501-K Combustor

At the present time researchers assume that a 1:1 correspondence exists between soot reduction and PM 2.5 emissions exists. Because PM2.5 and soot formation are highly three-dimensional processes, a 3D model of the 501K combustor is required. The numerical modeling completed here focused on the soot modeling [7] only. Figure 30 summarizes prediction of soot formation in the 501K combustor with and without electrostatic charging. The significant reduction in predicted soot concentration can be directly attributed to improved spray dispersion, elimination of droplet coalescence and accelerated secondary droplet breakup.

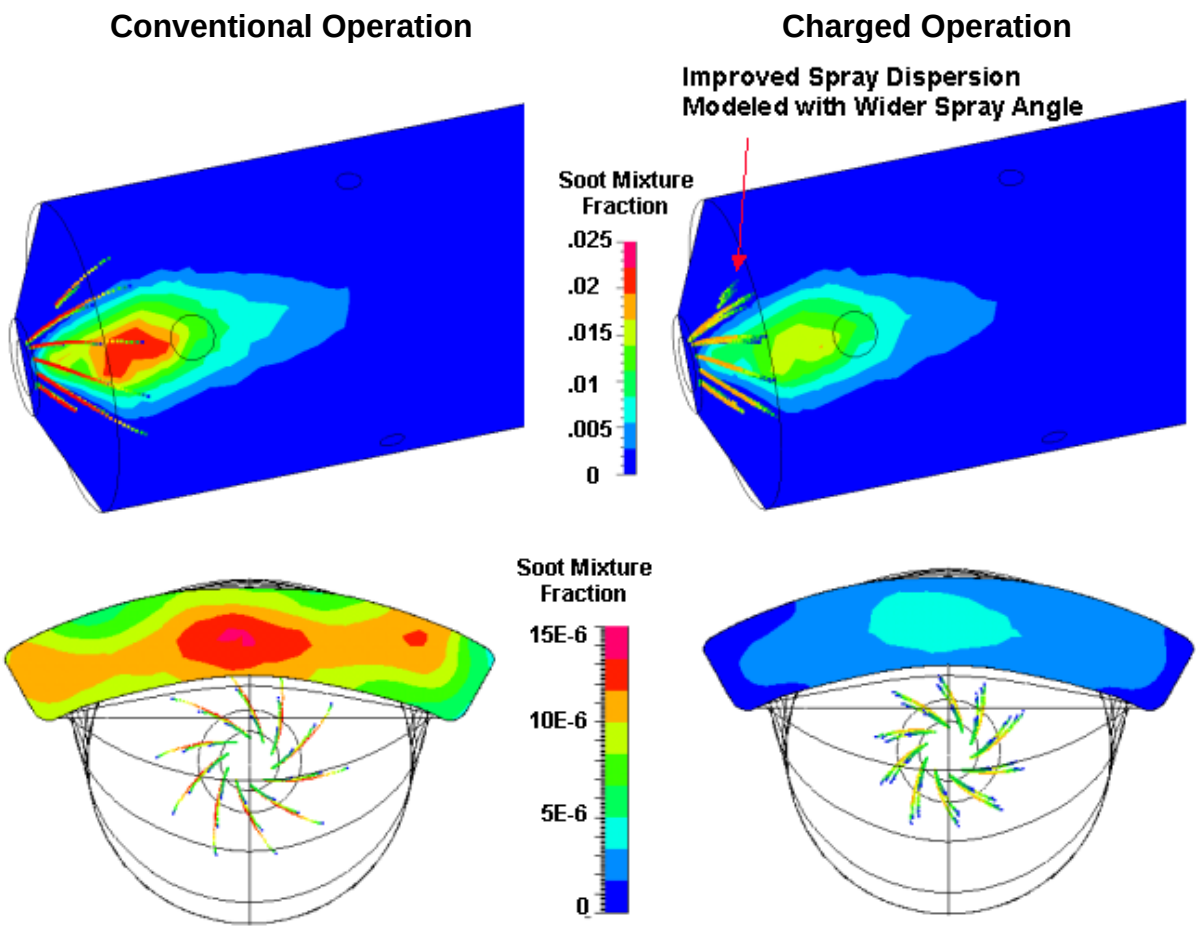

Figure 30. RRA 501-K Combustion Soot Predictions

The most significant result of this modeling effort is the quantum reduction in engine particulate emissions observed. Currently, the 501-K SAE Smoke Number averages approximately 50 as shown in Figure 31. This is well above the visible range and indicates a significant level of particulate matter in the exhaust as a result of the combination of dual orifice fuel injection and an excessively rich primary combustion zone. Although the basic combustor stoichiometry will not change with this injector modification, particulate matter reduction due to electrostatic charging was analytically shown to be first order due to secondary atomization breakup.

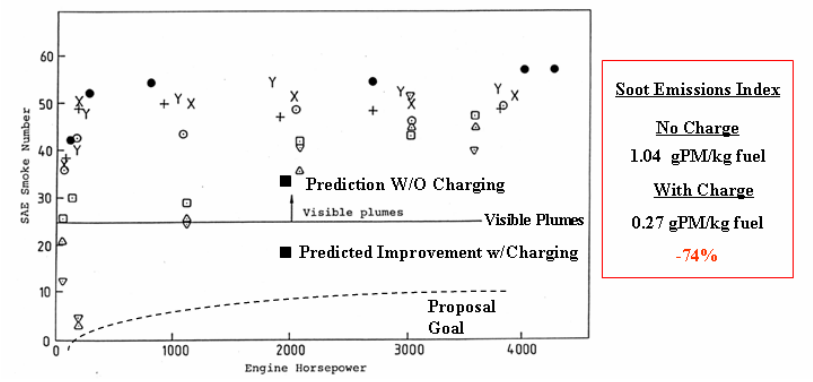

Figure 31. Smoke Number Measurements and Soot Prediction in the 501-K

In summary assessment of the electrostatic spray parameters has been completed to support selection of the optimum charging technique. Particular emphasis has been placed on characterizing the effect of increased charge density on droplet dispersion and uniformity. The interaction between the electrostatic charged fuel injection into the combustion flow field has been investigated.

5. RR501K ENGINE COMBUSTION SYSTEM IMPLEMENTATION

The RR 501-K gas turbine engine was recently upgraded to a Delavan air-blast nozzle. In this program these nozzles will be replaced with a complete electrostatic charged fuel atomization system consisting of the CFD Research Corp. electrostatic fuel nozzles, wiring harness and limited control system modifications capable of temporarily interfacing with the existing 501-K fuel control. The fuel injectors themselves will utilize the identical fuel manifold system.

5.1 Engine Electrostatic Fuel Injection System

Successful demonstration of the prototype configuration shown in Figure 13b and summarized in Figure 27 allowed CFDRC to pursue the final process of this demonstration program – fabrication and delivery of an engine set of fuel injectors. Ongoing coordination between CFDRC and NSWCCD resulted in the engine-configured injector shown in Figure 32. Structural optimization of this configuration is required before this nozzle can be fully implemented in an aggressive engine development test program.

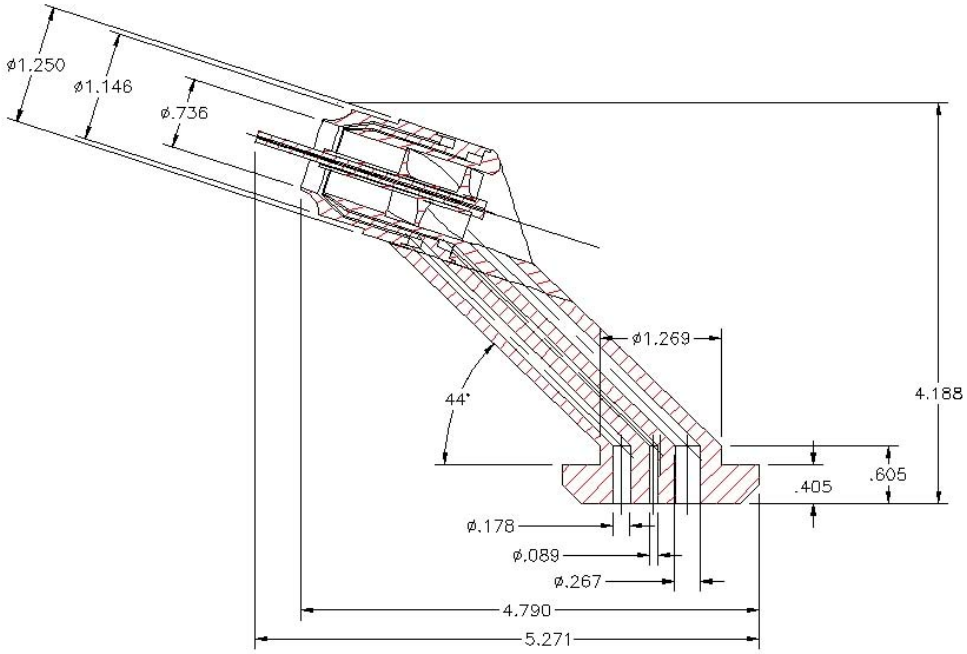

(a) RR 501K Detail Injector Design

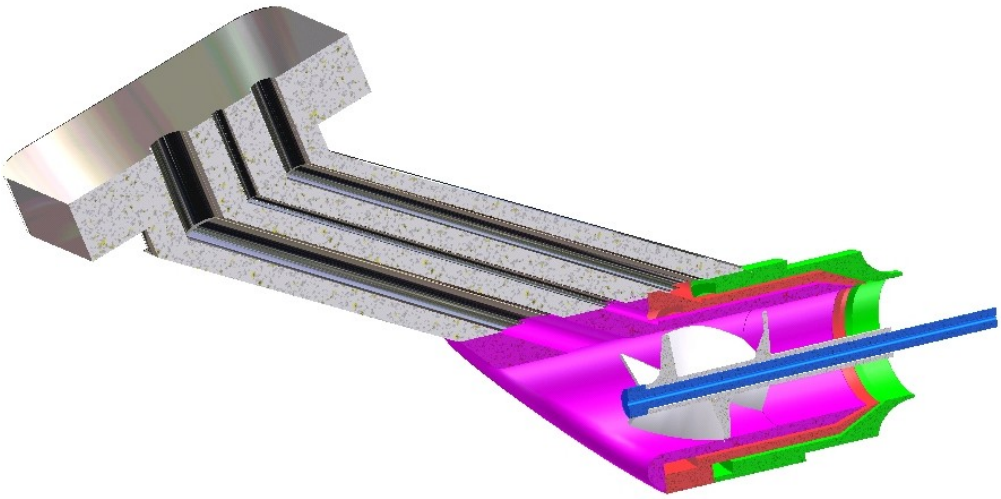

(b) RR 501K Injector Solid Model

Figure 32. RR 501K Engine Electrostatic Injector Design

A prototype engine injector was fabricated and sent to NSWCCD for final form and fit within the selected RR501K test engine. This injector is shown in Figure 32. Following the form, fit and function assessment six additional injectors were fabricated.

Figure 32. RR501K Prototype Engine Injector

This complete set of electrostatic charged injectors customized for operation within the RR501K combustion chamber are shown in figure 33.

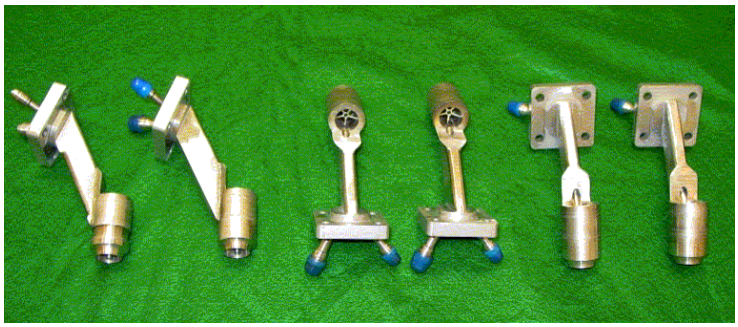

Figure 33. RR501K Engine Configured Electrostatic Charged Fuel Injector Set

Installation within an engine also required minor modifications to the fuel injection control system. These modifications included the addition of a PC, a variable high voltage power supply, an A/D card to measure fuel valve position and a D/A card to output a reference voltage. For each engine power setting and associated fuel flow, there an optimum voltage for maximizing the amount of charge imparted to the fuel droplets exists. The electrostatic controller used the position signal from the engine's liquid fuel valve to determine voltage and current flow to the electrostatic nozzles. The controller commanded the variable voltage supply shown in Figure 34 to provide the appropriate voltage to the nozzles. It is conceivable that in

order to maximize the advantages electrostatic charging offers the power supply will require two operating modes in the future. They are: 1) variation in voltage to control current flow into the spray as the air in the chamber becomes more conductive due to combustion ionization and/or 2) an ability to transition into pulsed mode operation in which a frequency controlled corona discharge is sustained.

AC Input	DC Output
120 VAC	0 – 80,000 Volts
500 Watts	0 – 7.5 mA

Figure 34. Customized Power Supply for Electrostatic Charge Control

It is important to note that when the air near the electrode is not heavily ionized there is little chance of spark discharge into the flow especially when this power supply is regulated to a voltage < 50 KV with very low current (< 50 microamps). Experimentation with non-reacting simplex charging has shown spark discharge begins to occur at voltage levels exceeding 100,000 V for the current levels under consideration within an air-breathing atmospheric combustion chamber. However, when the temperature near the electrode is significantly increased due to the presence of a reacting flow a corona discharge can ensue. When this happens a pulsed approach to the charging process may be required. This process is schematically shown in Figure 35.

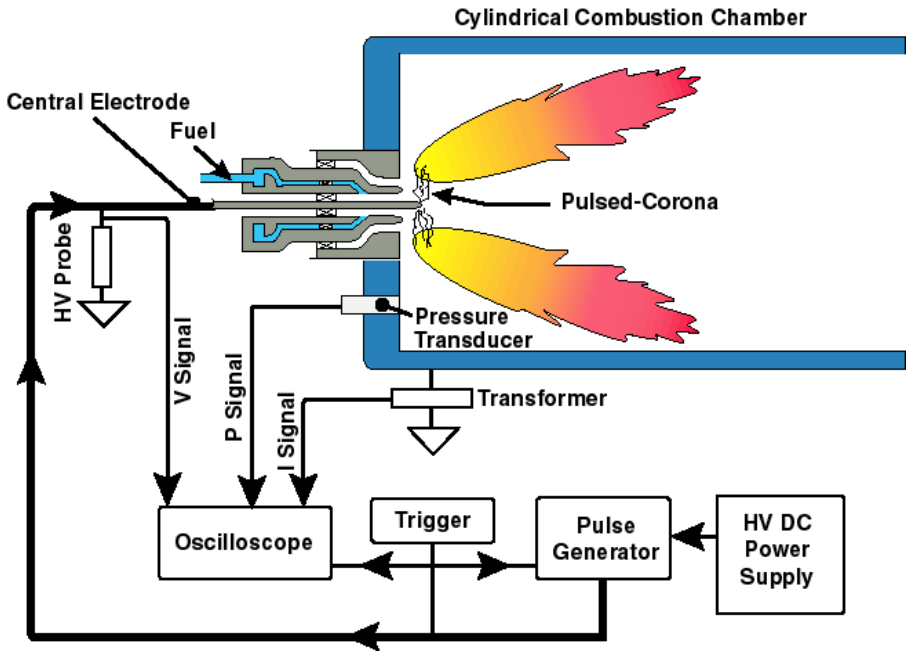

Figure 35. Schematic of Corona-discharge in a Laboratory Combustor and the Necessary Control Circuitry

In the future utilization of a pulsed corona within an electrostatic charged fuel injection process may be necessary to limit current flow into the combustion chamber at the voltages utilized for electrostatic charging. An effort to convert the power supply shown in Figure 34 into the schematically summarized power supply shown in Figure 35 was well outside the scope of this effort.

An initial schedule of voltage versus fuel flow was determined through lab experiments during the development of the RR501K electrostatic nozzle prototypes. The controller concept implemented into the engine is illustrated in Figure36.

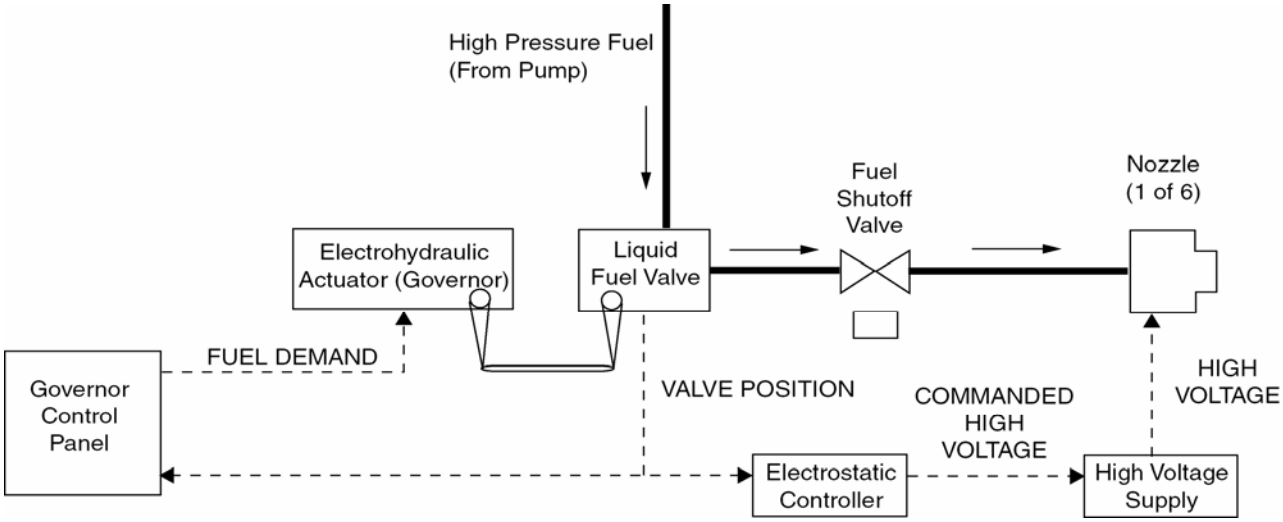

Figure 36. Electrostatic Fuel Nozzle Controller

5.2 Engine Implementation

The electrostatic fuel injection system described in section 5.1 was implemented in the RR501K engine shown in Figure 37 on two occasions May and August of 2005. Engineers and technicians from CFDRC and NSWCCD installed the electrostatic atomization nozzles and set up emissions instrumentation and data collection hardware. NSWCCD personnel performed all engine testing and emissions documentation.

Figure 37. RR 501K Gas Turbine at NSWCCD Philadelphia

The objective of this test program was to characterize and document the performance of a fuel injection system based on electrostatic fuel atomization technology when implemented in a 501-K17 Rolls-Royce gas turbine engine. These benefits were anticipated to include a reduction in CO and NOx emissions as well as a large reduction in PM 2.5 emissions

The electrostatic fuel atomization system delivered to NSWCCD for installation consisted of the following components: electrostatic fuel nozzles (6); wiring harness and controller/power supply. The installation of the electrostatic fuel nozzles was straightforward. They were a direct replacement for the current nozzles and used the same fuel and air assist manifolds. The only change was that each nozzle had a wire exiting through the mounting flange. Those six wires (one for each fuel nozzle) were connected to a terminal block and a single power wire was routed outside the module where it was attached to the power supply/controller. This electrostatic fuel nozzle installation is show in Figure 38.

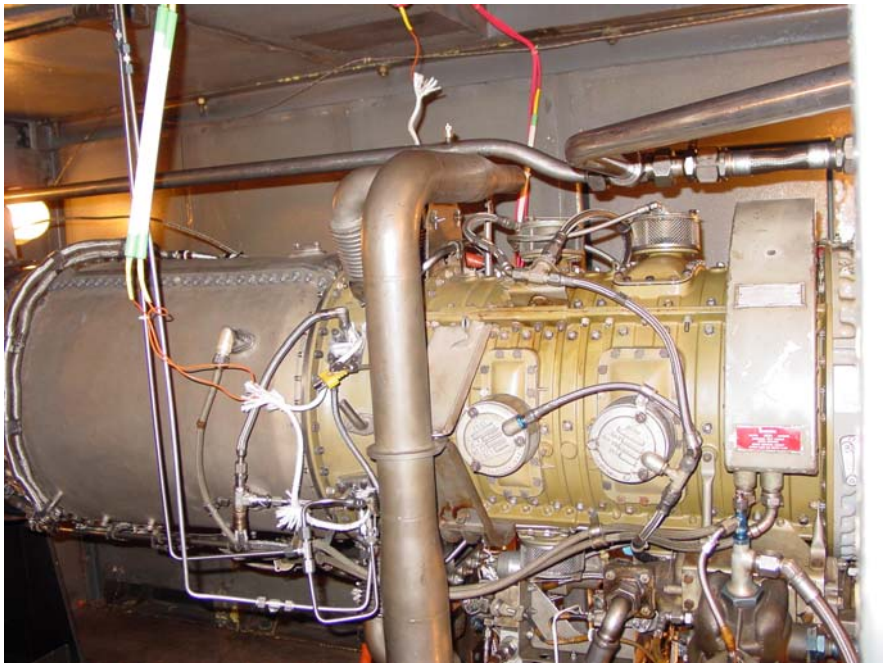

Figure 38. Photograph of Electrostatic Injector Installation within a RR501K Engine

Instrumentation and data acquisition systems that were utilized in the proof of concept testing included the following:

- Available LBES steady state and transient response instrumentation and data acquisitions systems to record engine/generator set steady state performance during stabilized operation and transient response performance during start-up cycle and load response testing.

- A heated line provide a gas sample from a probe inserted in the exhaust system to a continuous emissions monitoring system for measuring CO, CO2, O2, THC, NOx and SO2.

- A second probe was inserted in the exhaust system to obtain particle samples that were sent to a Scanning Mobility Particle Sizer (by TSI, Inc.) for determining particle size distributions and concentrations.

- A Sierra Instruments micro dilution test stand was also utilized to obtain particulate emissions (on a mass basis).

5.3 RR501K Engine Test and Evaluation

Engine test and evaluation included the development and a test procedure followed by execution of these test procedures during two independent test sequences.

Test Procedures

The following is an outline of the test procedures utilized to conduct all engine testing. A fuel sample was taken prior to the tests for analysis to document the properties of the fuel used in the test.

1. Conduct a generator set start-up cycle and stabilize at no-load operating conditions to document baseline start-up cycle. Record the available transient data during the start-up cycle.

2. Run the 501-K17/generator set to establish baseline steady state performance as well as baseline emissions and particulate levels. Monitor operation as power level is incrementally increased. Stabilize at power levels in 500 kW increments, from no-load to 2500kW. Record available steady state performance parameters as well as baseline emissions and particulate levels to document baseline operation.

3. Install the electrostatic atomization injection system.

4. After optimizing the electrostatic injection system, conduct a generator set start-up cycle and stabilize at no-load operations conditions. Record the available transient data during the start-up cycle.

5. With the electrostatic injection system optimized, monitor operation as power level is incrementally increased. Stabilize at power levels in 500 kW increments, from no-load to 2500kW. Record available steady state performance parameters as well as emissions and particulate levels to document operation.

6. Remove the electrostatic injection system and re-install the baseline fuel injection system.

Baseline Engine Testing

Baseline gaseous emissions were obtained prior to the installation of the electrostatic nozzles with the results being shown in table 5-1. The baseline particulate mass emissions are shown in Table 5-2. Average engine operating parameters recorded during the baseline emissions test are listed in Table 5-3. The engine testing was performed using JP-5 fuel. Selected fuel properties are shown in Table 5-4.

Table 5-1. Baseline Gaseous Emissions

Power (kW)	HC (ppm)	CO (ppm)	NOx (ppm)	SO2 (ppm)	CO2 (%)	O2 (%)
500	4.1	20.1	43	10	1.64	18.45
1000	3.6	11.8	59	12	1.98	17.96
1500	3.4	10.1	76	15	2.48	17.42
2000	3.3	13.3	103	17	2.94	16.85
2500	3.7	16.3	138	20	3.38	16.02

Table 5-2. Baseline Particle Mass Emissions

Power (kW)	**PM Mass (g/hr)**	**PM Mass (g/kW-hr)**
500	101.72	0.194
1000	113.8	0.114
1500	154.7	0.104
2000	208.5	0.104
2500	244.9	0.098

Table 5-3. Average Engine Operating Parameters

Power Output (kW)	Inlet Air Temp (ºF)	Engine RPM	Comp Exit P (PSIG)	Turbine Inlet T (ºF)	Fuel Pressure (PSIG)	Fuel Flow (GPM)	Exhaust Temp (ºF)
508	83.2	13839	90.6	1192	155	2.48	590
1004	83.8	13840	94.4	1327	182	3.03	685
1499	83.7	13840	98.6	1472	217	3.61	775
2010	85.1	13840	102.8	1630	261	4.27	875
2494	85.5	13840	107.1	1785	314	4.95	970

Table 5-4. Test Fuel Properties

Property	**Value**
Calculated Cetane Index	44.6
Density, kg/L @ 15ºC	0.809
Distillation Temp °C	10%: 188.5 50%: 208.5 90%: 237.0 E. P: 272.0
Flash Point, °C	62.5
Freezing Point, °C	-49.2
Heating Value, BTU/lb	18,532
Hydrogen Content, wt %	13.5
Total Acid Number, mg KOH/g	0.007
Total Aromatics, vol %	20.0
Total Sulfur, wt %	0.120
Viscosity, mm^2/second	5.0 @ -20°C

Electrostatic Injector Emissions Testing

The first electrostatic injector test series (May 10-12) was dedicated to debugging the engine starting sequence with the new electrostatic nozzles in place. A number of modifications were made to the engine starting fuel schedule over the two-day test period. Once these changes were completed the engine efficiently started on every occasion. Figure 39 depicts initial and final start schedule. This start schedule was so efficient it was incorporated into the main engine start routine and the current fuel injectors configuration. The key to consistent RR501K engine starting was to synchronize the fuel injection flow rate with the compressor speed to yield

optimal combustor light-off conditions. In most cases this entails “spiking” the fuel flow between 20-30% engine speed. Significantly more refinement of this engine starting process could be pursued up to and including biasing the engine start schedule for altitude and ambient conditions.

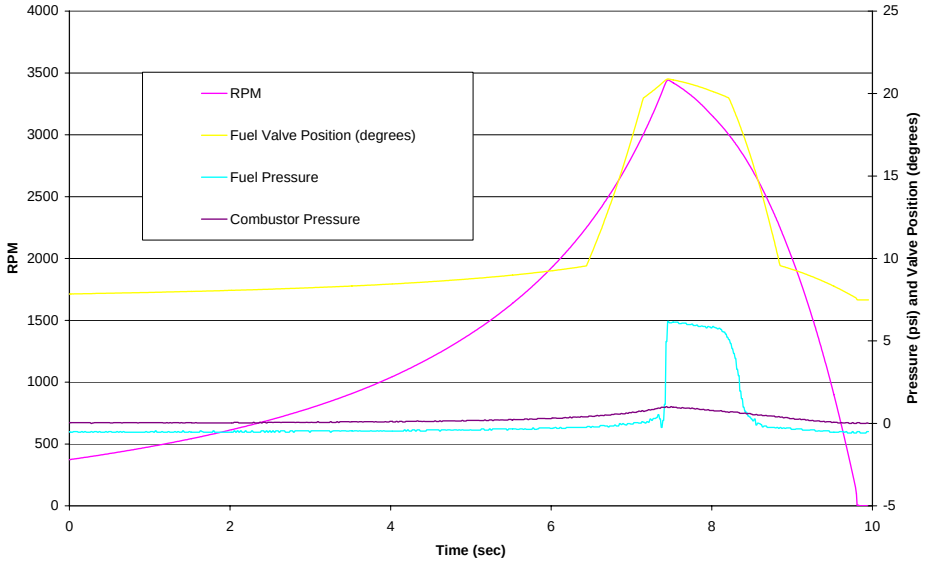

(a) Failed Start

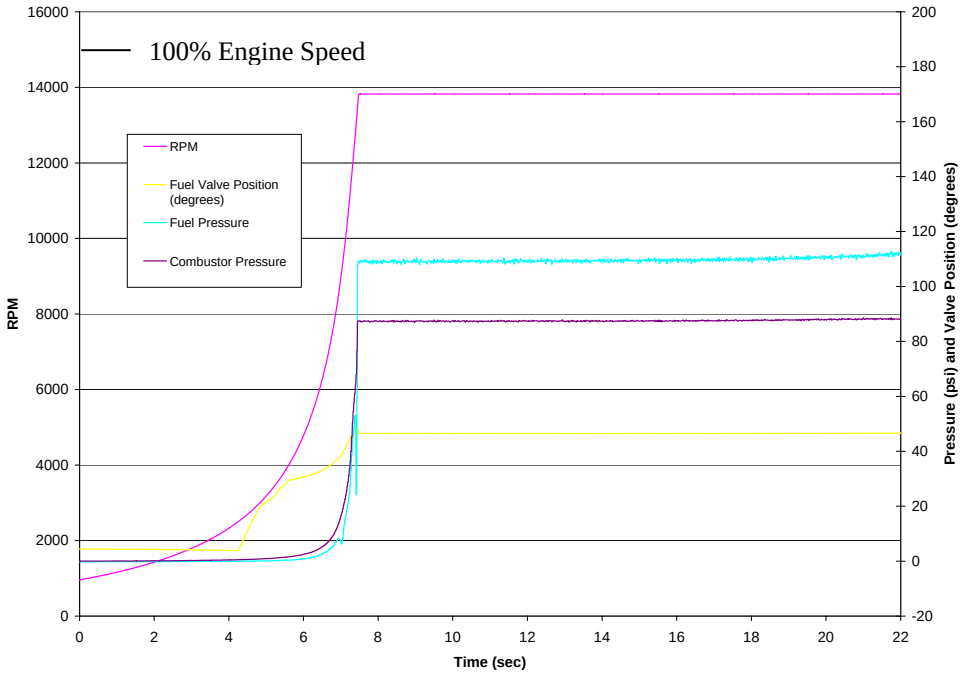

(b) Successful Start Using Fuel Spike at 22% N

Figure 39. RR501K Engine Starting with Electrostatic Fuel Injection

Once the engine starting procedures were quantified with the electrostatic nozzle the engine was accelerated to 100% idle speed. At this point a problem associated with the existing engine fuel manifold was encountered that resulted in a significant fuel leak around the engine. This situation precluded the collection of emissions data with the electrostatic nozzles. A second engine test was subsequently executed from August 23-25, 2005. On this occasion a critical thermal mechanical issue associated with the braze joint between the fuel tube and air-assist tube precluded operating the nozzle above idle speed. As a result the engine could not be operated long enough to gather emissions data with the new nozzles. Additional engine availability, as well as resources, precluded another attempt at testing the electrostatic nozzles within the RR501K engine.

6. SUMMARY

Electrostatic atomizers using an induction charging approach have been investigated and characterized. Diesel fuel has been successfully charged and atomized up to a flow rate of 250 lb./hr. Designs that integrate electrostatic atomization technology into a fuel nozzle/injector suitable for use in a gas turbine engine have been developed along with a controller. Prototype electrostatic fuel nozzles, suitable for engine installation were fabricated and tested both an ambient and engine test bed. Ambient test results indicate the potential to reduce gaseous emissions with electrostatic charging exists. Numerical simulations have indicated that electrostatic atomization has the potential to reduce particulate emissions by 80% from current engine levels. The Navy and CFDRC documented these results in ASME Paper GT-2004-54298. Actual engine testing was inclusive since the nozzles were not run above the engine idle condition long enough to collect emissions.

The work performed here demonstrated that electrostatic atomization technology could improve fuel spray characteristics. At low to moderate flow rates electrostatic atomization has a dramatic effect on droplet size and dispersion. At high flow rates these effects are less pronounced. However, at high flow rates electrostatics continue to improve overall atomization through improved secondary droplet breakup due to the charge on the fuel droplets. Although the engine test results are inclusive, the potential of electrostatic charging the fuel injection process remains to offer promise associated with enhancing combustion performance while reducing emissions, particularly particulate emissions.

7. REFERENCES

[1] www.navygasturbine.org

[2] Oglesby, S.J. and Nichols, G.B., Electrostatic Phenomena, Marcel Dekker, Inc., New York, 1978.

[3] Kelly, A.J., Electrostatic Atomization Devices, US Patent No. 4,255,777, March 1981.

[4] Law, S.E., Cooke, R., and Cooper, S., "Space Charge Suppression of Electrostatic-Induction Spray Charging," *Journal of Electrostatics*, 40891, pp. 603-608.

[5] Brown, C., "Laser Diffraction Sizing and qualitative Optical Patternation Results from Four Peanut Tips of an Electrostatic Atomizer," Report # ERC-CFD31-02-01, September 2002.

[6] CFD-ACE, Version 2003.0.29, CFD Research Corporation, 2003.

[7] Westbrook, C.K. and Dryer, F.L., "Simplified Reaction Mechanisms for the Oxidation of Hydrocarbon Fuels in Flames," Comb. Sc. and Tech, Vol. 27, pp. 31-43, 1981.

[8] Tolpadi, A.K., Davis, A.M., Mongis, H.C., and Lendstedt, R.P., "Soot Modeling in Gas Turbine Combustors," ASME 97-GT-149, 1997.

Proceedings of
ASME TURBO EXPO 2004
June 14-17, 2004, Vienna, Austria

GT-2004-54298

INSERTION OF ELECTROSTATICALLY CHARGED FUEL ATOMIZATION TECHNOLOGY INTO A US NAVY SHIPBOARD GAS TURBINE ENGINE

David P. Guimond
Naval Surface Warfare Center
Philadelphia, PA

Matthew E. Thomas
Roberto DiSalvo
Adam Elliot
D. Scott Crocker
CFDRC
Huntsville, AL

ABSTRACT

Recent breakthroughs in the field of hydrocarbon fuel electrostatic charging techniques have now permitted the opportunity for the Navy to consider implementing this technology into shipboard gas turbines. This research effort is focused toward electrostatic atomization insertion into a U.S. Navy Shipboard Rolls Royce Corporation 501-K research engine at the Naval Surface Warfare Center, Carderock Division (NSWCCD).

Specific milestones achieved thus far include:

(a) pray demonstration of an electrostatically boosted 501-K gas turbine fuel injector prototype at fuel flows from 40 PPH to 250 PPH.

(b) lectrostatic charging effect measurements on the droplet size and patternation of a 501-K simplex atomizer configuration.

(c) umerical modeling of the influence electrostatic charging has on secondary atomization breakup and predicted particulate emissions.

This paper documents results associated with injector conceptual design, electrode integration, atomization measurements, numerical modeling and fuel injection system integration. Preliminary results indicate electrostatic boosting may be capable of reducing particulate emissions up to 80% by inserting the appropriate fuel injector.

INTRODUCTION

The Rolls Royce Corporation (RRC) 501-K engine in Figure 1 serves as the prime mover for ship service gas turbine generator sets (SSGTGs) of the U.S. Navy's DDG 51 Class ships [1]. The 501-K engine features a single shaft with a 14-stage axial compressor, a combustor with six equally-spaced combustion liners, and a four-stage turbine. At the present time the RRC 501-K34 serves as the prime mover for SSGTGs on DD 963 and CG 43 Class ships.

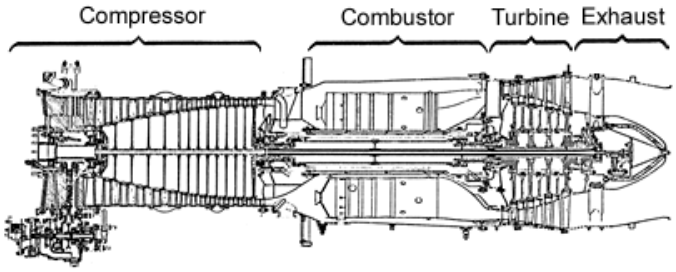

Figure 1. Rolls Royce Corporation 501-K Engine

The combustion section of the Navy's 501K engine shown in Figure 1 has traditionally proven to be where the bulk of the routine in-service maintenance takes place.

- The combustion liners historically last about 2,200 hours before replacement is required. The Navy is currently shifting to a new liner design in an effort to improve service life. The new effusion cooled liner is similar to other low emissions designs. Prototype effusion liners have operated in the Fleet for 15,000+ hours with only minor cracking noted.
- S Fuel nozzle reliability is difficult to quantify. They are typically the first components to be replaced when t troubleshooting engine starting problems. They are also replaced when the temperature spread between combustion E liners exceeds preset limits. The normal nozzle failure mode is that the pilot tip becomes clogged and prevents turbine starting. Fouling of the secondary flow passages is significantly less common. The current nozzle design is a N piloted dual entry type that lends itself to electrostatic charging.

ELECTROSTATIC CHARGING

The presence of electric charge on the fuel droplets within the well-defined geometry of the combustor allows for spray distance, angle, and charge levels to be adjusted for optimum evaporation and combustion. There are several methods available to impart charge to droplets. Among the most common we have induction charging, corona charging, and charge injection. Electrostatic spraying is an efficient and cost effective process to use in preparing fuel for combustion in gas turbine engines commonly found in Navy shipboard operations [1]. Using electronically controlled electrostatic atomization, droplet size and particularly dispersion can be manipulated, independent of flow velocity, aerodynamics or other mechanisms. As a result, the electrostatically boosted gas turbine engine fuel injection preparation approach described here offers significant potential in an engine insertion role. Figure 2 summarizes two fundamental electrostatic fuel charging approaches CFDRC has examined through the ambient gas turbine fuel injection demonstration phase. As a result of this reported development effort, the approach selected for test and evaluation in the RRC 501K industrial gas turbine engine is the induction charging approach.

Numerous different insulating materials have been evaluated. The most appropriate was determined to be a machineable aluminum oxide based material currently utilized in numerous high temperature glass manufacturing operations. This material offers maximum durability in a gas turbine fuel injector application while possessing extremely low electrical conductivity as well as machineability. The electrostatically charged fuel injection system has been fully integrated into the existing RRC 501-K engine fuel injector specifications. As of

Appendix A

Copyright © 2004 by ASME

the writing of this paper the injector in Figure 3 is undergoing combustion testing at ignition, idle and part power flow conditions.

Contact Charging [3]

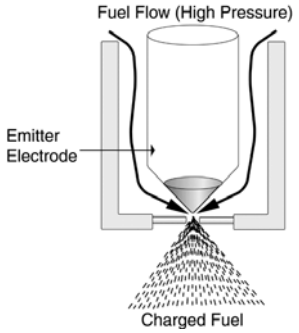

- Requires low fluid conductivity
- Demonstrated at low fuel flows (less than 10 PPH)
- Not commercially available
- Requires hydraulic power for atomization unavailable in 501K installations
- Susceptible to fuel coking

Induction Charging [4]

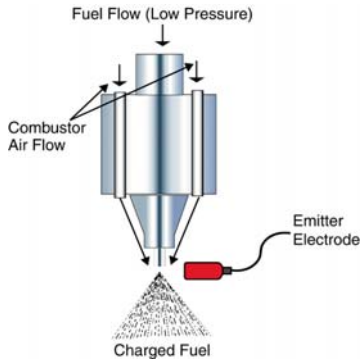

- Functional at any conductivity
- Demonstrated up to 250 PPH in a single injector
- Commercially demonstrated
- Requires pneumatic power for atomization available through combustor
- Failsafe operation (i.e. nozzle atomization operational without electrostatic charging)

Figure 2. Electrostatic Charging Approaches Considered for Implementation into an RRA 501-K Engine

ATOMIZER DESIGN

The 501-K fuel injector design process utilized here was broken down into two sequential steps. The first step was adaptation of the electrostatic atomization induction charging summarized in Figure 2 for operation in an RRC 501-K fuel injector. A full scale RRC 501K prototype injector assembly shown in Figure 3 has been fabricated with the capability to electrostatically charge up to 400 PPH of fuel flow using 1, 2, 3 or any combination of electrodes. The combustor dome swirler and air sweep cap are also shown in Figure 3 because they were an integral part of the design considerations. This air-assisted simplex design has been designated as the baseline configuration. The air assist passage was designed to utilize the identical air assist starting system operational within the current 501-K engine.

Figure 3. RRC501-K Engine Fuel Injector Featuring Electrostatic Charging

To accommodate the maximum fuel flow at 501K full power operation the simplex atomizer flow number must be at least 10. Flow numbers of both 10 and 18 are under final consideration for evaluation during combustion rig testing scheduled to commence in January 2004.

Figure 4 shows the test apparatus assembled to perform preliminary atomization evaluation of the simplex atomizer operating in an uncharged and charged mode. Energy Research Consultants (ERC) was tasked by CFDRC to obtain laser diffraction (LD) sizing data and qualitative optical patternation (QP) data from the simplex atomizer implemented in the injector shown in Figure 3.

Appendix A

Copyright © 2004 by ASME

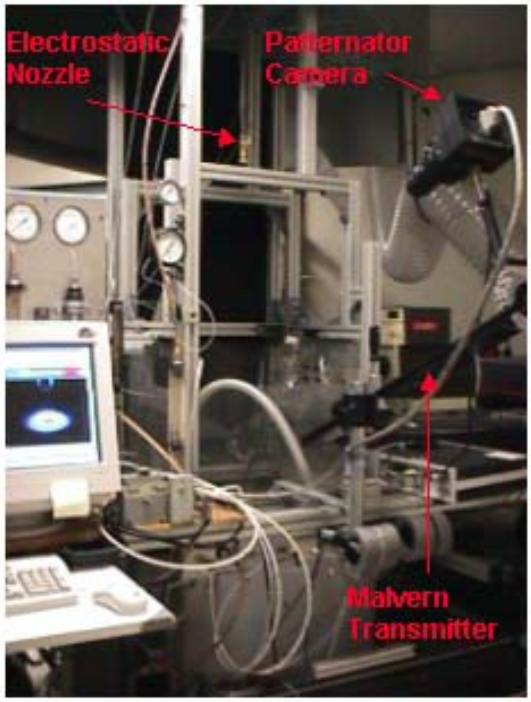

Equipment:

- Malvern 2600
- Data Acquisition
- Ventilation System
- Prototype Optical Patternator
- Nozzle Spray Apparatus

Figure 4. Atomization Testing Facility at ERC

With the unknown risk of highly atomized fuel in ambient air and high voltage present, early atomizer testing was conducted with distilled water to ensure a safe environment for this equipment. More recent findings also described here have demonstrated insufficient power is consumed during the induction charging process to initiate a spark. Due to the nature of the inductive charging process, the fundamental results of these tests are unaffected by the use of water.

Each atomizer was tested at four different pressures and four different positions with and without the electrostatic atomization. A total of 16 optical patternation tests and 32 SMD measurements were completed for each atomizer [5].

The radial locations were chosen based on the spray cone angle. The objective was to determine spray droplet size on a plane orthogonal to the axis of the spray at the center, at the edge, and approximately one inch beyond the spray cone angle.

For the optical patternation tests, the setup remained the same as in the SMD measurements. The camera for capturing the patternation data was a high speed electronic camera located above the spray cone. In each case, 9 images were obtained. The exposure varied from about 0.5 sec to about 4.0 sec in an effort to obtain relatively consistent pixel intensities from case to case. A laser power before the collimating lens was maintained at 200 mW to maximize the obscuration intensity measurement. Figure 5 depicts images associated with SMD and patternation testing in progress.

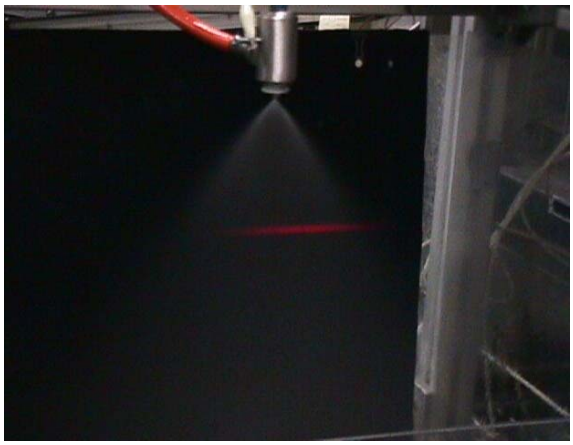

SMD Testing

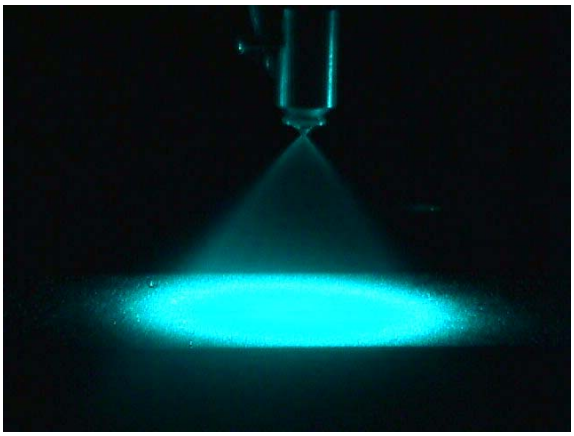

Optical Patternation Testing

Figure 5. Atomization Testing in Progress

Optical data processing involved an average of the 9 images for each case. A circular mask is placed at the nozzle geometric centerline of the affined image so that the corners of the images are not included in patternation analysis. A mask radius of 240 pixels (about 5.68 inches) was chosen. The patternation numbers were calculated by dividing the image into eight areas. Each image is divided into one circle near the center and seven annular areas, all within identical characteristic dimensions. For each area, the pixel intensities are summed. Results of typical optical patternation and SMD testing for the sprays are shown in Figures 6a through 6c.

Appendix A

Copyright © 2004 by ASME

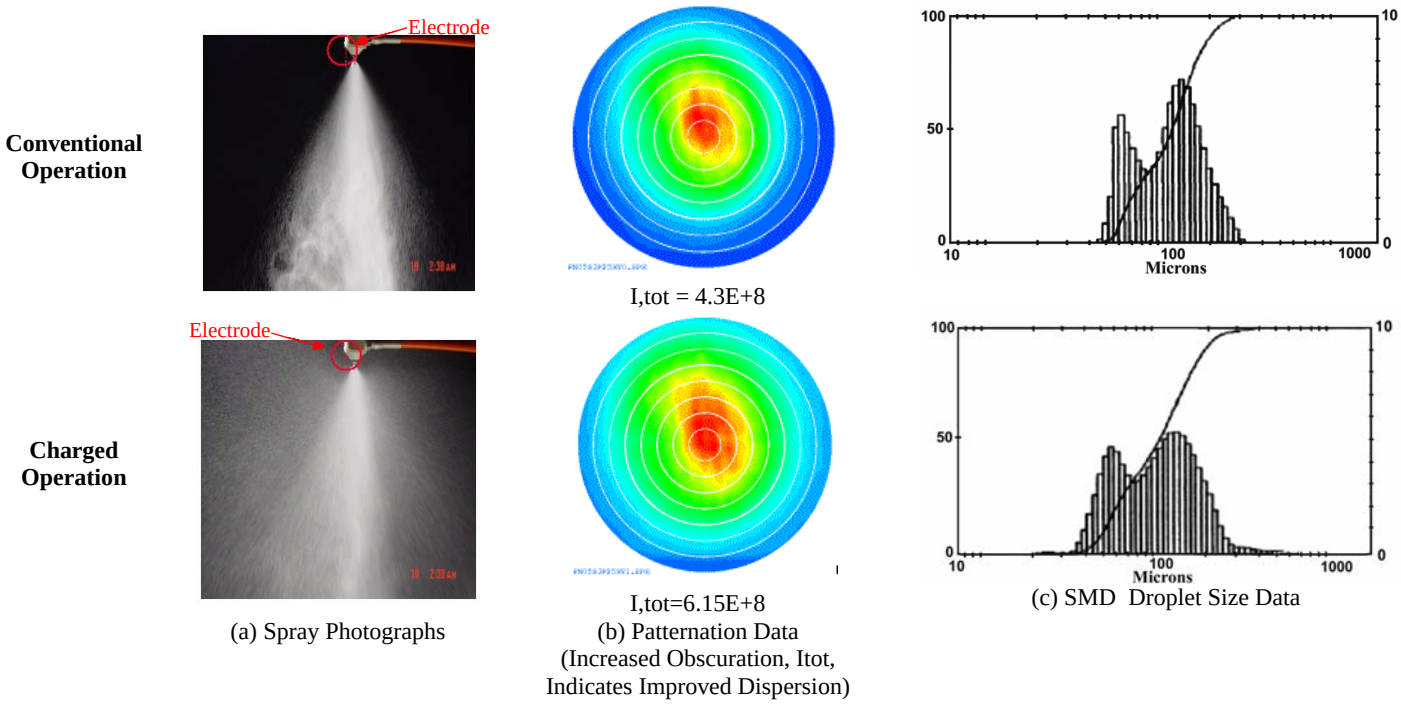

(a) Spray Photographs

(b) Patternation Data (Increased Obscuration, Itot, Indicates Improved Dispersion)

(c) SMD Droplet Size Data

Figure 6. Typical Atomization Test Results (FN – 10, w_f = 40 PPH)

The patternation images reveal that at lower flow rates the sprays are more spread out as a result of the electrostatic forces present. The effect of the electrostatic force is less pronounced with the higher flow rate sprays is due to the greater droplet density and velocity associated with the higher-pressure sprays. Figure 7 demonstrates the reduced dispersion which occurs at higher flow rates.

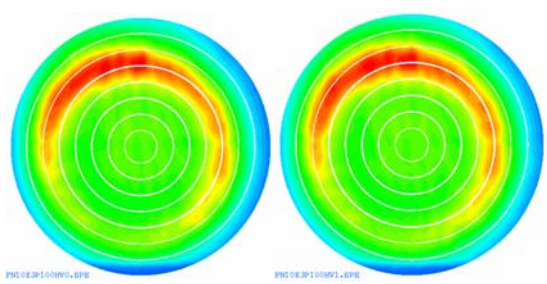

Figure 7. Reduced Droplet Dispersion at Increased Flow Rate (FN = 10, w_f = 150 PPH)

Numerical Modeling

Understanding of the electrostatic gas turbine spray combustion parameters in the 501-K gas turbine engine is required for selection of optimum spray patterns. CFDRC's numerical modeling efforts therefore have included assessment of the injector droplet size, distribution and spray, cone angle, as well as corresponding localized vaporization rates when operating in the 501-K engine. Numerous numerical simulations have been completed to evaluate electrostatic atomization spray pattern effects on 501-K engine performance.

The general purpose Computational Fluid Dynamic (CFD) software CFD-ACE$^+$ is being used to perform all numerical analyses. CFD-ACE$^+$ is a commercial software package developed by CFDRC [6]. The following basic capabilities are being utilized to support this analysis.

1. co-located, fully implicit and strongly conservative finite volume formulation;
2. solution of two- and three-dimensional Navier-Stokes equations for incompressible and compressible flows;
3. pressure-based solution algorithms including SIMPLE and a variant of SIMPLEC;
4. non-orthogonal curvilinear coordinates;
5. multi-block and many-to-one grid topology, allowing for local grid refinement;
6. unstructured grids with any cell type and with arbitrary interfaces at domain interfaces;
7. parallel processing;
8. second order central (with damping), second order upwind, and Osher-Chakravarthy spatial differencing schemes;
9. standard, low-Reynolds number, and RNG turbulence models for steady-state models;
10. instantaneous and finite-rate, one-step, and four-step heat release and emission kinetics models;
11. 2-scalar prescribed PDF, eddy breakup, and eddy dissipation turbulence-chemistry interaction models;
12. NO_x and CO emissions models;
13. conjugate heat transfer with radiation; and
14. spray models for trajectory tracking, vaporization, etc.

A key attribute of electrostatically charged fuel is the secondary atomization process. It has been shown the initial charge inductively injected into a droplet remains until the droplet strikes a grounded surface such as the chamber wall. To maintain equilibrium the droplet charges uniformly disperse themselves on the surface of the droplet as depicted in Figure 8. As the droplet mass and corresponding diameter decay due to evaporation the charge concentration on the droplet surface reaches a level that the repulsive forces due to charge exceed that of the retention force due to surface tension. A lumped parameter

Copyright © 2004 by ASME

model of this process has been constructed with the results also summarized in Figure 8.

The simulations completed here demonstrated the injector air swirler curved vanes minimize the air pressure drop and maximize the amount of airflow. This air also thermally protects the nozzle face, provides air to assist in atomization, and effectively prevents fuel from reaching the electrode casing. Numerous two-dimensional CFD simulations of injector operation have been completed. Axial velocity and temperature contours of the configuration shown in Figure 3 are depicted in Figure 10.

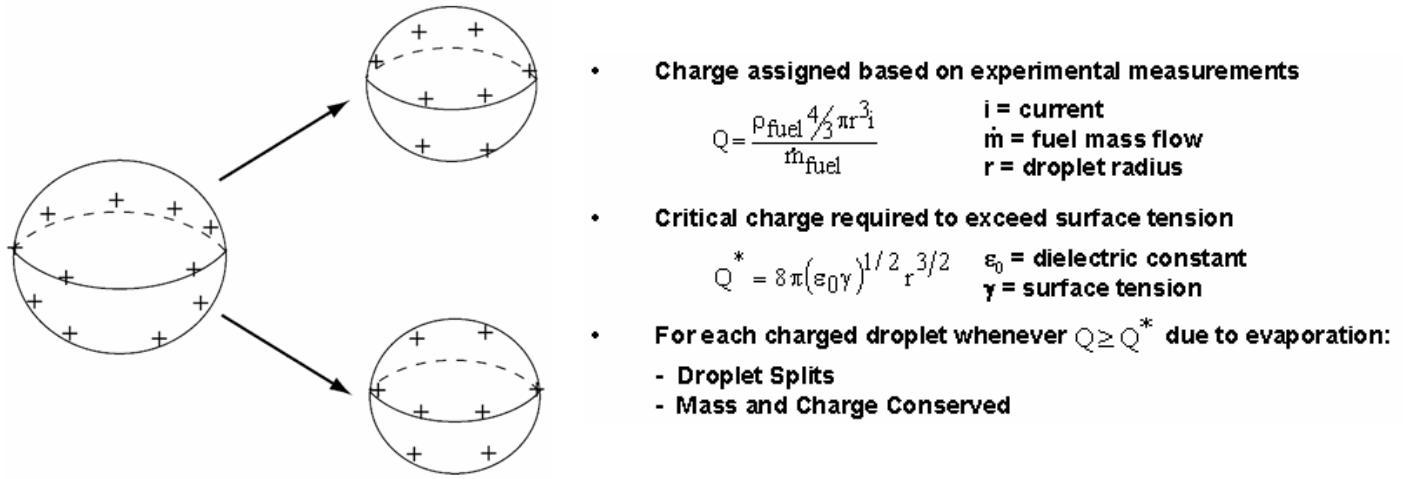

Figure 8. Secondary Atomization Breakup Model Due to Electrostatic Charging

Combustion is being modeled using a one-step finite rate reaction with equilibrium products of CO_2, H_2O, CO, H_2, OH, and O. The fuel is represented by the specie $C_{12}H_{23}$ with properties designed to imitate DF-2. The reaction rate is adapted from Westbrook and Dryer [7] with modifications that adjust for the equilibrium product flame temperature.

The 501-K combustor flow field inside and outside the liner has been modeled in order to provide the most accurate simulations possible. A baseline simulation performed on the 501-K combustor is shown in Figure 9.

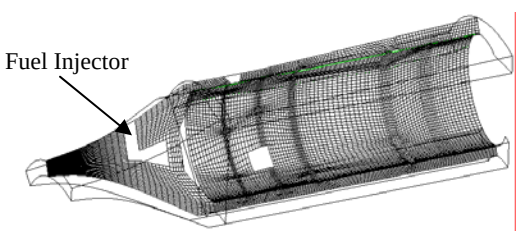

(a) Combustor Grid Model

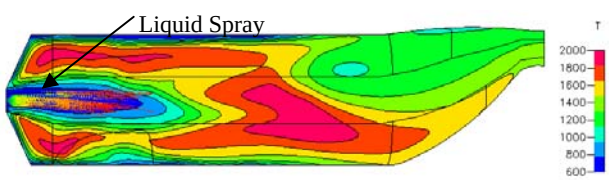

(b) Inner Combustor Temperature
(Plane Through Nozzle Centerline)

Figure 9. Simulation of Existing Allison 501-K Combustor

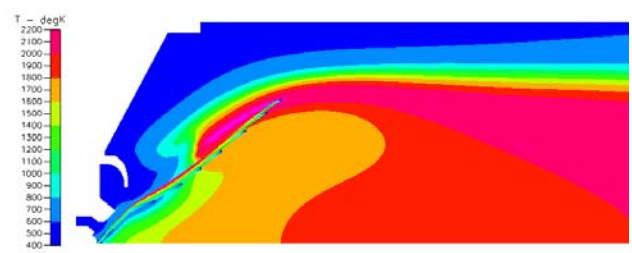

(a) Temperature Contours

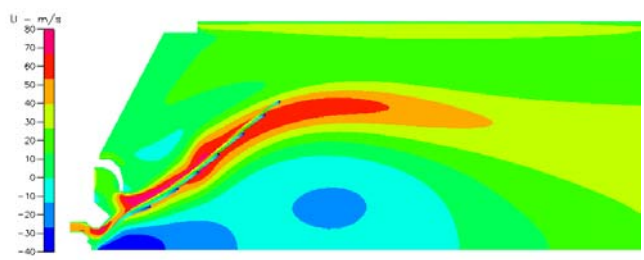

(b) Axial Velocity Contours

Figure 10. Two-Dimensional Injector Simulations at Fuel Injector/Combustor Interface

At this time it is assumed here that a 1:1 correspondence exists between soot reduction and particulate emissions reduction. Because particulate matter less than 2.5 micron characteristic diameter (PM2.5), as well as soot formation, is a highly three-dimensional process a 3D simulation of the 501K combustor was completed. For the sake of brevity in this paper only the soot modeling [8] results are summarized here. Figure 11 summarizes these predictions of soot formation in the 501K combustor with and without electrostatic charging. The significant reduction in predicted soot concentration can be directly attributed to improved spray dispersion and accelerated secondary droplet breakup.

Appendix A

Copyright © 2004 by ASME

The most significant anticipated result of this effort will be a reduction in engine particulate emissions. Currently, the 501-K SAE Smoke Number averages approximately 50 as shown in Figure 12. This is well above the visible range and indicates a significant level of particulate matter in the exhaust as a result of the combination of dual orifice fuel injection and an excessively rich primary combustion zone. Although the basic combustor stoichiometry will not change with this injector modification, particulate matter reduction due to electrostatic charging was analytically shown to be first order due to secondary atomization breakup. The soot formation process was illustrated in Figure 11 and the projected benefit of electrostatic charging is summarized in Figure 12. Approximately a five-fold reduction in PM2.5 is anticipated by reducing the SAE Smoke Number from 50 to 10.

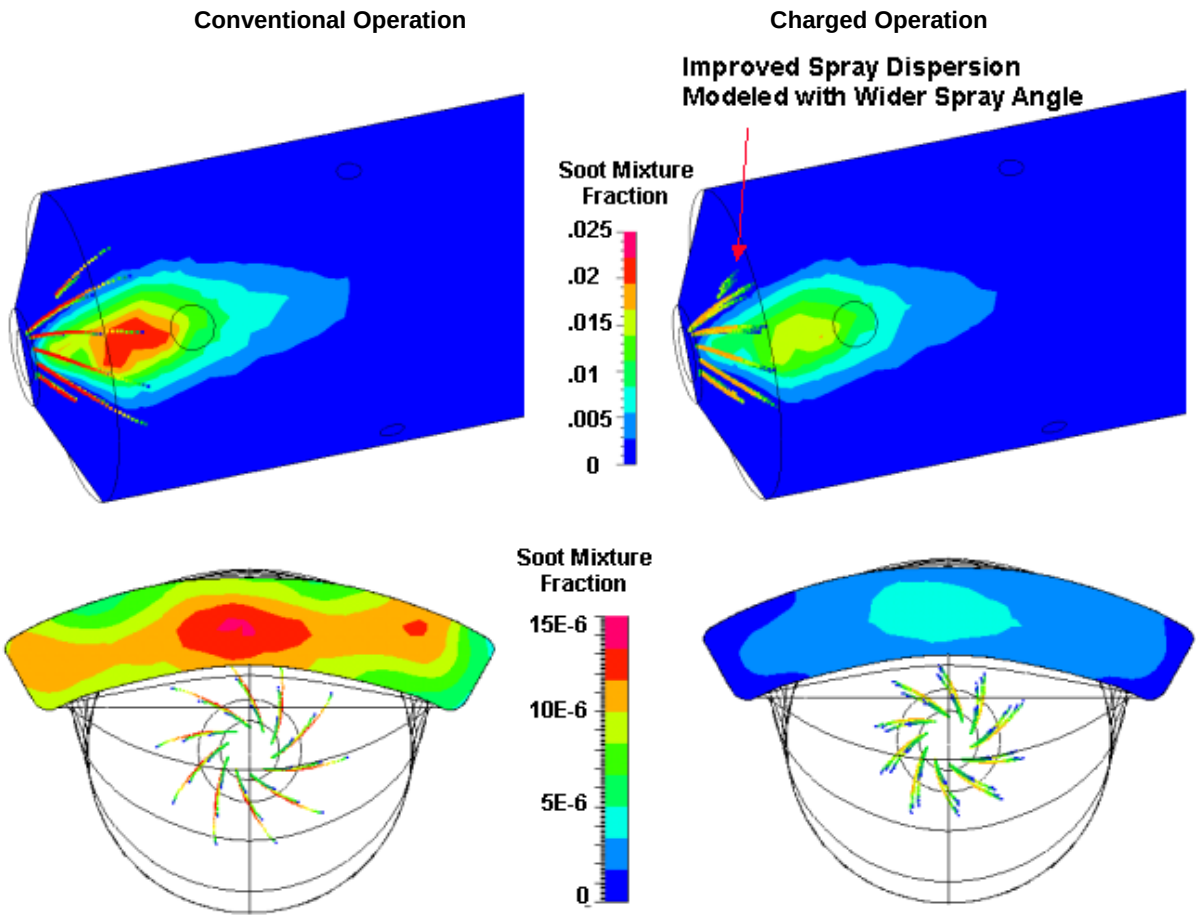

Figure 11. RRA 501-K Combustion Soot Predictions

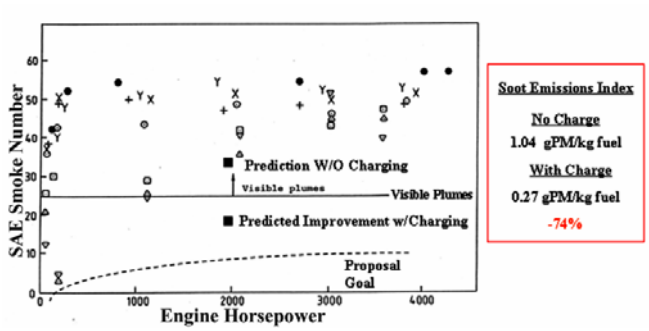

Figure 12. Smoke Number Measurements and Soot Prediction in the 501-K

Selected details of the electrostatic controller are summarized in Figure 13. Only two independent modifications of the existing controller are anticipated. The first is the addition of a controller which identifies and regulates power requirements associated with injecting charge into the fuel. The second is a customized power supply for this purpose.

Appendix A

Copyright © 2004 by ASME

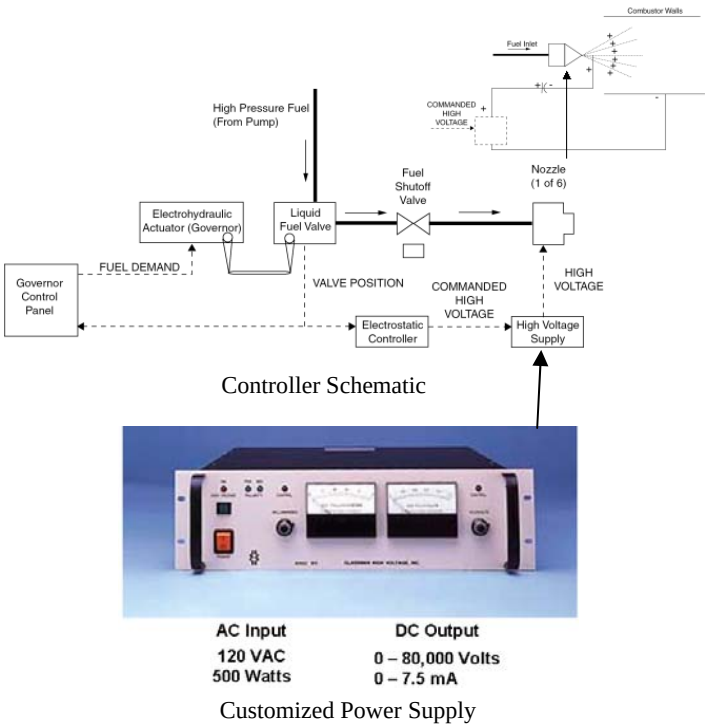

Figure 13. Electrostatic Charge Booster Controller Description

ENGINE DEMONSTRATION

A demonstration of electrostatic fuel atomization technology will be conducted using a Rolls Royce Corporation 501-K17 gas turbine engine located at the Naval Surface Warfare Center, Philadelphia Land Based Engineering Site (LBES). The 501-K17 engine is an earlier version of the 501-K34 engine currently used by the Navy. Successful operation in one of the Navy's 501-K17 research engines at the LBES test site shown in Figure 14 is the first step for any fuel injector under consideration for fleet retrofit.

Figure 14. NSWCCD/Philadelphia LBES Test Site

For this technology demonstration the exhaust emissions from 501-K17 at the LBES will be completely characterized using a variety of instrumentation. Gaseous emissions will be measured by drawing a sample of exhaust through a heated line into a continuous emissions monitoring system capable of measuring CO, CO_2, O_2, THC, NOx and SO_2. A second, cooled probe will be inserted close to the exit of the engine to obtain a representative sample of exhaust for particle sampling. The exhaust sample will be diluted with dry air at the tip of the probe to prevent water condensation and particle loss to the wall due to high temperature gradients, and to prevent saturation of the particle instrument. A Scanning Mobility Particle Sizer (SMPS) manufactured by TSI, Inc. will be used to measure particle size distributions and concentrations. The SMPS system consists of an Electrostatic Classifier and a Condensation Particle Counter along with a computerized data acquisition and control system. The SMPS system uses an electrical mobility detection technique by which the entire particle size distribution contained in the sample is measured to a high degree of accuracy. A micro dilution test stand manufactured by Sierra Instruments, typically used for diesel engines, will also be utilized to obtain particulate emission measurements on a mass basis.

A complete baseline of the 501-K17 engine with respect to performance and emissions characteristics will be obtained from idle to 2500 kW. The electrostatic fuel nozzles and controller will then be installed. A series of engine starts will be performed to confirm proper engine starting and operational characteristic with the electrostatic nozzles. This will be followed by a series of test runs at various loads to optimize the electrostatic fuel system operation and the amount of charge put into the fuel at various fuel flow and power levels. The emissions and performance characteristics of the 501-K17 while operating with the optimized electrostatic charged fuel nozzles will then be documented. The emphasis will be on low to mid power operation as this is region where the benefits of the charged fuel are expected to be greatest. Fail safe operation of the electrostatic fuel nozzles will also be demonstrated by starting and operating the engine with the charging circuit switched off to simulate a failure.

ACKNOWLEDGMENTS

The Strategic Environmental Research and Development Program (SERDP) has funded the development of electrostatic fuel atomization technology with an emphasis on reducing particulate matter (particularly PM2.5) and other emissions from gas turbine engines.

The authors would also like to thank the following:

Dr. David L. Black, of CFD Research Corporation, for his CFD modeling and swirler design efforts.

REFERENCES

[1] www.navygasturbine.org

[2] Oglesby, S.J. and Nichols, G.B., Electrostatic Phenomena, Marcel Dekker, Inc., New York, 1978.

[3] Kelly, A.J., Electrostatic Atomization Devices, US Patent No. 4,255,777, March 1981.

[4] Law, S.E., Cooke, R., and Cooper, S., "Space Charge Suppression of Electrostatic-Induction Spray Charging," *Journal of Electrostatics*, 40891, pp. 603-608.

[5] Brown, C., "Laser Diffraction Sizing and qualitative Optical Patternation Results from Four Peanut Tips of an Electrostatic Atomizer," Report # ERC-CFD31-02-01, September 2002.

[6] CFD-ACE, Version 2003.0.29, CFD Research Corporation, 2003.

[7] Westbrook, C.K. and Dryer, F.L., "Simplified Reaction Mechanisms for the Oxidation of Hydrocarbon Fuels in Flames," Comb. Sc. and Tech, Vol. 27, pp. 31-43, 1981.

[8] Tolpadi, A.K., Davis, A.M., Mongis, H.C., and Lendstedt, R.P., "Soot Modeling in Gas Turbine Combustors," ASME 97-GT-149, 1997.

Appendix A

Copyright © 2004 by ASME

Laser Diffraction Sizing and Qualitative Optical Patternation Results from Four Peanut Tips of an Electrostatic Atomizer

(Final Report)

prepared for
CFD Research Corporation

ENERGY RESEARCH CONSULTANTS

23342 South Pointe Drive, Suite E
Laguna Hills, CA 92653

Phone: (949) 583-1197
FAX: (949) 583-1198

September 2002

Report ERC-CFD31-02-1(b)

CFD PO Number: 02-176

Appendix-B

Table Of Contents

SUMMARY 1

FACILITY 1

TEXT MATRIX 2

FUEL SELECTION 9

LASER DIFFRACTION SIZING RESULTS 9

QUALITATIVE OPTICAL PATTERNATION RESULTS 1

COMMENTS ON FLOW DATA UNCERTAINTY 2

COMMENTS ON LASER DIFFRACTION DATA UNCERTAINTY 2

COMMENTS ON QUALITATIVE OPTICAL PATTERNATION DATA UNCERTAINTY 3

ELECTRONIC DATA 3

APPENDIX A – LASER DIFFRACTION DATA LISTINGS ..... ERROR! BOOKMARK NOT DEFINED.

List of Figures

FIGURE 1. FACILITY. 1
FIGURE 2. IMAGE NAMING SCHEME. 4
FIGURE 3. RAW IMAGE, PRIOR TO AFFINE TRANSFORM (FN30Z3P100HV0.SPE). 5
FIGURE 4. PATTERNATION NUMBERING SCHEME, IMAGE SCALE, AND INTENSITY SCALE. 5
FIGURE 5. RESULTS. 6

List of Tables

TABLE 1. LASER DIFFRACTION TEST MATRIX. 3
TABLE 2. QUALITATIVE OPTICAL PATTERNATION TEST MATRIX. 7
TABLE 3. LASER DIFFRACTION SIZING RESULTS. 10

Glossary

CFDRC	CFD Research Corporation
ERC	Energy Research Consultants
FN	Flow Number $\frac{lbs/hr}{\sqrt{psig}}$ (using calibrating fluid)
LD	Laser Diffraction
MI	Model Independent raw laser diffraction data
RR	Rosin Rammler fitted laser diffraction data
QP	Qualitative Optical Patternation

Summary

Energy Research Consultants (ERC) was tasked by CFD Research Corporation (CFDRD) to obtain laser diffraction (LD) sizing data and qualitative optical patternation (QP) data from four peanut tips of an electrostatic atomizer. Printouts of laser diffraction results were provided to CFDRC personnel during their visit to ERC. Electronic LD results in the form of an Excel file and QP results in the form of an intermediate report Word file were e-mailed to CFDRC as soon as they were available. This final report summarizes all of these previously submitted results. ERC was tasked with data collection, processing, compilation, and presentation, not data analysis. Some limited analysis is nonetheless presented in this final report.

Facility

A Malvern 2600 particle analyzer was used for the laser diffraction measurements. A prototype optical patternation system, developed by ERC, was used for the qualitative patternation measurements.

A photograph of the facility is shown in Figure 1.

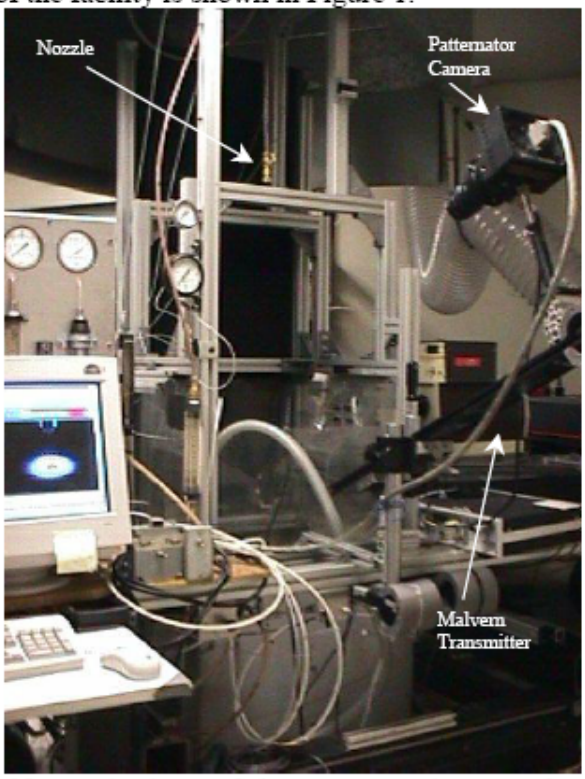

Note A photo of the exact nozzle setup for this particular project is not available. The nozzle setup in the above photo is very similar and the instrumentation shown above is identical.

Figure 1. Facility.

Appendix-B

Text Matrix

The test matrices for the laser diffraction and qualitative optical patternation results are presented in Table 1 and Table 2. All the text matrix points were chosen by CFDRC.

Appendix-B

Table 1. Laser Diffraction Test Matrix.

Run (#)	Peanut (FN)	Water P (psig)	Water Q (gph)	Y (inches)	Z (inches)	HV (on / off)	comment
12	0.5	25	0.365	0	3	0	
13	0.5	25	0.365	0	3	1	
14	0.5	50	0.524	0	3	0	
15	0.5	50	0.524	0	3	1	
28	0.5	50	0.524	0	3	0	repeat
30	0.5	50	0.524	0	3	1	repeat
29	0.5	50	0.524	0	3	0	repeat
31	0.5	50	0.524	0	3	1	repeat
16	0.5	100	0.712	0	3	0	
17	0.5	100	0.712	0	3	1	
18	0.5	145	0.820	0	3	0	
19	0.5	145	0.820	0	3	1	
32	0.5	145	0.820	0	3	0	repeat
34	0.5	145	0.820	0	3	1	repeat
33	0.5	145	0.820	0	3	0	repeat
35	0.5	145	0.820	0	3	1	repeat
42	0.5	25	0.392	-1	3	0	
43	0.5	25	0.392	-1	3	1	
40	0.5	50	0.524	-1	3	0	
41	0.5	50	0.524	-1	3	1	
38	0.5	100	0.766	-1	3	0	
39	0.5	100	0.766	-1	3	1	
36	0.5	145	0.820	-1	3	0	
37	0.5	145	0.820	-1	3	1	
44	0.5	25	0.392	-2	3	0	
45	0.5	25	0.392	-2	3	1	
46	0.5	50	0.524	-2	3	0	
47	0.5	50	0.524	-2	3	1	
48	0.5	100	0.766	-2	3	1	
49	0.5	145	0.820	-2	3	1	
26	0.5	25	0.392	0	2	0	
27	0.5	25	0.392	0	2	1	
24	0.5	50	0.524	0	2	0	
25	0.5	50	0.524	0	2	1	
50	0.5	50	0.524	0	2	0	repeat
52	0.5	50	0.524	0	2	1	repeat
51	0.5	50	0.524	0	2	0	repeat
53	0.5	50	0.524	0	2	1	repeat
22	0.5	100	0.739	0	2	0	
23	0.5	100	0.739	0	2	1	
20	0.5	145	0.820	0	2	0	
21	0.5	145	0.820	0	2	1	

Notes: 1. Malvern data file name: cfd31_a.db0

Appendix-B

Table 1. Laser Diffraction Test Matrix (continued).

Run (#)	Peanut (FN)	Water P (psig)	Water Q (gph)	Y (inches)	Z (inches)	HV (on / off)	comment
16	3	25	2.072	0	3	0	
17	3	25	2.072	0	3	1	
14	3	50	2.947	0	3	0	
36	3	50	2.947	0	3	0	repeat
37	3	50	2.947	0	3	0	repeat
15	3	50	2.947	0	3	1	
12	3	100	4.099	0	3	0	
13	3	100	4.099	0	3	1	
38	3	100	4.099	0	3	0	repeat
40	3	100	4.099	0	3	1	repeat
39	3	100	4.099	0	3	0	repeat
41	3	100	4.099	0	3	1	repeat
10	3	145	4.917	0	3	0	
11	3	145	4.917	0	3	1	
18	3	25	2.072	-1	3	0	
21	3	25	2.072	-1	3	1	
19	3	25	2.072	-1	3	0	repeat
22	3	25	2.072	-1	3	1	repeat
20	3	25	2.072	-1	3	0	repeat
23	3	25	2.072	-1	3	1	repeat
24	3	50	2.947	-1	3	0	
25	3	50	2.947	-1	3	1	
26	3	100	4.099	-1	3	0	
27	3	100	4.099	-1	3	1	
28	3	145	4.917	-1	3	0	
29	3	145	4.917	-1	3	1	
35	3	50	2.947	-2	3	0	
34	3	50	2.947	-2	3	1	
32	3	100	4.099	-2	3	0	
31	3	100	4.099	-2	3	1	
33	3	145	4.917	-2	3	0	
30	3	145	4.917	-2	3	1	
2	3	25	2.072	0	2	0	
3	3	25	2.072	0	2	1	
4	3	50	2.947	0	2	0	
5	3	50	2.947	0	2	1	
6	3	100	4.099	0	2	0	
7	3	100	4.099	0	2	1	
8	3	145	4.917	0	2	0	
9	3	145	4.917	0	2	1	

Notes: 1. Malvern data file name: cfd31_b.db0

Appendix-B

Table 1. Laser Diffraction Test Matrix (continued).

Run (#)	Peanut (FN)	Water P (psig)	Water Q (gph)	Y (inches)	Z (inches)	HV (on / off)	comment
2	7.4	25	5.238	0	3	0	
3	7.4	25	5.238	0	3	1	
4	7.4	50	7.513	0	3	0	
5	7.4	50	7.513	0	3	1	
6	7.4	100	10.560	0	3	0	
7	7.4	100	10.560	0	3	1	
8	7.4	145	12.710	0	3	0	
9	7.4	145	12.710	0	3	1	
16	7.4	25	5.303	-2.1	3	0	
17	7.4	25	5.303	-2.1	3	1	
14	7.4	50	7.478	-2.1	3	0	
15	7.4	50	7.478	-2.1	3	1	
12	7.4	100	10.560	-2.1	3	0	
13	7.4	100	10.560	-2.1	3	1	
10	7.4	145	12.710	-2.1	3	0	
11	7.4	145	12.710	-2.1	3	1	
18	7.4	25	5.303	-3.1	3	0	
19	7.4	25	5.303	-3.1	3	1	
20	7.4	50	7.374	-3.1	3	1	
21	7.4	100	10.560	-3.1	3	0	
22	7.4	100	10.560	-3.1	3	1	
23	7.4	145	12.710	-3.1	3	1	
34	7.4	25	5.303	0	2	0	
35	7.4	25	5.303	0	2	1	
32	7.4	50	7.409	0	2	0	
33	7.4	50	7.409	0	2	1	
26	7.4	100	10.560	0	2	0	
27	7.4	100	10.560	0	2	1	
28	7.4	100	10.560	0	2	0	repeat
30	7.4	100	10.560	0	2	1	repeat
29	7.4	100	10.560	0	2	0	repeat
31	7.4	100	10.560	0	2	1	repeat
24	7.4	145	12.710	0	2	0	
25	7.4	145	12.710	0	2	1	

Notes: 1. Malvern data file name: cfd31_c.db0

2. A shaded cell indicates flow above the range of the rotometer. Flow was calculated based on pressure from an average flow number for that peanut. The average flow number was calculated from all of the points where a rotometer reading for that peanut could be taken.

Appendix-B

Table 1. Laser Diffraction Test Matrix (concluded).

Run (#)	Peanut (FN)	Water P (psig)	Water Q (gph)	Y (inches)	Z (inches)	HV (on / off)	comment
10	10	25	6.691	0	3	0	
11	10	25	6.691	0	3	1	
12	10	50	9.336	0	3	0	
13	10	50	9.336	0	3	1	
14	10	100	13.200	0	3	0	
15	10	100	13.200	0	3	1	
16	10	145	15.900	0	3	0	
17	10	145	15.900	0	3	1	
24	10	25	6.556	-2.5	3	0	
27	10	25	6.556	-2.5	3	1	
25	10	25	6.556	-2.5	3	0	repeat
28	10	25	6.556	-2.5	3	1	repeat
26	10	25	6.556	-2.5	3	0	repeat
29	10	25	6.556	-2.5	3	1	repeat
22	10	50	9.336	-2.5	3	0	
23	10	50	9.336	-2.5	3	1	
20	10	100	13.200	-2.5	3	0	
21	10	100	13.200	-2.5	3	1	
18	10	145	15.900	-2.5	3	0	
19	10	145	15.900	-2.5	3	1	
30	10	25	6.556	-3.5	3	0	
31	10	25	6.556	-3.5	3	1	
32	10	50	9.336	-3.5	3	1	
33	10	100	13.200	-3.5	3	0	
34	10	100	13.200	-3.5	3	1	
35	10	145	15.900	-3.5	3	1	
8	10	25	6.691	0	2	0	
9	10	25	6.691	0	2	1	
6	10	50	9.336	0	2	0	
7	10	50	9.336	0	2	1	
3	10	100	13.200	0	2	0	
4	10	100	13.200	0	2	1	
1	10	145	15.900	0	2	0	
5	10	145	15.900	0	2	0	
2	10	145	15.900	0	2	1	

Notes: 1. Malvern data file name: cfd31_d.db0

2. A shaded cell indicates flow above the range of the rotometer. Flow was calculated based on pressure from an average flow number for that peanut. The average flow number was calculated from all of the points where a rotometer reading for that peanut could be taken.

Appendix-B

Table 2. Qualitative Optical Patternation Test Matrix.

Image #	Flow Number ($pph / \sqrt{psig}$)	Pressure (psig)	High Voltage (off / on)	Axial Position (inches)
1	0.5	25	Off	3
2	0.5	25	On	3
3	0.5	50	Off	3
4	0.5	50	On	3
5	0.5	100	Off	3
6	0.5	100	On	3
7	0.5	145	Off	3
8	0.5	145	On	3
9	1.0	25	Off	3
10	1.0	25	On	3
11	1.0	50	Off	3
12	1.0	50	On	3
13	1.0	100	Off	3
14	1.0	100	On	3
15	1.0	145	Off	3
16	1.0	145	On	3
17	3.0	25	Off	3
18	3.0	25	On	3
19	3.0	50	Off	3
20	3.0	50	On	3
21	3.0	100	Off	3
22	3.0	100	On	3
23	3.0	145	Off	3
24	3.0	145	On	3
25	7.4	25	Off	3
26	7.4	25	On	3
27	7.4	50	Off	3
28	7.4	50	On	3
29	7.4	100	Off	3
30	7.4	100	On	3
31	7.4	145	Off	3
32	7.4	145	On	3

Appendix-B

Table 2. Qualitative Optical Patternation Test Matrix (concluded).

Image #	Flow Number ($pph/\sqrt{psig}$)	Pressure (psig)	High Voltage (off / on)	Axial Position (inches)
33	0.5	25	Off	2
34	0.5	25	On	2
35	0.5	50	Off	2
36	0.5	50	On	2
37	0.5	100	Off	2
38	0.5	100	On	2
39	0.5	145	Off	2
40	0.5	145	On	2
41	1.0	25	Off	2
42	1.0	25	On	2
43	1.0	50	Off	2
44	1.0	50	On	2
45	1.0	100	Off	2
46	1.0	100	On	2
47	1.0	145	Off	2
48	1.0	145	On	2
49	3.0	25	Off	2
50	3.0	25	On	2
51	3.0	50	Off	2
52	3.0	50	On	2
53	3.0	100	Off	2
54	3.0	100	On	2
55	3.0	145	Off	2
56	3.0	145	On	2
57	7.4	25	Off	2
58	7.4	25	On	2
59	7.4	50	Off	2
60	7.4	50	On	2
61	7.4	100	Off	2
62	7.4	100	On	2
63	7.4	145	Off	2
64	7.4	145	On	2

Appendix-B

Fuel Selection

Fuel was desired to be used in the present study, but water was ultimately chosen by CFDRC.

Note that the flow numbers provided in Table 1 and Table 2 were nominal numbers provided by CFDRC, based on calibrating fluid, not measured by ERC. Data to compute a measured flow number, with water, were provided to CFDRC in the Excel laser diffraction data file.

Laser Diffraction Sizing Results

Laser diffraction droplet size data were obtained following the test matrix outlined in Table 1. The 300 mm receiver lens was used which offered a size range from 1.5 to 564 microns. The entire spray was contained with about 1.4 times the lens focal length to avoid vignetting. Since obscurations were less than 0.50 (50%) in all cases, D32 size corrections for obscuration effects were not required.

The laser diffraction sizing results are tabulated in Table 3.

The laser diffraction listings printed from the Malvern are included in **Error! Reference source not found.**. These listings include a plot of the percent volume histogram and a table of the histogram. They are organized based on Table 1. The left panel of the double sided copy includes the HV0 case while the right panel includes the HV1 cases. When data are not available, to retain this presentation format, a blank page is inserted. Additional data presentation, in the form of scatter plots for example, were specifically not requested by CFDRC.

Raw unfitted Model Independent (MI) data were requested by CFDRC. Only Model Independent raw data are tabulated in Table 3 and included in **Error! Reference source not found.**. Note that the electronic data provided to CFDRC does include fitted Rosin Rammler (RR) histogram information.

CFDRC selected some cases for repeat. These cases were repeated twice, providing a total of three measurements. A discussion of laser diffraction uncertainty, based on analysis of these repeats, and also based on past experience, is included in the section Comments on Laser Diffraction Data Uncertainty.

Appendix-B

Table 3. Laser DIffraction Sizing Results (continued).

Run (#)	Peanut (FN)	P avg (psig)	Q (gph)	Y (inches)	Z (inches)	HV (on / off)	comment ()	obscur (%)	MI D32 (microns)	MI D43 (microns)	MI Dv0.1 (microns)	MI Dv0.5 (microns)	MI Dv0.9 (microns)
16	3	25	2.072	0	3	0		0.220	84.88	125.50	47.09	121.40	205.43
17	3	25	2.072	0	3	1		0.226	83.75	125.10	45.93	119.70	207.26
14	3	50	2.947	0	3	0		0.225	53.39	85.70	30.41	73.37	152.26
36	3	50	2.947	0	3	0	repeat	0.220	52.84	85.40	29.78	72.84	152.25
37	3	50	2.947	0	3	0	repeat	0.218	53.39	85.99	30.35	73.52	153.33
15	3	50	2.947	0	3	1		0.233	52.67	84.54	30.30	71.25	150.30
12	3	100	4.099	0	3	0		0.226	43.12	74.43	22.34	59.89	139.14
13	3	100	4.099	0	3	1		0.231	42.77	74.14	22.34	59.37	138.90
38	3	100	4.099	0	3	0	repeat	0.224	42.95	73.87	22.26	59.51	138.15
40	3	100	4.099	0	3	1	repeat	0.225	43.14	74.14	22.59	59.41	138.61
39	3	100	4.099	0	3	0	repeat	0.221	43.48	74.50	22.89	60.05	138.88
41	3	100	4.099	0	3	1	repeat	0.225	42.92	74.32	22.53	59.63	139.11
10	3	145	4.917	0	3	0		0.241	38.43	68.63	19.75	54.51	131.75
11	3	145	4.917	0	3	1		0.244	38.34	68.32	19.69	54.15	131.27
18	3	25	2.072	-1	3	0		0.108	101.10	124.20	58.56	117.90	197.03
21	3	25	2.072	-1	3	1		0.130	90.79	118.20	52.37	107.90	196.49
19	3	25	2.072	-1	3	0	repeat	0.108	100.20	124.00	57.75	117.20	197.63
22	3	25	2.072	-1	3	1	repeat	0.132	89.70	117.90	51.39	107.50	196.67
20	3	25	2.072	-1	3	0	repeat	0.104	102.70	123.90	60.56	120.00	195.54
23	3	25	2.072	-1	3	1	repeat	0.132	89.64	118.40	51.25	107.60	198.22
24	3	50	2.947	-1	3	0		0.181	75.78	96.65	46.34	84.76	162.00
25	3	50	2.947	-1	3	1		0.194	73.57	94.72	45.34	80.82	159.69
26	3	100	4.099	-1	3	0		0.205	59.04	79.11	35.78	63.77	139.11
27	3	100	4.099	-1	3	1		0.210	58.92	78.21	36.36	63.05	141.27
28	3	145	4.917	-1	3	0		0.218	52.50	71.90	31.62	56.83	133.53
29	3	145	4.917	-1	3	1		0.221	52.02	71.74	31.10	56.66	133.98
35	3	50	2.947	-2	3	0		0.060	93.96	109.10	60.65	101.20	166.79
34	3	50	2.947	-2	3	1		0.078	85.86	102.10	56.59	90.60	163.89
32	3	100	4.099	-2	3	0		0.100	88.77	105.70	56.58	98.16	166.58
31	3	100	4.099	-2	3	1		0.107	86.46	103.70	55.02	94.80	165.36
33	3	145	4.917	-2	3	0		0.117	86.96	103.40	54.77	97.00	159.48
30	3	145	4.917	-2	3	1		0.123	85.81	102.60	53.97	95.60	159.93
2	3	25	2.072	0	2	0		0.224	89.61	134.60	46.01	128.40	215.73
3	3	25	2.072	0	2	1		0.226	91.50	136.20	46.54	129.40	218.00
4	3	50	2.947	0	2	0		0.214	56.09	92.66	29.63	85.05	164.04
5	3	50	2.947	0	2	1		0.217	55.19	91.70	29.51	83.24	165.11
6	3	100	4.099	0	2	0		0.209	46.69	82.56	23.67	70.81	151.51
7	3	100	4.099	0	2	1		0.210	46.11	82.05	23.67	70.06	150.22
8	3	145	4.917	0	2	0		0.218	42.75	78.20	20.99	66.03	145.60
9	3	145	4.917	0	2	1		0.218	42.85	78.71	21.02	66.45	147.02

Notes: 1. Malvern data file name: cfd31_b.db0

Appendix-B

Table 3. Laser DIffraction Sizing Results (continued).

Run (#)	Peanut (FN)	P avg (psig)	Q (gph)	Y (inches)	Z (inches)	HV (on / off)	comment ()	obscur (%)	MI D32 (microns)	MI D43 (microns)	MI Dv0.1 (microns)	MI Dv0.5 (microns)	MI Dv0.9 (microns)
2	7.4	25	5.238	0	3	0		0.293	98.89	157.00	51.36	142.60	265.59
3	7.4	25	5.238	0	3	1		0.297	99.28	156.90	51.59	142.40	266.59
4	7.4	50	7.513	0	3	0		0.289	66.99	114.40	35.86	96.02	207.50
5	7.4	50	7.513	0	3	1		0.294	66.98	112.10	36.39	94.18	203.83
6	7.4	100	10.560	0	3	0		0.308	53.09	98.49	26.60	79.32	187.87
7	7.4	100	10.560	0	3	1		0.311	53.00	98.34	26.56	78.61	187.86
8	7.4	145	12.710	0	3	0		0.327	47.22	89.82	22.70	72.79	173.01
9	7.4	145	12.710	0	3	1		0.329	47.24	89.85	22.78	72.82	173.69
16	7.4	25	5.303	-2.1	3	0		0.060	118.80	157.30	75.32	137.60	252.07
17	7.4	25	5.303	-2.1	3	1		0.085	104.60	137.10	65.24	117.00	240.36
14	7.4	50	7.478	-2.1	3	0		0.116	100.30	126.90	63.29	113.20	212.52
15	7.4	50	7.478	-2.1	3	1		0.131	94.45	121.90	59.79	105.70	209.12
12	7.4	100	10.560	-2.1	3	0		0.159	93.23	118.60	58.21	106.50	197.34
13	7.4	100	10.560	-2.1	3	1		0.168	91.35	116.90	57.32	103.80	196.65
10	7.4	145	12.710	-2.1	3	0		0.185	93.71	116.40	56.30	106.60	188.72
11	7.4	145	12.710	-2.1	3	1		0.190	92.95	116.00	56.18	105.70	188.66
18	7.4	25	5.303	-3.1	3	0		0.014	119.20	133.20	80.55	125.60	195.30
19	7.4	25	5.303	-3.1	3	1		0.026	100.70	119.10	65.74	106.10	191.41
20	7.4	50	7.374	-3.1	3	1		0.033	94.47	107.00	66.40	94.74	163.63
21	7.4	100	10.560	-3.1	3	0		0.020	90.31	100.40	63.72	92.13	146.98
22	7.4	100	10.560	-3.1	3	1		0.024	87.56	97.85	61.64	88.70	145.26
23	7.4	145	12.710	-3.1	3	1		0.019	84.30	96.47	59.11	87.55	143.40
34	7.4	25	5.303	0	2	0		0.285	101.00	156.70	51.69	145.50	254.79
35	7.4	25	5.303	0	2	1		0.291	100.70	156.60	50.99	145.20	256.59
32	7.4	50	7.409	0	2	0		0.277	72.33	120.70	36.68	109.10	209.66
33	7.4	50	7.409	0	2	1		0.281	72.29	121.40	36.76	109.00	211.39
26	7.4	100	10.560	0	2	0		0.287	57.89	105.50	28.67	94.47	191.95
27	7.4	100	10.560	0	2	1		0.290	56.96	104.20	28.47	93.58	190.17
28	7.4	100	10.560	0	2	0	repeat	0.287	57.83	105.20	28.47	94.23	191.30
30	7.4	100	10.560	0	2	1	repeat	0.288	57.95	105.60	28.81	94.45	192.07
29	7.4	100	10.560	0	2	0	repeat	0.288	57.86	105.10	28.61	94.28	190.86
31	7.4	100	10.560	0	2	1	repeat	0.288	57.74	105.10	28.77	93.95	191.24
24	7.4	145	12.710	0	2	0		0.306	53.13	99.06	25.51	90.53	179.67
25	7.4	145	12.710	0	2	1		0.303	52.84	99.47	25.53	90.02	181.76

Notes: 1. Malvern data file name: cfd31_c.db0

2. A shaded cell indicates flow above the range of the rotometer. Flow was calculated based on pressure from an average flow number for that peanut. The average flow number was calculated from all of the points where a rotometer reading for that peanut could be taken.

Appendix-B

Table 3. Laser Diffraction Sizing Results (concluded).

Run (#)	Peanut (FN)	P avg (psig)	Q (gph)	Y (inches)	Z (inches)	HV (on / off)	comment ()	obscur (%)	MI D32 (microns)	MI D43 (microns)	MI Dv0.1 (microns)	MI Dv0.5 (microns)	MI Dv0.9 (microns)
10	10	25	6.691	0	3	0		0.258	100.30	162.80	51.50	149.20	282.66
11	10	25	6.691	0	3	1		0.263	99.83	162.40	51.34	148.10	285.27
12	10	50	9.336	0	3	0		0.268	73.76	126.60	38.74	109.00	222.95
13	10	50	9.336	0	3	1		0.272	73.43	126.10	38.91	107.50	223.08
14	10	100	13.200	0	3	0		0.292	60.51	113.00	30.05	93.04	210.30
15	10	100	13.200	0	3	1		0.292	60.52	113.10	30.09	92.80	210.53
16	10	145	15.900	0	3	0		0.309	55.18	104.70	26.31	88.07	196.96
17	10	145	15.900	0	3	1		0.309	55.70	107.20	27.06	88.60	201.52
24	10	25	6.556	-2.5	3	0		0.032	135.40	162.80	84.68	151.50	245.45
27	10	25	6.556	-2.5	3	1		0.058	116.90	149.60	69.01	130.50	241.23
25	10	25	6.556	-2.5	3	0	repeat	0.038	134.70	164.40	83.62	151.60	251.41
28	10	25	6.556	-2.5	3	1	repeat	0.057	117.50	151.10	68.77	132.40	243.13
26	10	25	6.556	-2.5	3	0	repeat	0.037	135.70	164.40	85.09	151.60	250.01
29	10	25	6.556	-2.5	3	1	repeat	0.057	117.90	152.10	69.09	132.70	245.60
22	10	50	9.336	-2.5	3	0		0.080	110.90	132.80	69.32	120.10	210.76
23	10	50	9.336	-2.5	3	1		0.096	105.30	128.20	65.56	112.80	208.65
20	10	100	13.200	-2.5	3	0		0.125	101.10	125.50	60.68	112.60	203.67
21	10	100	13.200	-2.5	3	1		0.133	98.84	124.40	59.61	109.20	204.19
18	10	145	15.900	-2.5	3	0		0.160	96.38	121.80	57.78	111.90	196.59
19	10	145	15.900	-2.5	3	1		0.162	96.50	121.50	57.86	111.00	196.51
30	10	25	6.556	-3.5	3	0		0.008	135.30	152.20	92.31	141.60	222.30
31	10	25	6.556	-3.5	3	1		0.020	111.10	133.50	70.75	118.70	210.87
32	10	50	9.336	-3.5	3	1		0.029	102.40	115.30	71.78	103.10	174.88
33	10	100	13.200	-3.5	3	0		0.023	95.26	106.10	68.06	96.16	155.75
34	10	100	13.200	-3.5	3	1		0.029	92.56	103.20	66.32	93.06	152.96
35	10	145	15.900	-3.5	3	1		0.038	91.78	108.50	62.20	99.93	164.43
8	10	25	6.691	0	2	0		0.264	104.10	162.90	52.26	158.50	277.81
9	10	25	6.691	0	2	1		0.269	104.00	163.50	51.73	158.20	280.35
6	10	50	9.336	0	2	0		0.270	80.04	139.20	40.56	125.90	236.40
7	10	50	9.336	0	2	1		0.271	79.88	139.90	40.53	125.40	239.48
3	10	100	13.200	0	2	0		0.288	65.54	122.80	32.56	109.70	216.75
4	10	100	13.200	0	2	1		0.288	65.01	121.90	32.40	108.90	215.64
1	10	145	15.900	0	2	0		0.302	60.94	117.40	29.66	105.00	209.87
5	10	145	15.900	0	2	0		0.301	61.06	116.40	29.73	105.30	207.55
2	10	145	15.900	0	2	1		0.301	60.43	116.70	29.27	104.80	208.95

Notes: 1. Malvern data file name: cfd31_d.db0

2. A shaded cell indicates flow above the range of the rotometer. Flow was calculated based on pressure from an average flow number for that peanut. The average flow number was calculated from all of the points where a rotometer reading for that peanut could be taken.

Appendix-B

Qualitative Optical Patternation Results

After careful consideration of various scenarios for conducting patternation, a quick turnaround, qualitative strategy was selected for the current study. The downstream patternation distance was selected at a location far enough downstream such that the nozzle hardware did not obstruct optical access but not far enough downstream where the spray diameter exceeded the laser sheet width (which was about 5.5 inches). Two axial positions of 2 and 3 inches downstream of the nozzle exit were examined for all cases.

The CCD camera was placed at an angle of 24 degrees above the horizontal (see Figure 1). In each case, 9 images were obtained. The exposure varied from about 0.5 sec to about 4.0 sec in an effort to obtain relatively consistent pixel intensities from case to case. In all cases, at least 4.5 seconds (0.5 sec * 9 images) of data were obtained (the total exposure time associated with all 9 images). The laser power before the collimating lens was maintained at 200 mW.

The data processing involved the following. For each case, the 9 images were averaged. Since the camera obtained images at an angle, the image was affine transformed. A circular mask was placed at the nozzle geometric centerline of the affined image so that the corners of the images were not included in patternation analysis. A mask radius of 240 pixels (about 5.68 inches) was chosen.

The patternation numbers were calculated as follows. The image was divided into eight areas, one circle near the center and seven annular areas. Eight equal radii were suggested by CFD. The eight areas were the same for all the images, chosen from the biggest spray image obtained. For each area, the pixel intensities were summed (denoted as I,s). The total sum was obtained (denoted as I,tot). The patternation number for each of the eight areas was determined as I,s / I,tot * 100.

The results are presented as follows. First, Figure 2 summarizes the image naming scheme. Figure 3 shows an example raw image (FN30Z3P100HV0.SPE), prior to being affine transformed. Figure 4 summarizes the patternation numbering scheme, image scaling, and the intensity color scale. Figure 5 presents the results in the form of affine transformed images and patternation numbers. The Figure 5 results are presented in the order outlined by the test matrix in Table 2. Note that the left panel has the high voltage off (denoted by HV0), while the right panel has the high voltage on (denoted by HV1). Images of the scattering from the droplets were obtained rather than images of fluorescence from the droplets. As a result, the intensities measured are representative of the distribution of surface area rather than mass.

The image results reveal that the lower flow rate sprays are more spread out with the high voltage on. The effect of the high voltage is much less pronounced with the higher flow rate sprays. Some of the sprays were solid cone for all the pressures tested at a given axial plane, while other sprays were hollow cone for all the pressures tested, again, at a given axial plane. Some of the sprays started out as solid cone at the lower pressures and became hollow cones at the higher pressures. Both these results (the spreading and "solidity" of the spray) were consistent with visual observations made during data collection.

It should be noted that the attached results are qualitative, not quantitative. CFDRC requested qualitative results rather than quantitative results, to make the data collection more efficient. Quantitative results can be obtained using advanced data collection and data processing techniques, but such an approach was beyond the scope of the present work. The attached qualitative results must be interpreted with the following clarifications in mind. Great care was taken to create a laser sheet that was uniform ("top hat") in intensity across the sheet

using specialized optics. However, any variations in sheet intensity were not quantified or accounted for in the patternation analysis. Care was taken to maintain constant laser power from image to image, however, again, this was not quantified. The laser sheet intensity is attenuated as it travels through the spray (right to left on the attached images in Figure 5). The scattering signal is attenuated as it travels from the spray to the camera (top to bottom on the attached images in Figure 5). Both the illumination attenuation and signal attenuation affects were not corrected. The presence of these uncontrolled issues must be kept in mind when comparing patternation from various nozzle and conditions.

Despite the purposeful lack of complete treatment of these effects, these particular sprays, combined with the use of the specialized optics, allow for effective use of optical patternation, especially as it is applied to comparative results from various nozzles and conditions tested herein. Although the results are qualitative, they are nonetheless very useful. Images with the high voltage off and then on were taken back to back, thereby minimizing any system variations such as laser power drift, which were not accounted for, as described above.

Comments on Flow Data Uncertainty

Flow meter accuracy and measured repeatability contribute to the overall uncertainty in the in the flow rate. The calibration of the rotometer used to measure the flow rate was recently check using a catch and weigh method taking several points over the entire range of the rotometer. The flow measurement accuracy was 5%. Several conditions were repeated offering data for repeatability analysis. The measured repeatability of the flow settings was within 2.4%. The total uncertainty in the flow rates is +/- 7.4%. The repeatability was clearly quite good and the majority of the flow rate uncertainty is associated with the flowmeter accuracy.

The water pressure gauges chosen were grade B which are accurate to ± 2% of the middle portion of the scale (the portion of the scale at which many of the measurements were made).

Comments on Laser Diffraction Data Uncertainty

Prior to application to the current project, the alignment and measurement accuracy of the laser diffraction system was checked using a calibration reticle. This reticule consists of a known particle size distribution deposited onto a piece of glass. The particular reticule used has a Rosin Rammler particle size distribution with X = 50 and N = 2. The reticule is used by placing it in the path of the beam and measuring the size as would be done with a spray. The results of the reticule sizing were consistent with past experience with this particular reticule (i.e., X values were 50 +/-2 and N was 2.2). This calibration remained similar for both charged and uncharged sprays and these measurements were typically taken "back to back" to minimize the effect of any random errors.

In addition to absolute accuracy, repeatability of the measurements was assessed for select conditions. Based on 8 conditions which were each repeated twice (thereby providing three measurements of the same condition), the average variation in the measured SMD (based on Model Independent treatment) was 0.92% of the measured SMD. This repeatability is ver good.

Appendix B

Comments on Qualitative Optical Patternation Data Uncertainty

The qualitative optical patternation is indeed qualitative. The analysis conducted was directed at allowing comparison between the global features of the spray with and without charging. The utility of the images is the direct comparison of the uncharged and right charged spray structures. Images for each condition were taken back to back for cases with and without charge to minimize any random errors. Care was taken to minimize the effects of laser sheet intensity variation and energy drift, but they were not explicitly monitored. As was discussed in the section Qualitative Optical Patternation Results, care should be taken when considering symmetry features. Additional details can be found in the section Qualitative Optical Patternation Results.

Electronic Data

A CD is attached at the end of this report. It contains this report in Word 97 format. Any tables contained in the Word file can be copied to an Excel file if desired. Any images contained in the Word file can be copied to other places as needed. The CD also contains and Excel file, previously submitted to CFDRC, that summarizes the laser diffraction results. Finally, the CD contained a series of digital images obtained by CFDRC during the testing and previously submitted to CFDRC.

```
FN05Z3P25HV0.SPE
|    | |  |
|    | |  |
|    | |  High voltage
|    | |  0 for off
|    | |  1 for on
|    | |
|    | Pressure
|    | 25  for  25 psig
|    | 50  for  50 psig
|    | 100 for 100 psig
|    | 145 for 145 psig
|    |
|   Axial Position
|   2 for 2 inches downstream
|   3 for 3 inches downstream
|
Flow number
05 for 0.5
10 for 1.0
30 for 3.0
74 for 7.4
```

Figure 2. Image Naming Scheme.

Appendix B

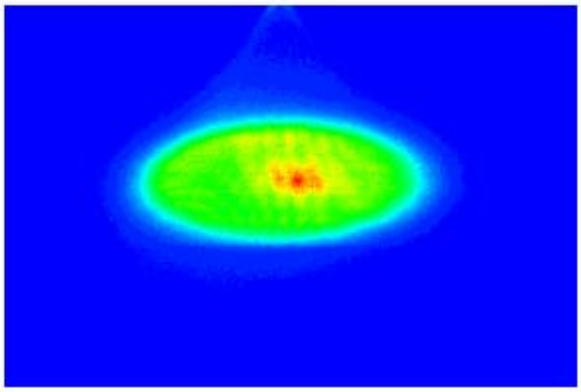

Figure 3. Raw Image, Prior to Affine Transform (FN30Z3P100HV0.SPE).

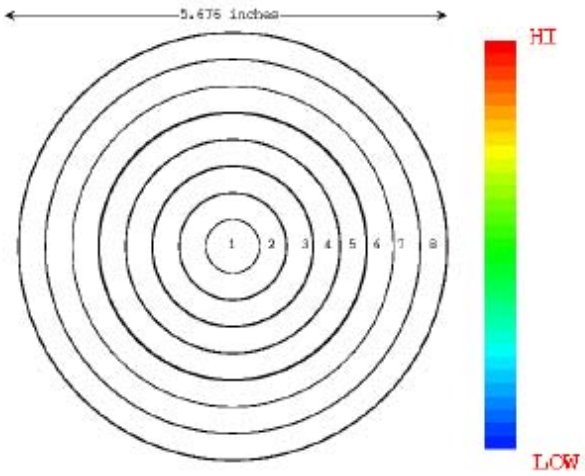

Figure 4. Patternation Numbering Scheme, Image Scale, and Intensity Scale.

Appendix B

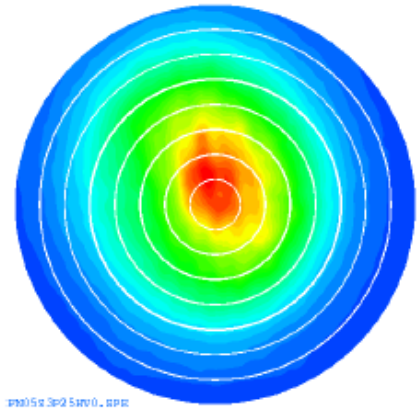

FN05Z3P25HV0.SPE

RING#	I,s	I,s/I,tot (%)
1	1.97969E+07	4.61
2	5.17662E+07	12.05
3	7.09702E+07	16.52
4	7.64231E+07	17.79
5	7.06724E+07	16.45
6	5.78486E+07	13.47
7	4.53542E+07	10.56
8	3.66680E+07	8.54

I,tot = 4.29500E+08

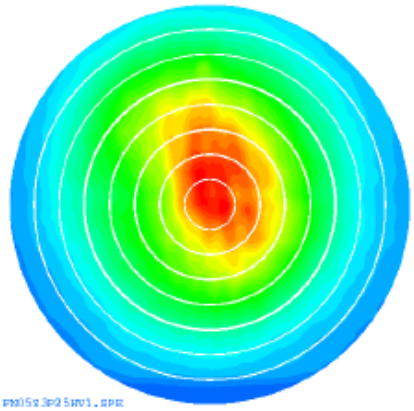

FN05Z3P25HV1.SPE

RING#	I,s	I,s/I,tot (%)
1	2.21136E+07	3.59
2	5.90367E+07	9.59
3	8.57843E+07	13.94
4	9.98985E+07	16.23
5	1.01750E+08	16.53
6	9.38039E+07	15.24
7	8.26377E+07	13.43
8	7.04666E+07	11.45

I,tot = 6.15492E+08

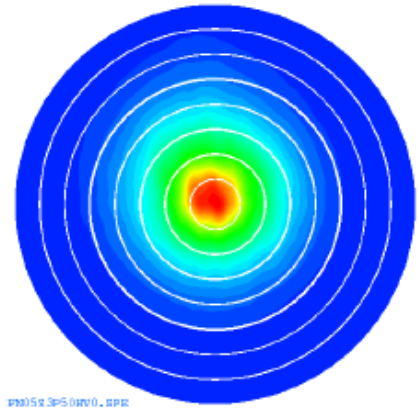

FN05Z3P50HV0.SPE

RING#	I,s	I,s/I,tot (%)
1	4.46818E+07	10.61
2	8.64304E+07	20.53
3	8.49681E+07	20.18
4	6.93742E+07	16.47
5	5.01124E+07	11.90
6	3.51494E+07	8.35
7	2.68552E+07	6.38
8	2.35212E+07	5.59

I,tot = 4.21093E+08

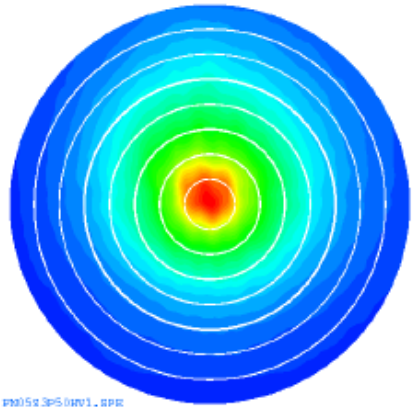

FN05Z3P50HV1.SPE

RING#	I,s	I,s/I,tot (%)
1	4.43360E+07	6.32
2	9.74018E+07	13.89
3	1.13653E+08	16.21
4	1.12184E+08	16.00
5	1.02313E+08	14.59
6	8.91672E+07	12.71
7	7.68362E+07	10.96
8	6.54398E+07	9.33

I,tot = 7.01332E+08

Figure 5. Results.

Appendix B

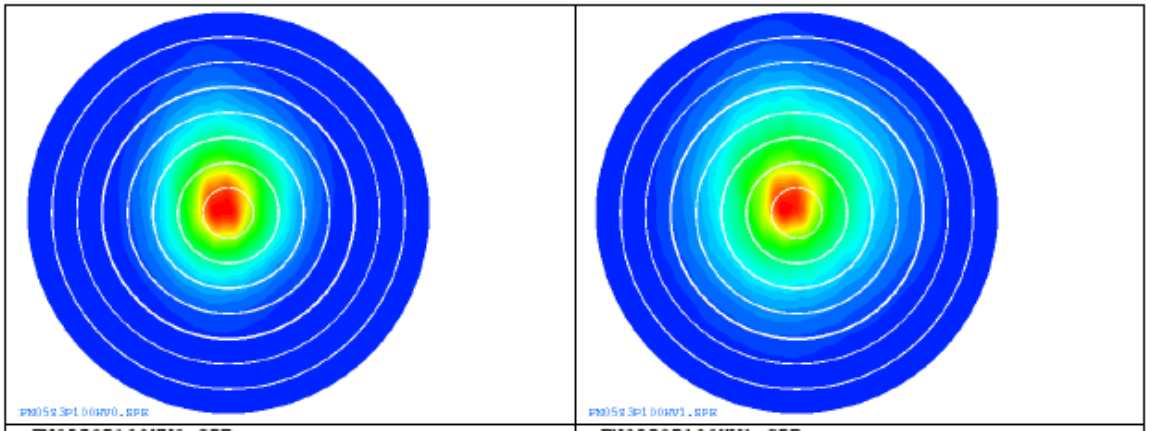

FN05Z3P100HV0.SPE

RING#	I,s	I,s/I,tot (%)
1	6.05167E+07	12.63
2	1.16634E+08	24.35
3	1.05038E+08	21.93
4	7.66802E+07	16.01
5	5.05137E+07	10.54
6	3.17232E+07	6.62
7	2.11902E+07	4.42
8	1.67446E+07	3.50
I,tot =	4.79041E+08	

FN05Z3P100HV1.SPE

RING#	I,s	I,s/I,tot (%)
1	5.27019E+07	8.78
2	1.08415E+08	18.06
3	1.15673E+08	19.27
4	1.05467E+08	17.57
5	8.59299E+07	14.31
6	6.20996E+07	10.35
7	4.16414E+07	6.94
8	2.83521E+07	4.72
I,tot =	6.00280E+08	

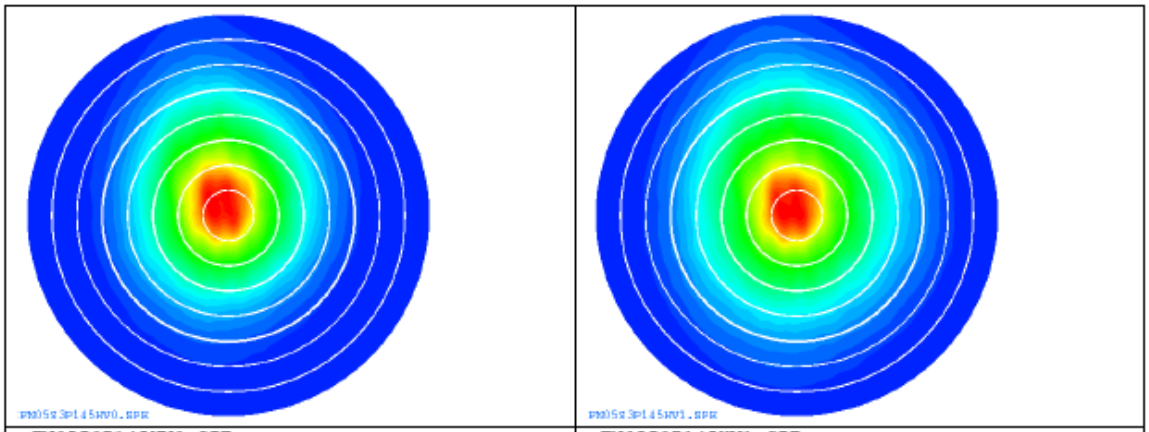

FN05Z3P145HV0.SPE

RING#	I,s	I,s/I,tot (%)
1	6.28368E+07	8.48
2	1.42531E+08	19.22
3	1.58949E+08	21.44
4	1.38993E+08	18.75
5	1.02780E+08	13.86
6	6.70096E+07	9.04
7	4.11382E+07	5.55
8	2.71677E+07	3.66
I,tot =	7.41405E+08	

FN05Z3P145HV1.SPE

RING#	I,s	I,s/I,tot (%)
1	6.07618E+07	7.06
2	1.37119E+08	15.93
3	1.61930E+08	18.81
4	1.60623E+08	18.66
5	1.37516E+08	15.98
6	1.00588E+08	11.69
7	6.36983E+07	7.40
8	3.85224E+07	4.48
I,tot =	8.60758E+08	

Figure 5. Results (continued).

Appendix B

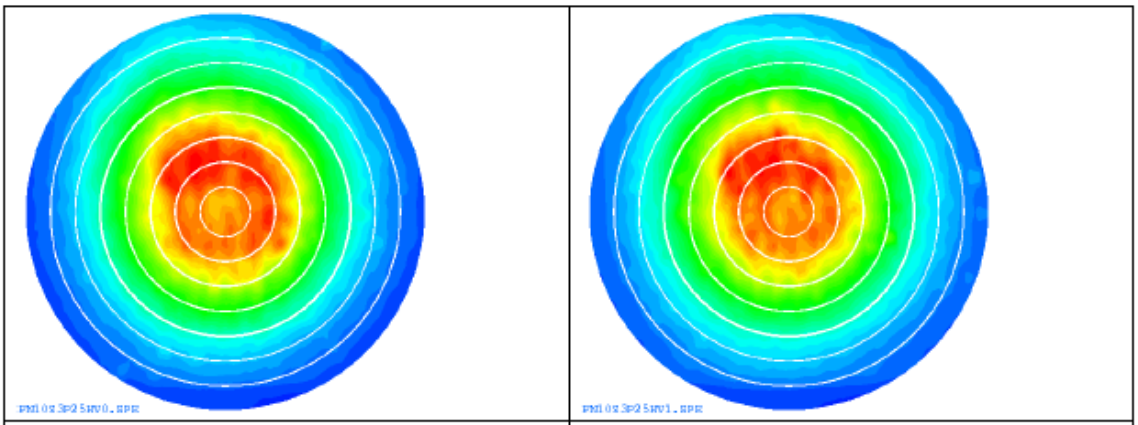

FN10Z3P25HV0.SPE

RING#	I,s	I,s/I,tot (%)
1	1.43594E+07	3.44
2	4.58393E+07	10.99
3	7.16826E+07	17.18
4	7.89812E+07	18.93
5	7.17099E+07	17.19
6	5.77117E+07	13.83
7	4.44013E+07	10.64
8	3.25917E+07	7.81
I,tot =	4.17277E+08	

FN10Z3P25HV1.SPE

RING#	I,s	I,s/I,tot (%)
1	1.45985E+07	3.45
2	4.50687E+07	10.65
3	6.98196E+07	16.49
4	7.72070E+07	18.24
5	7.24990E+07	17.13
6	6.02392E+07	14.23
7	4.78479E+07	11.30
8	3.60424E+07	8.51
I,tot =	4.23322E+08	

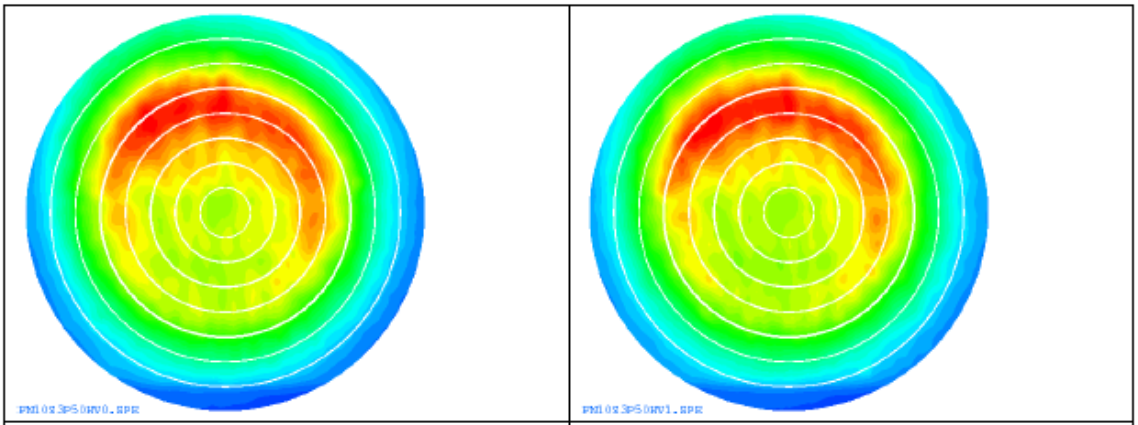

FN10Z3P50HV0.SPE

RING#	I,s	I,s/I,tot (%)
1	1.11098E+07	2.01
2	3.53496E+07	6.41
3	6.02936E+07	10.94
4	9.06525E+07	16.44
5	1.14346E+08	20.74
6	1.05366E+08	19.11
7	7.92882E+07	14.38
8	5.49735E+07	9.97
I,tot =	5.51379E+08	

FN10Z3P50HV1.SPE

RING#	I,s	I,s/I,tot (%)
1	1.09632E+07	1.96
2	3.46523E+07	6.20
3	5.92322E+07	10.60
4	9.02443E+07	16.15
5	1.15327E+08	20.64
6	1.07462E+08	19.23
7	8.27990E+07	14.82
8	5.81894E+07	10.41
I,tot =	5.58869E+08	

Figure 5. Results (continued).

Appendix B

Appendix B

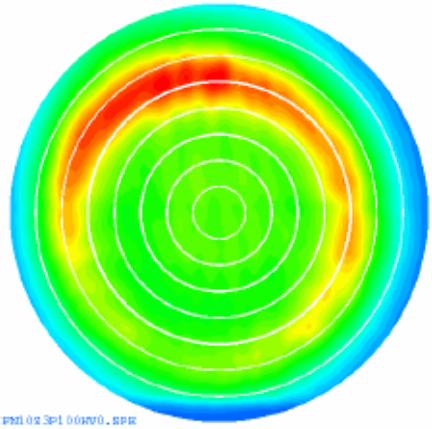

FN10Z3P100HV0.SPE

RING#	I,s	I,s/I,tot (%)
1	3.34705E+07	1.67
2	1.01752E+08	5.07
3	1.62540E+08	8.10
4	2.30131E+08	11.47
5	3.57424E+08	17.81
6	4.78477E+08	23.84
7	4.01911E+08	20.02
8	2.41350E+08	12.03

I,tot = 2.00705E+09

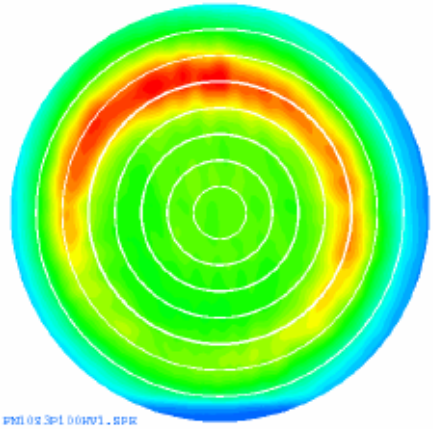

FN10Z3P100HV1.SPE

RING#	I,s	I,s/I,tot (%)
1	3.29791E+07	1.65
2	9.97132E+07	4.99
3	1.59943E+08	8.00
4	2.27676E+08	11.39
5	3.54422E+08	17.74
6	4.72324E+08	23.64
7	4.02545E+08	20.15
8	2.48620E+08	12.44

I,tot = 1.99822E+09

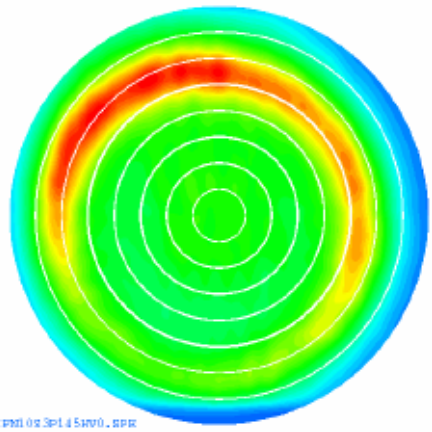

FN10Z3P145HV0.SPE

RING#	I,s	I,s/I,tot (%)
1	3.04229E+07	1.58
2	9.04904E+07	4.69
3	1.42480E+08	7.38
4	1.96551E+08	10.18
5	2.99032E+08	15.49
6	4.63560E+08	24.02
7	4.48944E+08	23.26
8	2.58599E+08	13.40

I,tot = 1.93008E+09

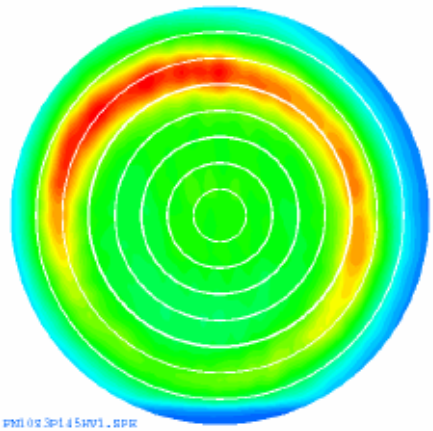

FN10Z3P145HV1.SPE

RING#	I,s	I,s/I,tot (%)
1	3.07953E+07	1.57
2	9.16441E+07	4.69
3	1.44308E+08	7.38
4	1.99264E+08	10.19
5	3.03455E+08	15.51
6	4.70037E+08	24.03
7	4.54721E+08	23.25
8	2.61719E+08	13.38

I,tot = 1.95594E+09

Figure 5. Results (continued).

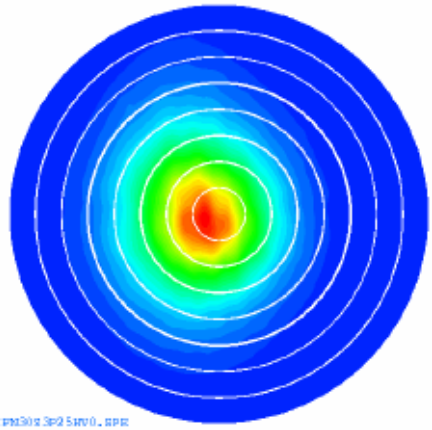

FN30Z3P25HV0.SPE

RING#	I,s	I,s/I,tot (%)
1	4.67611E+07	9.24
2	1.06974E+08	21.13
3	1.11030E+08	21.93
4	8.68815E+07	17.16
5	6.19829E+07	12.24
6	4.19161E+07	8.28
7	2.88794E+07	5.70
8	2.17931E+07	4.31
I,tot =	5.06218E+08	

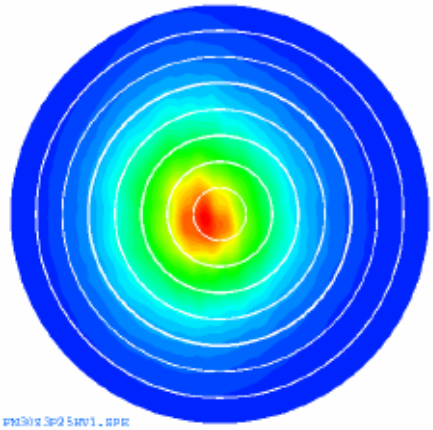

FN30Z3P25HV1.SPE

RING#	I,s	I,s/I,tot (%)
1	4.18491E+07	7.26
2	1.00031E+08	17.36
3	1.13451E+08	19.69
4	1.01529E+08	17.62
5	8.25561E+07	14.33
6	6.14696E+07	10.67
7	4.39123E+07	7.62
8	3.14610E+07	5.46
I,tot =	5.76259E+08	

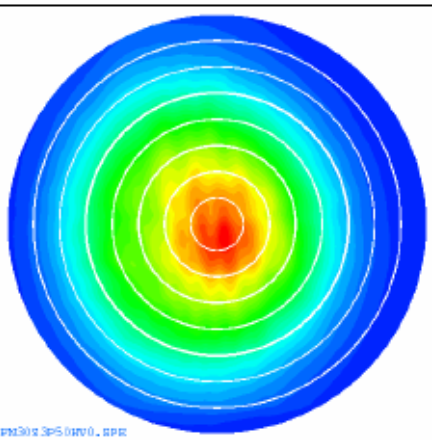

FN30Z3P50HV0.SPE

RING#	I,s	I,s/I,tot (%)
1	7.08054E+07	4.69
2	1.91168E+08	12.66
3	2.66649E+08	17.66
4	2.91175E+08	19.28
5	2.66212E+08	17.63
6	2.02150E+08	13.38
7	1.36964E+08	9.07
8	8.51836E+07	5.64
I,tot =	1.51031E+09	

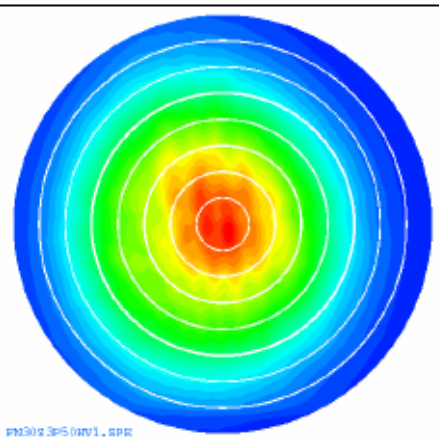

FN30Z3P50HV1.SPE

RING#	I,s	I,s/I,tot (%)
1	6.95010E+07	4.36
2	1.87793E+08	11.78
3	2.68589E+08	16.85
4	3.03988E+08	19.07
5	2.87344E+08	18.02
6	2.24682E+08	14.09
7	1.55406E+08	9.75
8	9.69638E+07	6.08
I,tot =	1.59427E+09	

Figure 5. Results (continued).

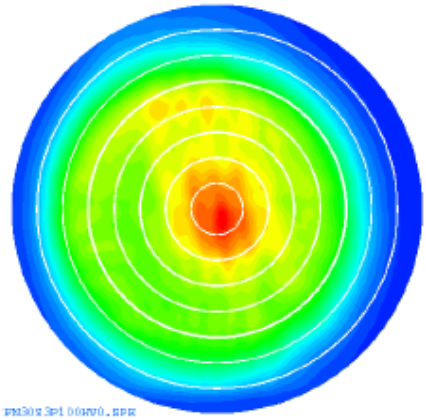

FN30Z3P100HV0.SPE

RING#	I,s	I,s/I,tot (%)
1	6.57380E+07	3.36
2	1.74515E+08	8.91
3	2.55675E+08	13.06
4	3.35254E+08	17.12
5	4.06896E+08	20.78
6	3.78069E+08	19.31
7	2.31482E+08	11.82
8	1.10476E+08	5.64

I,tot = 1.95811E+09

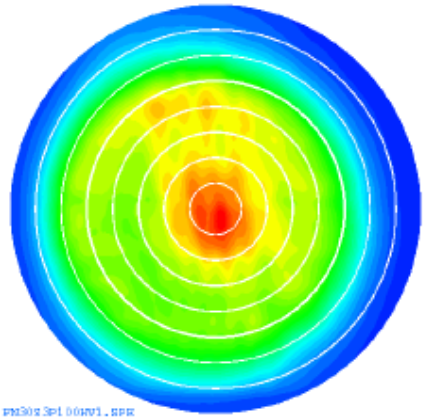

FN30Z3P100HV1.SPE

RING#	I,s	I,s/I,tot (%)
1	6.58259E+07	3.29
2	1.75526E+08	8.77
3	2.58143E+08	12.89
4	3.40795E+08	17.02
5	4.16614E+08	20.80
6	3.89631E+08	19.46
7	2.40602E+08	12.01
8	1.15419E+08	5.76

I,tot = 2.00256E+09

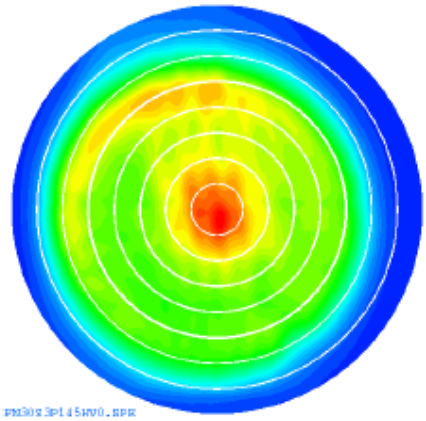

FN30Z3P145HV0.SPE

RING#	I,s	I,s/I,tot (%)
1	7.46096E+07	3.29
2	1.92729E+08	8.49
3	2.78137E+08	12.25
4	3.63527E+08	16.01
5	4.72939E+08	20.83
6	4.92880E+08	21.71
7	2.82967E+08	12.47
8	1.12146E+08	4.94

I,tot = 2.26993E+09

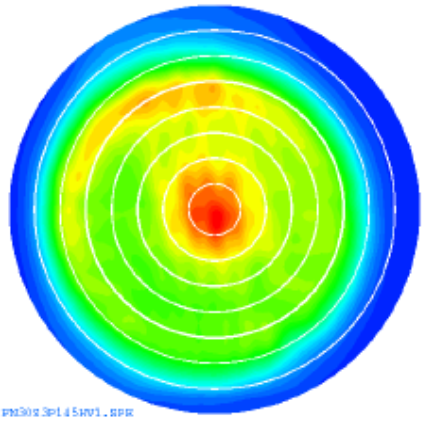

FN30Z3P145HV1.SPE

RING#	I,s	I,s/I,tot (%)
1	7.46996E+07	3.26
2	1.92854E+08	8.42
3	2.78710E+08	12.17
4	3.66033E+08	15.98
5	4.78053E+08	20.87
6	4.98099E+08	21.75
7	2.87354E+08	12.55
8	1.14697E+08	5.01

I,tot = 2.29050E+09

Figure 5. Results (continued).

Appendix B

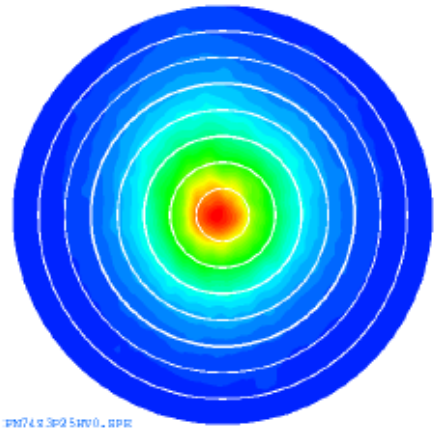

FN74Z3P25HV0.SPE

RING#	I,s	I,s/I,tot (%)
1	2.90428E+07	8.48
2	6.22160E+07	18.17
3	6.51285E+07	19.02
4	5.58009E+07	16.30
5	4.54027E+07	13.26
6	3.55689E+07	10.39
7	2.77839E+07	8.12
8	2.14315E+07	6.26
I,tot =	3.42375E+08	

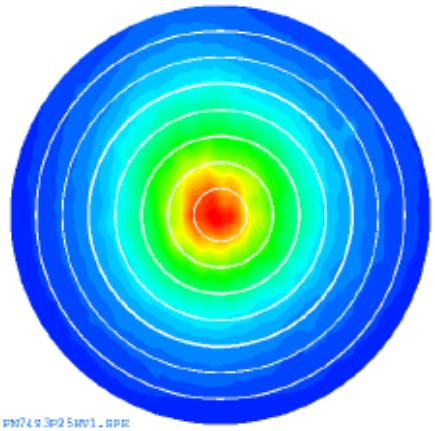

FN74Z3P25HV1.SPE

RING#	I,s	I,s/I,tot (%)
1	2.40303E+07	6.47
2	5.74188E+07	15.47
3	6.67683E+07	17.99
4	6.12308E+07	16.50
5	5.31064E+07	14.31
6	4.45259E+07	12.00
7	3.59013E+07	9.67
8	2.81596E+07	7.59
I,tot =	3.71141E+08	

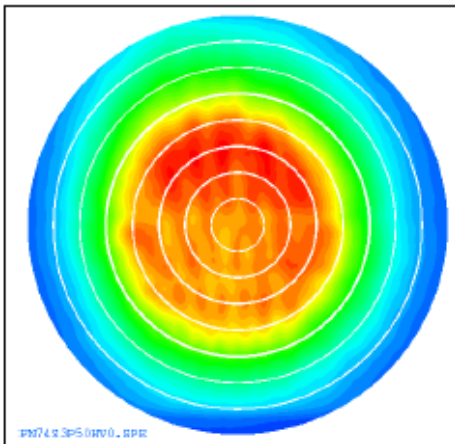

FN74Z3P50HV0.SPE

RING#	I,s	I,s/I,tot (%)
1	4.79857E+07	2.68
2	1.47876E+08	8.26
3	2.53240E+08	14.15
4	3.42160E+08	19.12
5	3.50149E+08	19.56
6	2.85325E+08	15.94
7	2.13348E+08	11.92
8	1.49830E+08	8.37
I,tot =	1.78991E+09	

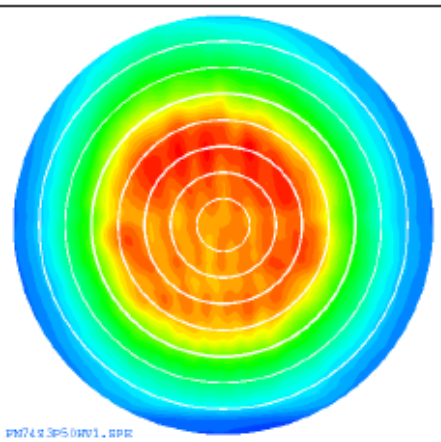

FN74Z3P50HV1.SPE

RING#	I,s	I,s/I,tot (%)
1	4.74161E+07	2.60
2	1.44699E+08	7.93
3	2.48930E+08	13.64
4	3.41880E+08	18.73
5	3.55961E+08	19.50
6	2.97638E+08	16.30
7	2.27145E+08	12.44
8	1.61956E+08	8.87
I,tot =	1.82563E+09	

Figure 5. Results (continued).

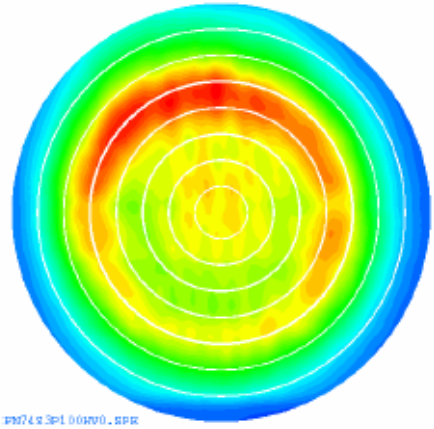

FN74Z3P100HV0.SPE

RING#	I,s	I,s/I,tot (%)
1	5.16955E+07	2.18
2	1.51060E+08	6.38
3	2.39431E+08	10.11
4	3.44814E+08	14.56
5	5.01120E+08	21.16
6	5.12306E+08	21.63
7	3.54935E+08	14.99
8	2.12684E+08	8.98
I,tot =	2.36805E+09	

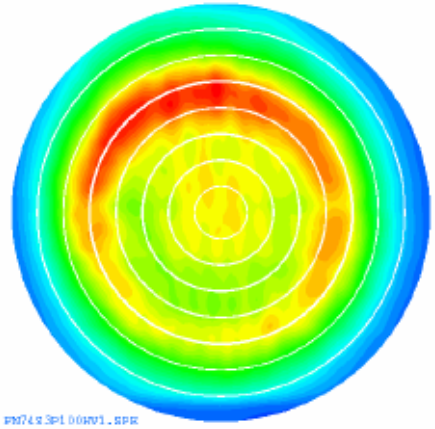

FN74Z3P100HV1.SPE

RING#	I,s	I,s/I,tot (%)
1	5.16846E+07	2.16
2	1.50724E+08	6.29
3	2.38938E+08	9.97
4	3.45427E+08	14.41
5	5.04640E+08	21.05
6	5.21487E+08	21.75
7	3.64330E+08	15.20
8	2.20285E+08	9.19
I,tot =	2.39752E+09	

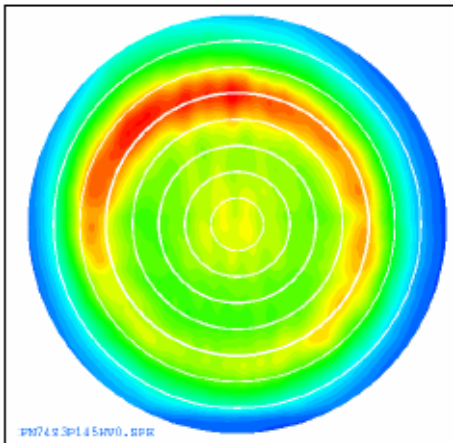

FN74Z3P145HV0.SPE

RING#	I,s	I,s/I,tot (%)
1	4.32580E+07	2.11
2	1.22713E+08	6.00
3	1.90085E+08	9.29
4	2.63233E+08	12.86
5	4.02731E+08	19.68
6	4.93789E+08	24.13
7	3.46721E+08	16.94
8	1.83789E+08	8.98
I,tot =	2.04632E+09	

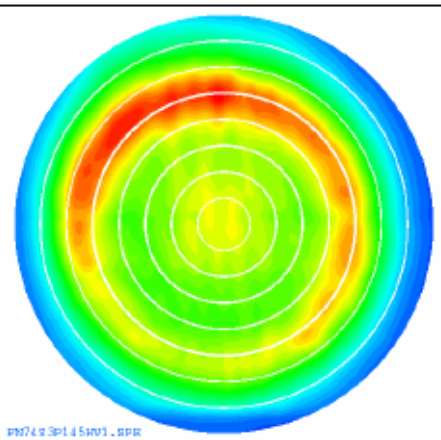

FN74Z3P145HV1.SPE

RING#	I,s	I,s/I,tot (%)
1	4.31658E+07	2.10
2	1.22871E+08	5.97
3	1.90138E+08	9.24
4	2.63677E+08	12.82
5	4.04037E+08	19.65
6	4.96499E+08	24.14
7	3.49690E+08	17.00
8	1.86595E+08	9.07
I,tot =	2.05667E+09	

Figure 5. Results (continued).

Appendix B

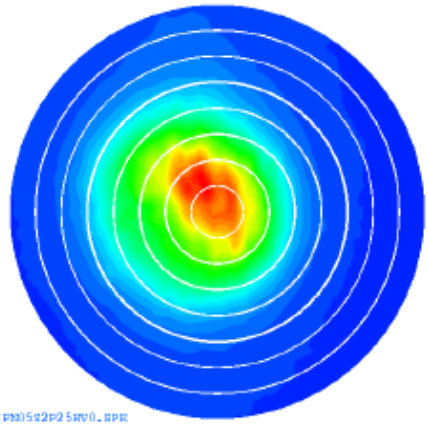

FN05Z2P25HV0.SPE

RING#	I,s	I,s/I,tot (%)
1	1.36757E+07	7.05
2	3.45786E+07	17.83
3	3.88021E+07	20.00
4	3.27846E+07	16.90
5	2.42765E+07	12.51
6	1.81366E+07	9.35
7	1.58591E+07	8.18
8	1.58700E+07	8.18
I,tot =	1.93983E+08	

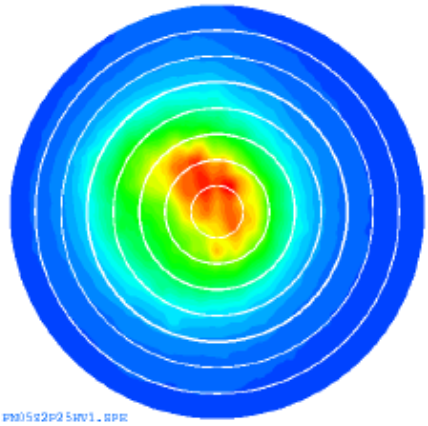

FN05Z2P25HV1.SPE

RING#	I,s	I,s/I,tot (%)
1	1.12074E+07	5.85
2	2.96817E+07	15.50
3	3.53503E+07	18.46
4	3.24392E+07	16.94
5	2.66471E+07	13.91
6	2.10999E+07	11.02
7	1.80759E+07	9.44
8	1.70329E+07	8.89
I,tot =	1.91534E+08	

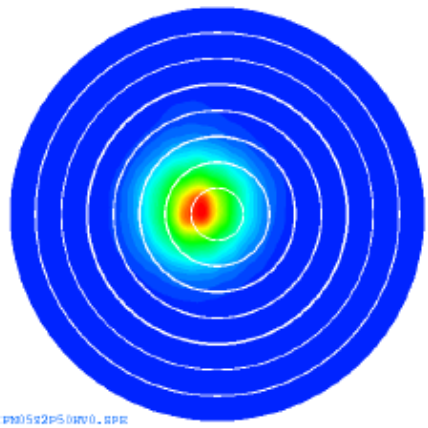

FN05Z2P50HV0.SPE

RING#	I,s	I,s/I,tot (%)
1	3.75188E+07	15.09
2	6.85156E+07	27.56
3	5.03800E+07	20.27
4	2.87844E+07	11.58
5	1.82081E+07	7.32
6	1.49673E+07	6.02
7	1.47252E+07	5.92
8	1.54790E+07	6.23
I,tot =	2.48578E+08	

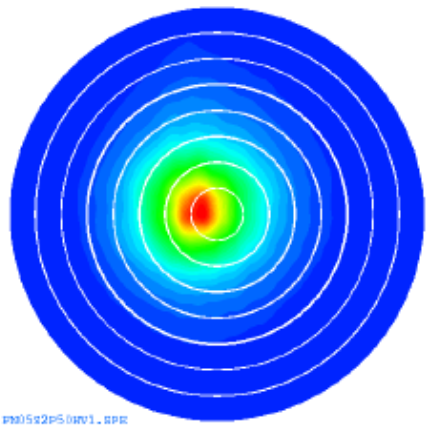

FN05Z2P50HV1.SPE

RING#	I,s	I,s/I,tot (%)
1	3.28137E+07	10.34
2	6.74335E+07	21.25
3	6.34110E+07	19.98
4	4.84304E+07	15.26
5	3.60241E+07	11.35
6	2.73074E+07	8.60
7	2.22300E+07	7.00
8	1.97550E+07	6.22
I,tot =	3.17405E+08	

Figure 5. Results (continued).

Appendix B

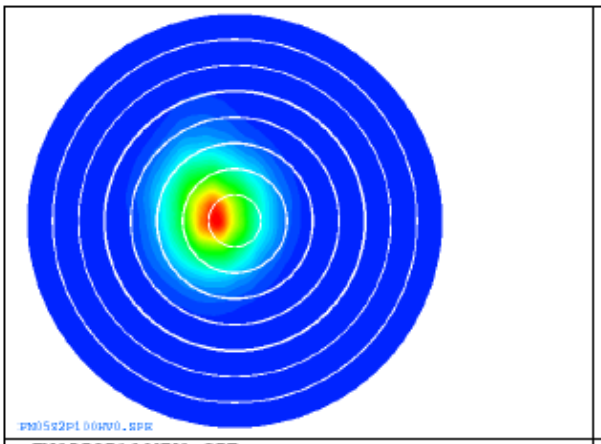

FN05Z2P100HV0.SPE

RING#	I,s	I,s/I,tot (%)
1	3.77920E+07	14.80
2	7.37175E+07	28.87
3	5.69091E+07	22.29
4	3.31736E+07	12.99
5	1.88599E+07	7.39
6	1.28297E+07	5.02
7	1.11392E+07	4.36
8	1.09007E+07	4.27

I,tot = 2.55322E+08

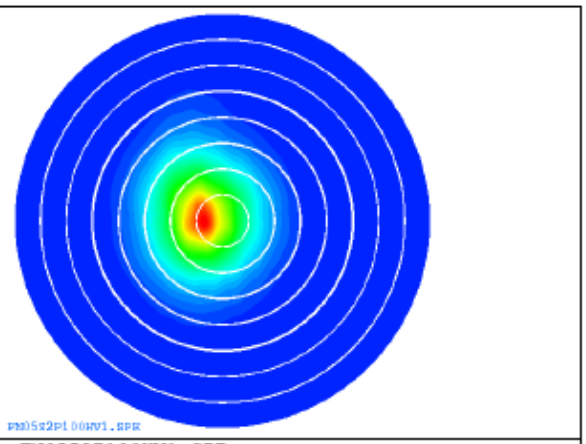

FN05Z2P100HV1.SPE

RING#	I,s	I,s/I,tot (%)
1	5.02362E+07	13.71
2	1.01849E+08	27.80
3	8.61332E+07	23.51
4	5.34964E+07	14.60
5	2.91000E+07	7.94
6	1.77595E+07	4.85
7	1.43467E+07	3.92
8	1.34982E+07	3.68

I,tot = 3.66420E+08

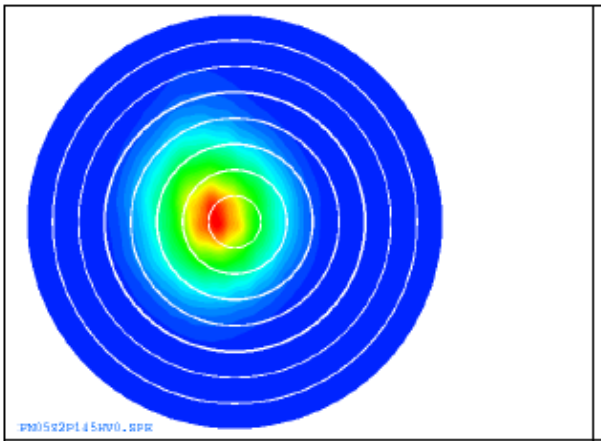

FN05Z2P145HV0.SPE

RING#	I,s	I,s/I,tot (%)
1	5.56405E+07	11.62
2	1.21201E+08	25.32
3	1.15802E+08	24.19
4	8.00257E+07	16.72
5	4.59522E+07	9.60
6	2.58961E+07	5.41
7	1.83486E+07	3.83
8	1.58245E+07	3.31

I,tot = 4.78690E+08

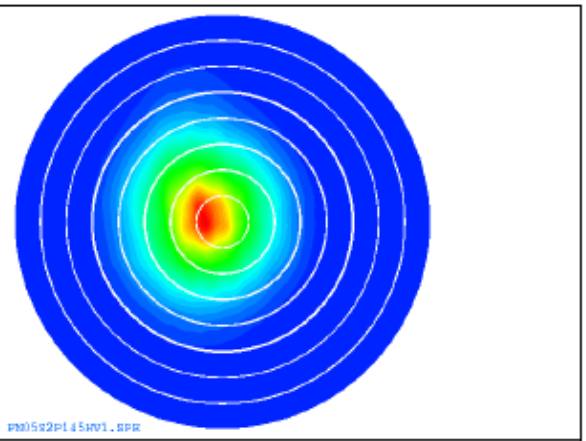

FN05Z2P145HV1.SPE

RING#	I,s	I,s/I,tot (%)
1	5.67075E+07	11.17
2	1.23409E+08	24.32
3	1.22714E+08	24.18
4	8.91952E+07	17.57
5	5.14981E+07	10.15
6	2.80692E+07	5.53
7	1.93828E+07	3.82
8	1.65567E+07	3.26

I,tot = 5.07533E+08

Figure 5. Results (continued).

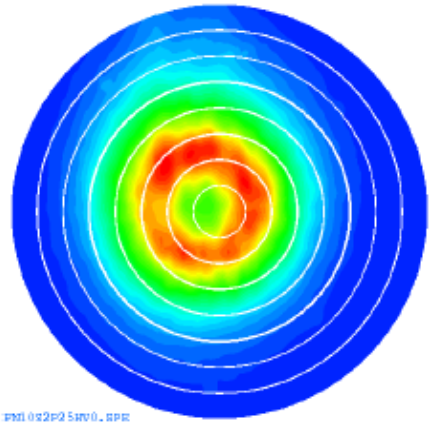

FN10Z2P25HV0.SPE

RING#	I,s	I,s/I,tot (%)
1	3.36020E+07	4.39
2	1.19005E+08	15.54
3	1.79105E+08	23.38
4	1.61598E+08	21.10
5	1.14207E+08	14.91
6	7.33595E+07	9.58
7	4.93406E+07	6.44
8	3.57719E+07	4.67

I,tot = 7.65989E+08

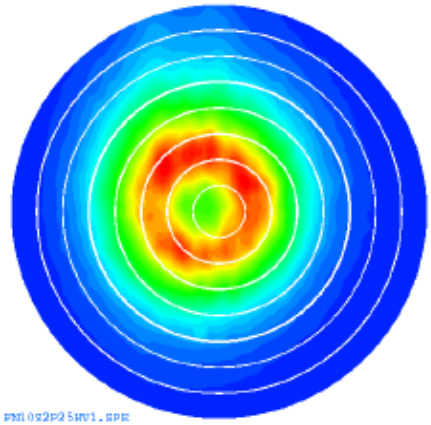

FN10Z2P25HV1.SPE

RING#	I,s	I,s/I,tot (%)
1	3.34174E+07	4.25
2	1.18792E+08	15.11
3	1.79448E+08	22.82
4	1.64709E+08	20.95
5	1.18472E+08	15.07
6	7.82953E+07	9.96
7	5.36127E+07	6.82
8	3.95017E+07	5.02

I,tot = 7.86248E+08

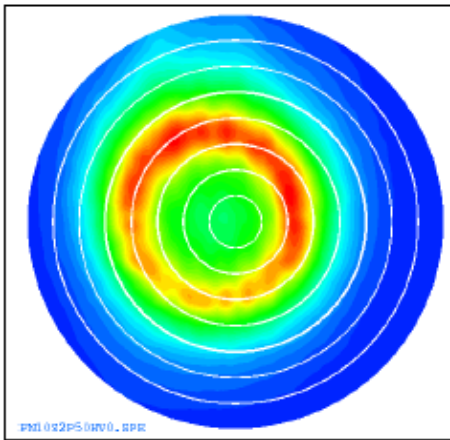

FN10Z2P50HV0.SPE

RING#	I,s	I,s/I,tot (%)
1	2.22992E+07	2.25
2	8.24221E+07	8.30
3	1.78115E+08	17.94
4	2.36893E+08	23.86
5	2.06628E+08	20.81
6	1.30441E+08	13.14
7	8.10917E+07	8.17
8	5.50023E+07	5.54

I,tot = 9.92893E+08

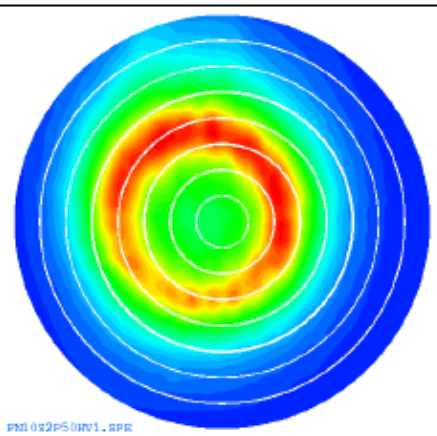

FN10Z2P50HV1.SPE

RING#	I,s	I,s/I,tot (%)
1	2.22034E+07	2.21
2	8.21407E+07	8.17
3	1.78235E+08	17.72
4	2.38570E+08	23.72
5	2.09916E+08	20.87
6	1.33538E+08	13.28
7	8.38412E+07	8.34
8	5.71505E+07	5.68

I,tot = 1.00560E+09

Figure 5. Results (continued).

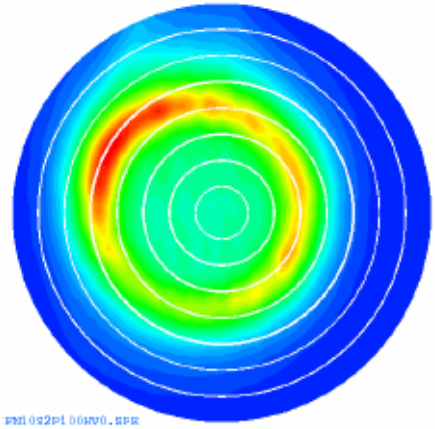

FN10Z2P100HV0.SPE

RING#	I,s	I,s/I,tot (%)
1	2.35463E+07	1.89
2	7.54287E+07	6.05
3	1.63107E+08	13.07
4	2.83375E+08	22.71
5	3.15787E+08	25.31
6	2.11268E+08	16.93
7	1.08921E+08	8.73
8	6.61302E+07	5.30
I,tot =	1.24756E+09	

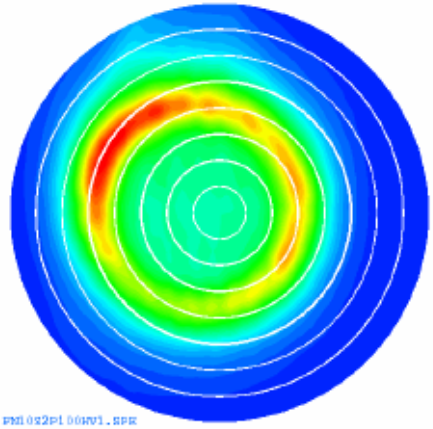

FN10Z2P100HV1.SPE

RING#	I,s	I,s/I,tot (%)
1	2.36422E+07	1.88
2	7.57525E+07	6.04
3	1.63430E+08	13.02
4	2.84176E+08	22.64
5	3.17946E+08	25.33
6	2.12964E+08	16.97
7	1.10000E+08	8.76
8	6.71440E+07	5.35
I,tot =	1.25505E+09	

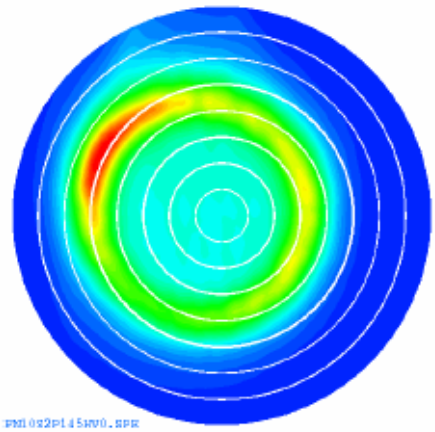

FN10Z2P145HV0.SPE

RING#	I,s	I,s/I,tot (%)
1	1.91179E+07	1.81
2	5.92696E+07	5.61
3	1.18827E+08	11.25
4	2.34047E+08	22.16
5	2.77393E+08	26.27
6	2.04062E+08	19.32
7	9.16845E+07	8.68
8	5.15710E+07	4.88
I,tot =	1.05597E+09	

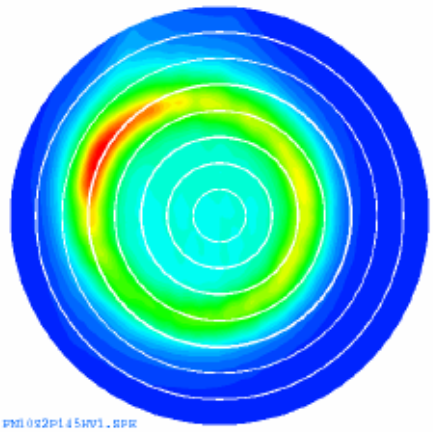

FN10Z2P145HV1.SPE

RING#	I,s	I,s/I,tot (%)
1	1.93575E+07	1.82
2	5.99000E+07	5.63
3	1.20031E+08	11.28
4	2.36463E+08	22.21
5	2.79775E+08	26.28
6	2.04434E+08	19.21
7	9.24507E+07	8.69
8	5.20515E+07	4.89
I,tot =	1.06446E+09	

Figure 5. Results (continued).

Appendix B

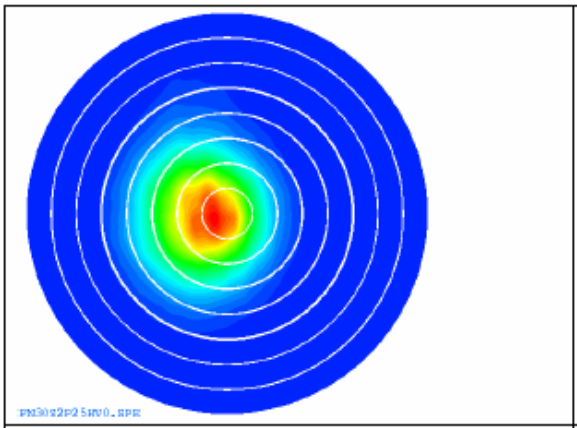

FN30Z2P25HV0.SPE

RING#	I,s	I,s/I,tot (%)
1	3.87162E+07	12.28
2	8.04657E+07	25.52
3	7.45558E+07	23.65
4	4.87247E+07	15.45
5	2.81904E+07	8.94
6	1.76043E+07	5.58
7	1.40020E+07	4.44
8	1.30530E+07	4.14
I,tot =	3.15312E+08	

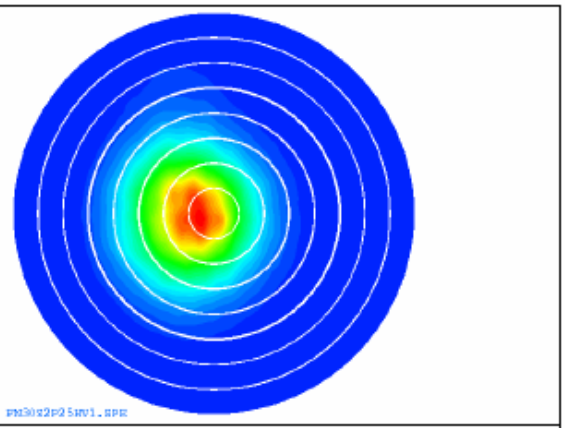

FN30Z2P25HV1.SPE

RING#	I,s	I,s/I,tot (%)
1	3.71249E+07	11.04
2	8.03301E+07	23.88
3	7.88721E+07	23.45
4	5.54096E+07	16.47
5	3.39723E+07	10.10
6	2.09429E+07	6.23
7	1.57256E+07	4.68
8	1.39778E+07	4.16
I,tot =	3.36355E+08	

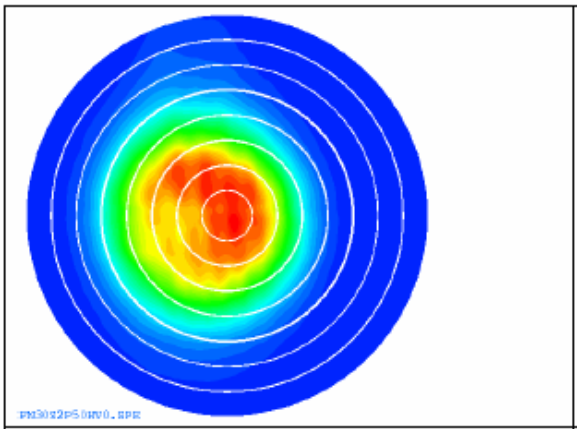

FN30Z2P50HV0.SPE

RING#	I,s	I,s/I,tot (%)
1	5.35496E+07	6.47
2	1.48617E+08	17.96
3	1.97118E+08	23.82
4	1.79409E+08	21.68
5	1.17595E+08	14.21
6	6.34354E+07	7.66
7	3.86547E+07	4.67
8	2.92476E+07	3.53
I,tot =	8.27626E+08	

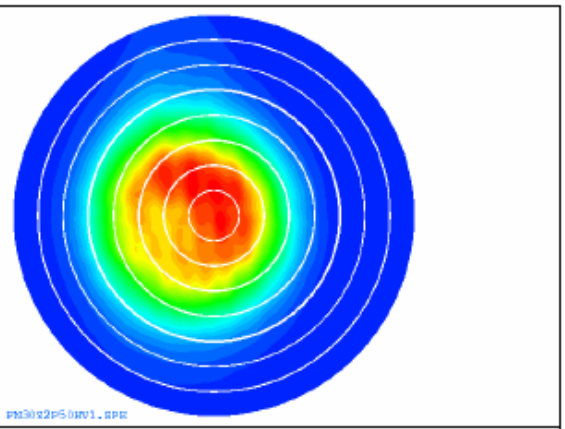

FN30Z2P50HV1.SPE

RING#	I,s	I,s/I,tot (%)
1	5.32411E+07	6.26
2	1.49419E+08	17.57
3	2.01389E+08	23.68
4	1.85684E+08	21.83
5	1.23068E+08	14.47
6	6.69308E+07	7.87
7	4.05073E+07	4.76
8	3.01855E+07	3.55
I,tot =	8.50426E+08	

Figure 5. Results (continued).

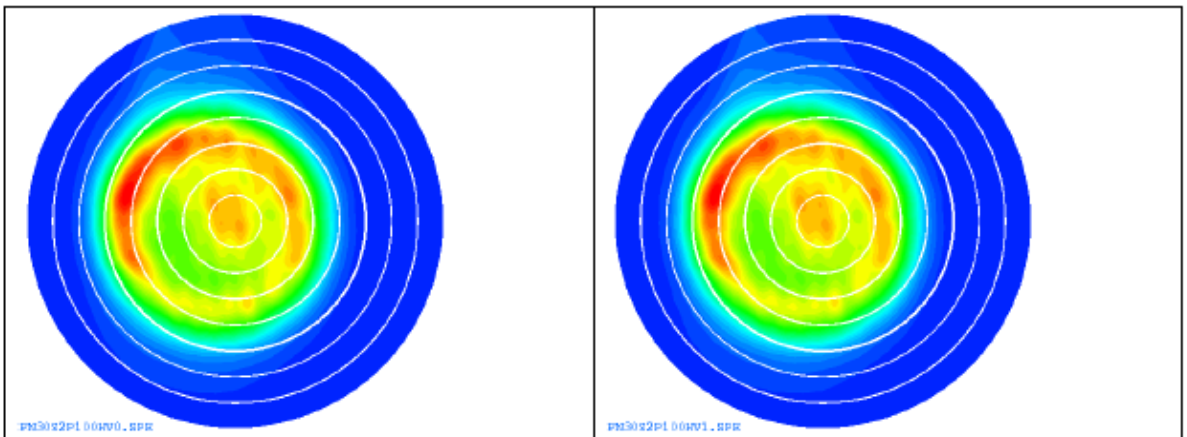

FN30Z2P100HV0.SPE

RING#	I,s	I,s/I,tot (%)
1	4.65653E+07	4.60
2	1.27413E+08	12.58
3	2.13049E+08	21.03
4	2.59102E+08	25.58
5	2.07677E+08	20.50
6	8.52168E+07	8.41
7	4.18745E+07	4.13
8	3.21724E+07	3.18
I,tot =	1.01307E+09	

FN30Z2P100HV1.SPE

RING#	I,s	I,s/I,tot (%)
1	4.71718E+07	4.61
2	1.29154E+08	12.61
3	2.15652E+08	21.06
4	2.61219E+08	25.51
5	2.09061E+08	20.42
6	8.65773E+07	8.45
7	4.25744E+07	4.16
8	3.25921E+07	3.18
I,tot =	1.02400E+09	

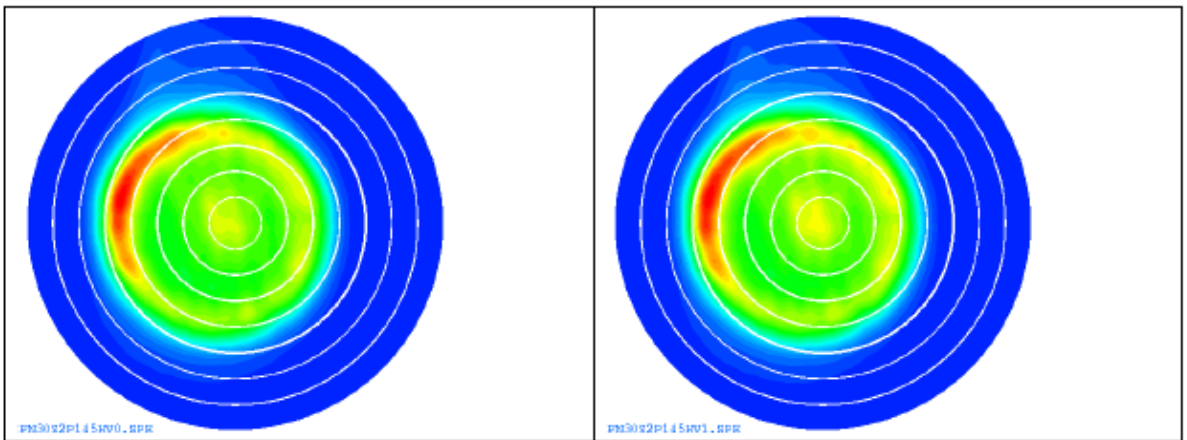

FN30Z2P145HV0.SPE

RING#	I,s	I,s/I,tot (%)
1	5.11027E+07	4.44
2	1.35040E+08	11.73
3	2.27503E+08	19.76
4	3.06128E+08	26.58
5	2.62027E+08	22.75
6	9.22571E+07	8.01
7	4.29960E+07	3.73
8	3.45069E+07	3.00
I,tot =	1.15156E+09	

FN30Z2P145HV1.SPE

RING#	I,s	I,s/I,tot (%)
1	5.23205E+07	4.51
2	1.36800E+08	11.79
3	2.29953E+08	19.81
4	3.08157E+08	26.55
5	2.62381E+08	22.61
6	9.28964E+07	8.00
7	4.33942E+07	3.74
8	3.47396E+07	2.99
I,tot =	1.16064E+09	

Figure 5. Results (continued).

Appendix B

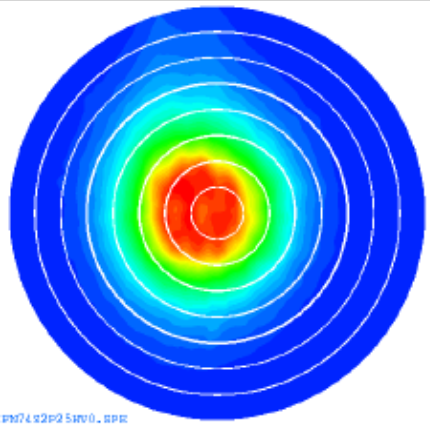

FN74Z2P25HV0.SPE

RING#	I,s	I,s/I,tot (%)
1	3.93065E+07	7.97
2	1.04816E+08	21.25
3	1.16744E+08	23.67
4	8.69037E+07	17.62
5	5.80021E+07	11.76
6	3.85123E+07	7.81
7	2.74764E+07	5.57
8	2.15135E+07	4.36
I,tot =	4.93274E+08	

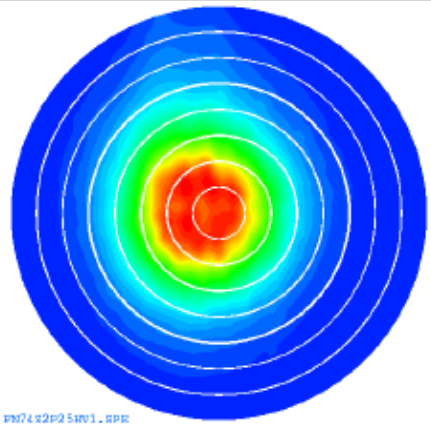

FN74Z2P25HV1.SPE

RING#	I,s	I,s/I,tot (%)
1	3.83103E+07	7.61
2	1.01614E+08	20.19
3	1.16214E+08	23.09
4	8.99253E+07	17.87
5	6.20040E+07	12.32
6	4.16978E+07	8.28
7	3.01293E+07	5.99
8	2.34320E+07	4.66
I,tot =	5.03327E+08	

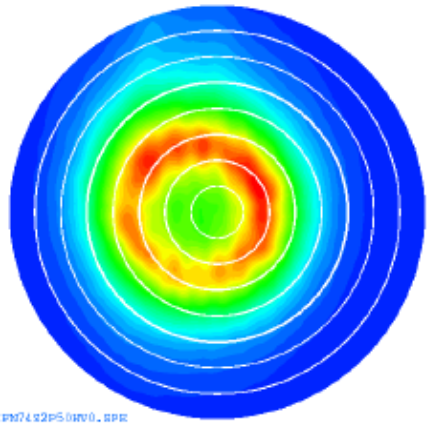

FN74Z2P50HV0.SPE

RING#	I,s	I,s/I,tot (%)
1	2.82489E+07	3.40
2	1.03056E+08	12.41
3	1.82119E+08	21.94
4	1.94062E+08	23.38
5	1.40472E+08	16.92
6	8.69886E+07	10.48
7	5.58330E+07	6.73
8	3.94299E+07	4.75
I,tot =	8.30209E+08	

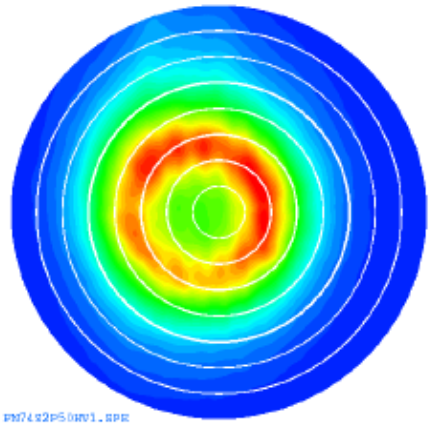

FN74Z2P50HV1.SPE

RING#	I,s	I,s/I,tot (%)
1	2.82591E+07	3.36
2	1.02868E+08	12.24
3	1.82210E+08	21.67
4	1.94897E+08	23.18
5	1.43333E+08	17.05
6	8.98459E+07	10.69
7	5.83250E+07	6.94
8	4.10076E+07	4.88
I,tot =	8.40746E+08	

Figure 5. Results (continued).

Appendix B

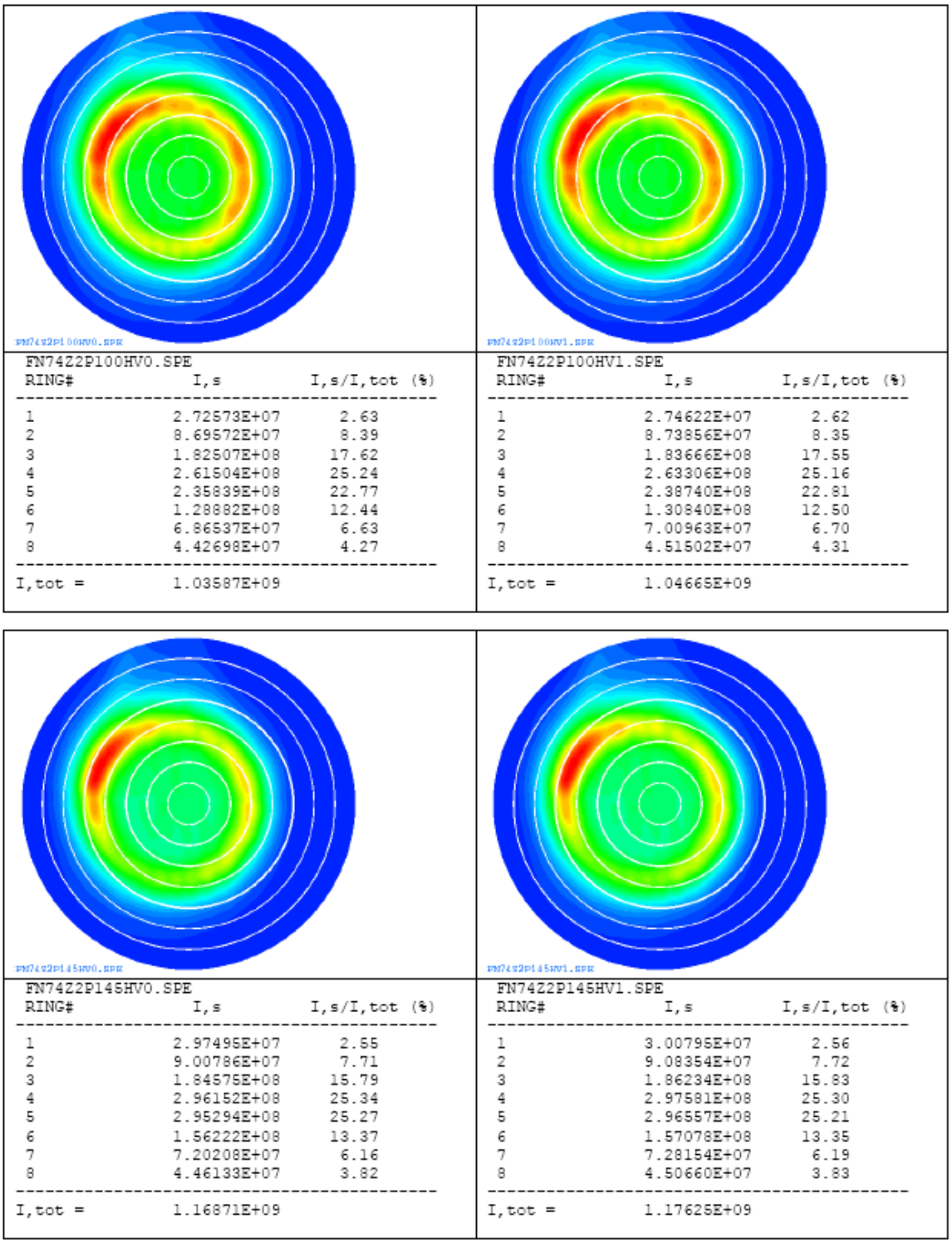

Figure 5. Results (concluded).

Appendix B

Appendix B